ACTA FACULTATIS TECHNICAE

TECHNICKÁ UNIVERZITA VO ZVOLENE

2

ROČNÍK: XXIII
ZVOLEN 2018

Medzinárodný zbor recenzentov / International Reviewers Board

OBSAH

VEDECKÉ ČLÁNKY

VEDECKÉ ČLÁNKY

RESEARCH OF RAYLEIGH-BÉNARD'S CONVECTION IN A HEATED FLUID LAYER

VÝSKUM RAYLEIGHOVEJ-BÉNARD KONVEKCIE VO VRSTVE VYHRIEVANEJ KVAPALINY

Zuzana Brodnianská[1], Elena Pivarčiová[2], Mohammad Emal Qazizada[2]

Zuzana Brodnianská[1], Elena Pivarčiová[2], Mohammad Emal Qazizada[2]
[1]Department of Environmental and Forestry Technology, Faculty of Environmental and Manufacturing Technology, Technical University in Zvolen, Studentska 26, 960 53, Zvolen, Slovak Republic, zuzana.brodnianska@tuzvo.sk
[2]Department of Manufacturing and Automation Technology, Faculty of Environmental and Manufacturing Technology, Technical University in Zvolen, T. G. Masaryka 24, 960 53, Zvolen, Slovak Republic, elena.pivarciova@tuzvo.sk, m.emalqazizada@yahoo.com

ABSTRACT: This contribution is dealt with experimental research of Rayleigh-Bénard´s convection in a heated fluid layer. The holographic interferometry optical method was used for the visualization of temperature distributions in the investigated area. The conductive, transition and convection regimes in heated fluid layer were evaluated from interferograms. Transient flow regime has occurred at Ra = 1037, at heating time of 65 s. From the temperature fields of interferograms were created graphic progress of temperature changes of fluid layer during its heating at different heights of layer H.

Key words: Rayleigh-Bénard›s convection, transient regime, holographic interferometry, fluid layer

ABSTRAKT: Príspevok sa zaoberá experimentálnym výskumom Rayleigh-Bénardovej konvekcie vo vrstve ohrievanej kvapaliny. Pre vizualizáciu rozloženia teplôt v skúmanom prostredí bola použitá optická metóda holografickej interferometrie. Z obrazov interferogramov bol vyhodnotený kondukčný, prechodový a konvekčný režim prúdenia v ohrievanej tekutine. Prechodový režim prúdenia nastal pri Ra = 1037, v čase ohrevu 65 s. Z teplotných polí interferogramov boli vytvorené grafické priebehy teplotných zmien kvapaliny počas jej ohrevu v rôznych výškach vrstvy H.

Kľúčové slová: Rayleigh-Bénardova konvekcia, prechodový režim, holografická interferometria, vrstva kvapaliny

INTRODUCTION

Heat transfer by natural convection in horizontal layer of fluid has been studied by several authors. In most experiments, the liquid layer is heated from below and cooled from above. The heat is transferred through the channel in liquid layer up to a certain

temperature difference, and in this regime the liquid is stable. After the critical temperature difference particles of liquid have a tendency to move vertically. At this point, begins convection. In convection regime, being generated hexagonal cells called Bénard's cells (Bénard, 1901). At this point, the particle motion depends on two forces competing each other: resistance forces and viscous forces.

The first experiments have taken place at the beginning of twentieth century (Bénard, 1901) and theoretical studies were realized a few years later (Rayleigh, 1916). Enhancement of convection by appropriate regulation of convective cell size achieved by Domaradzki (Domaradzki, 1989). The Author's team (Cerisier et al, 1998) analyzed start of convection in horizontal layer of fluid between two plates with different thicknesses and different thermal conductivity. Prakash and Koster (Prakash and Koster, 1996) examined Rayleigh-Bénard's problem in two immiscible fluids. Practical applications of this problems are demonstrated in the cooling of electronic devices and heat reservoirs.

In the case of that horizontal layer of liquid is warmed from top and a black body is placed on the bottom of the liquid vessel, the heat absorbed by black bodies. Thus, the liquid layer is heated from below and creates a temperature gradient, which we encounter in classic Rayleigh-Bénard´s problem of thermal instability. Kozanoglu in his work (Kozanoglu, 1993) also confirmed this statement. This phenomenon can be observed for example, in solar lakes.

In our experimental investigation we warmed liquid (distilled water) from top and at the bottom of container of liquid we sited a black body. For visualization of temperature fields in observed environment we used holographic interferometry method. Images of interferograms were recorded at time intervals during heating of liquid and allow us to evaluate the flow transient regime in the liquid, as well as the behavior of liquid during heating. The temperature differences ΔT were determined from interferogram images in examined liquid at height H and calculated values Ra for conduction regime, transient regime and convection regime.

RAYLEIGH-BÉNARD´S INSTABILITY

Rayleigh-Bénard′s convection is a type of natural convection occurring in a horizontal layer of liquid heated from below. Initial movement is increased in fluid of lower density from bottom layer heated. This increase is spontaneously arranged in a regular design of cells - Bénard′s cells. Because it's upper and lower level density gradient, gravity is trying to get cooler and pull a dense liquid from top to bottom. The gravitational force acts against viscous force in fluid. The equilibrium of these two forces are expressed by a dimensionless parameter called Rayleigh's number (Kozanoglu and Cruz, 2003):

$$Ra = \frac{g \cdot \beta \left(T_1 - T_2\right) H^3}{\nu \cdot \kappa} \tag{1}$$

where, g – gravitational acceleration [m/s^2],
β – thermal expansion coefficient [K^{-1}],
T_2 – the temperature of top surface [K],
T_1 – the temperature of bottom surface [K],
H – height of fluid layer [m],

ν – kinematic viscosity [m^2/s],
κ – heat diffusivity [m^2/s],

The heat diffusivity is calculated according to this formula:

$$\kappa = \frac{\lambda}{\rho \cdot c} \tag{2}$$

where, λ – thermal conductivity coefficient [W/(m.K)],
ρ – density of fluid [kg/m^3],
c – specific heat capacity [J/(kg.K)].

When *Ra* number increases, gravitational forces become more dominant with the critical number Ra_c, conventional cells start to appear. Ra_c can be obtained analytically for a variety of different boundary conditions. The simplest case are two free boundary margins, which Lord Rayleigh solved in 1916 by obtaining $Ra_c = 27/4.\pi^4 \approx 657.51$ in the case of a solid bottom surface and an unfilled top surface, the critical Rayleigh number occurs at $Ra_c = 1100.65$ (Drazin and Reid, 2004).

Rayleigh-Bénard′s convection can occur in three different cases. The fluid is enclosed between two solid surfaces, or fluid is between free surfaces, or fluid is between solid and free surface (e.g. air). When the fluid is between free surfaces, it is unrealistic. The most common occurrence in the industry and household is the case, when fluid is occur between solid and free surfaces (Fig. 1).

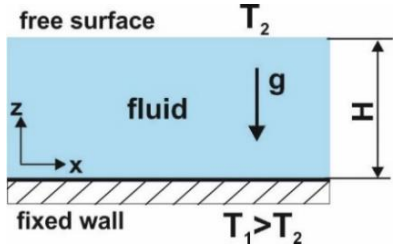

Fig. 1 Case of Rayleigh-Bénard´s instability – fluid between fixed and free surfaces
Obr. 1 Prípad Rayleigh-Bénard instability – tekutina medzi pevným a voľným povrchom
T_1 – temperature on lower fixed wall, T_2 – temperature on top free surface, H – height of fluid layer, g – gravitational acceleration

Gravity causes, that warmer (lighter) liquids are hovering against cooler (heavier) fluids and buoyancy forces are trying to bring the fluid into motion. Such heat-driven motion is called convection and occurs naturally everywhere, where there are sufficiently large local changes in the temperature of the liquid (Nemec et al., 2016).

At a certain time the peripheral temperature changes, the resulting heat changes of temperature in liquid, hence its density and result of the convection is with velocity of field **v**. Analytical vision of convection is obtained from Boussinesq equations for incompressible liquid (Lautrup, 2011):

$$\frac{\partial \Delta T}{\partial t} + (\mathbf{v}.\boldsymbol{\nabla})\Delta T = \kappa\, \boldsymbol{\nabla}^2 \Delta T \tag{3}$$

$$\frac{\partial \mathbf{v}}{\partial t} + (\mathbf{v}.\boldsymbol{\nabla})\mathbf{v} = \frac{\boldsymbol{\nabla}\Delta p}{\rho_0} + \nu\boldsymbol{\nabla}^2\mathbf{v} - \beta\Delta T\boldsymbol{g}_0 \tag{4}$$

$$\boldsymbol{\nabla}.\mathbf{v} = 0 \tag{5}$$

where, $\mathbf{v}$ – velocity field [-],
ΔT – temperature difference [K],
t – time [s],
ρ_0 – density [kg/m^3],
Δp – pressure difference [Pa].

The detailed source of the Boussinesq approximation is reported in literature (Tritton, 1988).

Thermal expansion coefficient β is for all kinds of isotropic matter defined as relative decrease in density per unit of temperature increase at constant pressure (Lautrup, 2011):

$$\beta = -\left(\frac{\partial \rho}{\partial T}\right)_p \tag{6}$$

We may calculate change in density:

$$\Delta\rho = -\beta\Delta T\rho \tag{7}$$

Vertical and horizontal velocity are takes the form:

$$v_z = -\frac{\kappa\Theta}{G}\cos k_x x(\nabla_z^2 - k_x^2)\, f(z) \tag{8}$$

$$v_x = -\frac{\kappa\Theta}{Gk_x}\sin k_x x(\nabla_z^2 - k_x^2)\, f'(z) \tag{9}$$

where, $f(z)$ – a dimensionless function of z, $f'(z) = df(z)/dz$,
G – vertical temperature gradient.

The third velocity component v_y does not participate ($v_y = 0$) (Lautrup, 2011).

EXPERIMENTAL INVESTIGATION

In our experiment, we observed the flow transient regime in fluid layer in free convection, the bottom surface of liquid being bounded by a black body and the top surface being free and heated. The scheme of the experimental device is illustrated in Fig. 2. The liquid was in a glass container CF with dimensions of 200 mm × 70 mm × 180 mm. On the bottom of container was polystyrene insulation (IS) with a thickness of 30 mm, to prevent thermal outflow. On this polystyrene layer was the aluminum layer with a thickness of 10 mm (BB) coated with black color (Koleda et al., 2017). The work capacity use distilled water filled to a height of 40 mm from the black surface. The liquid was heated by a 1200 W heat source (HS), which located 350 mm above the liquid level (Kotšmíd et al, 2015). Temperature at the liquid level and at the bottom of liquid was measured by K-type thermocouples (Koleda et al., 2016). The temperature values were recorded during heating into ALMEMO 2590-4AS datalogger (Dzurňák, 2017).

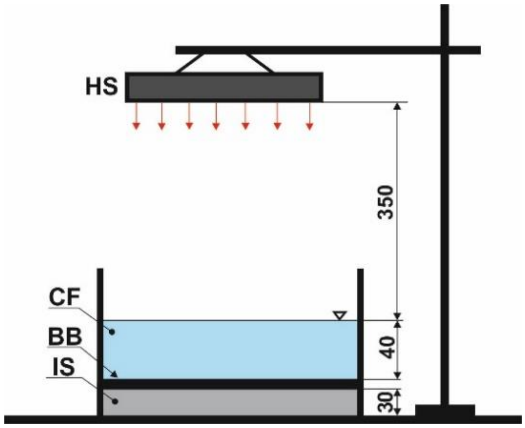

Fig. 2 Experimental description scheme
Obr. 2 Schéma experimentálnej zostavy
HS – heat source, CF – container with fluid (distilled water), BB – black body,
IS – insulation (dimensions are in mm)

In Fig. 3 illustrating the diagram of energy balance during the heating of liquid by source of thermal radiation from top. The total radiation intensity G is applied to the level of liquid, while part of radiation energy is reflected from the level of fluid Φ and the other part is absorbed by surface and guided through a layer of liquid α. Part of radiation that reaches the bottom of liquid layer is absorbed by black body G_{bb} (Kozanoglu and Cruz, 2003).

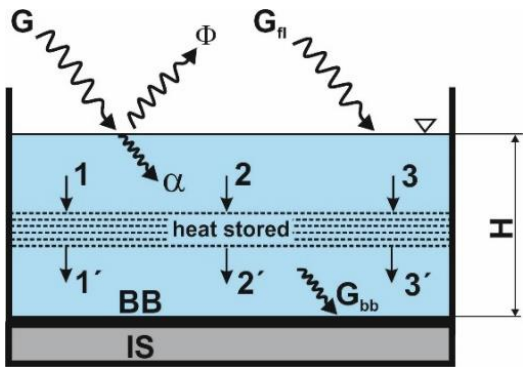

Fig. 3 Processes running during heating the container of liquid
Obr. 3 Procesy prebiehajúce v nádobe počas ohrevu kvapaliny
G – total radiation intensity, G_{fl}– intensity of radiation affecting water level, Φ – part of reflected radiation from surface, α – part of absorbed radiation, G_{bb} – radiation intensity reaching the bottom of vessel, BB – black body, IS – insulation, H – height of studied layer,
1 – convection coming in, 1´ – convection going out, 2 – conduction coming in,
2´ – conduction going out, 3 – absorption coming in, 3´ – absorption going out

For visualization of temperature fields in examined environments used holographic interferometry method in real-time. The scheme of holographic version of Mach-Zehnder interferometer used shown in Fig. 4.

Laser beam from helium-neon laser reflected from mirror (Z_1) is divided on the dividing plate (D) point to two waves – object wave (OV) and reference wave (RV). Mirrors (Z_2, Z_3) and a mirror placed in a cardan axis (KZ) the waves were directed to holographic plate (H) location. Object and reference waves have been expanded and aligned to a diameter of 8 cm using telescopic systems (T_1, T_2). The telescopic system consists of microscopic lenses (MO_1, MO_2), apertures (C_1, C_2) and objectives (O_1, O_2). The object wave (OV) pass away through the investigated place, and therefore a container with fluid (CF) filled with liquid, and fell on a holographic plate (H) mounted in holder (DH). The reference wave (RV) fell on mirror (KZ) stored in a cardan hinge and consequently to a holographic plate (H), where both waves interfered. Images of holographic interferograms were recorded through ground glass (M) to the camera (K) and then evaluated in software developed for analysis of temperature fields.

The optical method of holographic interferometry has been able to give a comprehensive image, an idea of size and shape of temperature field at a given time, and the shape of temperature field at a given time then analyze it to understand the observed phenomenon (Koleda and Koleda, 2014).

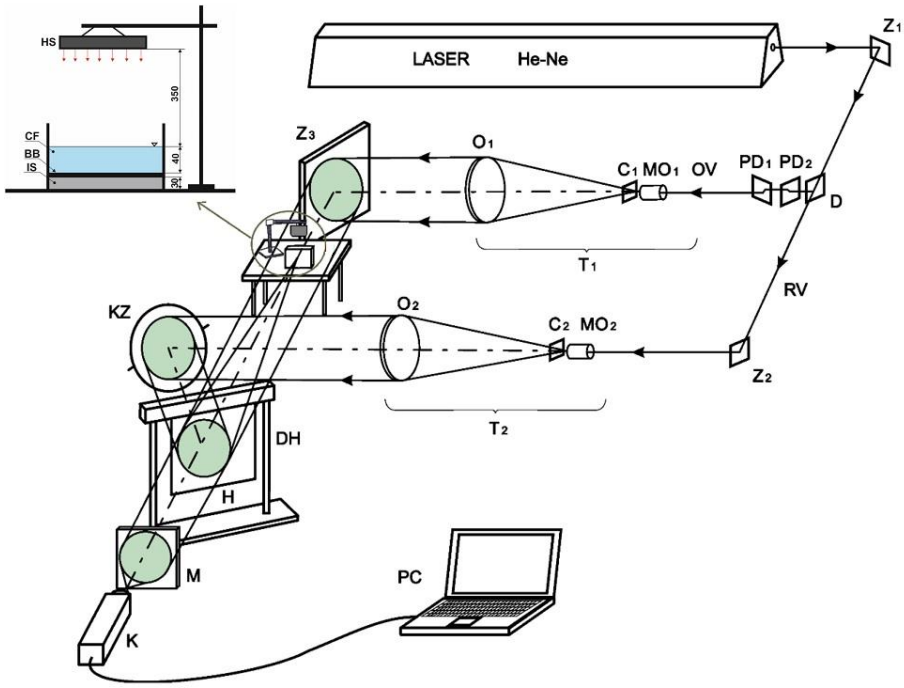

Fig. 4 Scheme of a holographic variant Mach-Zehnder interferometer
Obr. 4 Schéma holografického variantu Mach-Zehnderovho interferometra
LASER – Helium-neon laser, OV – object wave, RV – reference wave, D – divider,
H – holographic plate, DH – holographic plate holder, KZ – mirror in a cardan axis,
O_1, O_2 – objectives, Z_1, Z_2, Z_3 – mirrors, C_1, C_2 – aperture holes, MO_1, MO_2 – microscopic lenses,
PD_1, PD_2 – plane-parallel sheets, T_1, T_2 – telescopic structures, M – ground glass,
K– CCD camera, PC – computer with hardware and software equipment

RESULTS AND DISCUSSION

During continuous heating of liquid in the interval of 30 seconds images of holographic interferograms were recorded in real-time (Fig. 5). Images of interferograms allowed us to monitor and record changes in temperature profiles in heated liquid at the same time evaluate the critical transition between conduction and convection in liquid.

From the qualitative analysis of images of holographic interferograms (Fig. 5) appearance, that the temperature profiles in the time range of 0 to 65 seconds correspond to the conduction regime, and after 65 seconds starts the convection regime. Heating the liquid level began to create interference fringes (Fig. 5b) and their number increased with increasing temperature flown.

In the works (Rayleigh, 1916 and Chandrasekkar, 1961), critical numbers were obtained in the range 1026 to 1051. The theoretical critical Ra_c number for one empty and one heated area the value reaches to 1100.65 (Chandrasekkar, 1961). In our case we can see the transition of conduction regime to quantum can be observed in Fig. 5d, where the value is reached to $Ra_c = 1036$.

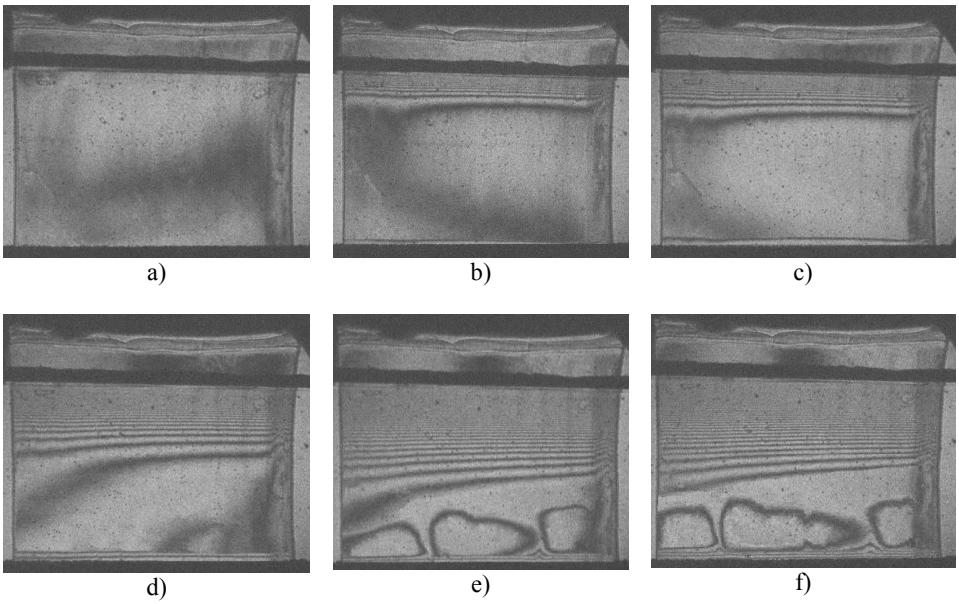

Fig. 5 Images of holographic interferograms of temperature fields in studied environment
Obr. 5 Obrazy holografických interferogramov teplotných polí v skúmanom prostredí
a) start of heating, $t = 0$ s b) $t = 20$ s (conduction), $Ra = 22$,
c) $t = 40$ s (conduction), $Ra = 599$,d) $t = 65$ s (transition), $Ra = Ra_{crit} = 1037$,
e) $t = 130$ s (convection), $Ra = 12701$, f) $t = 160$ s (convection), $Ra = 18959$

By estimating images of holographic interferograms (Fig. 5) we have obtained a temperature distribution in investigated place during the progressive heating. The *Ra* values for individual heaters were calculated according to formula (1).

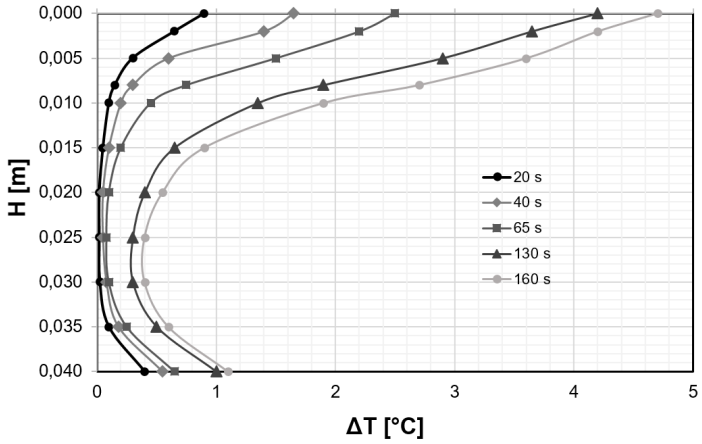

Fig. 6 Distribution of temperatures in investigated environment during heated
Obr. 6 Rozloženie teplôt v skúmanom prostredí počas ohrevu

The temperature differences ΔT in investigated liquid were quantitatively evaluated from interference fringes of individual interferograms. In conversion regime clearly shows the shape change of interference fringes (Fig. 5e, 5f). The heat flow through the liquid absorbed by black body at bottom and thus the liquid heated from below. A temperature gradient generated, which we created the classic Rayleigh-Bénard´s problem of thermal instability. During the convection regime at $t = 130$ s (Fig. 5e), in the lower part of container of fluid began to form conventional Bénard convection cells.

In Fig. 6 shows the temperature differences during heating of liquid at different depths from heated level. At a distance of $H = 0.018$ m from liquid level, at heating time $t = 65$ s, the transition occurs in flow regime. Temperature differences ΔT have a decreasing tendency towards the bottom of container during liquid heated. Due to black body, temperature gradient formed at the bottom of container at $H = 0.04$ m.

CONCLUSION

The problem of Rayleigh-Bénard instability is the problem of convection inside in liquid. This instability occurs in a liquid enclosed between two infinite horizontal planes at different temperatures on each side of liquid. In this paper, we focused on Rayleigh--Bénard's convection in the case of, when heated liquid between the solid and unfilled surface (air).

In this paper, we concentrated on visualization of temperature fields in liquid layer, which heated by heat radiator from top and surrounded by a black body from below. The heating of liquid managed to form temperature fields in investigated environment which were recorded by non-contact holographic interferometry method in real time. Temperature differences were determined from interferogram images in liquid ΔT at the height H, which were formed during slow heating of liquid. The temperature field observed as a whole and it is possible to record heat change also above the black body.

From the qualitative and quantitative analysis of the interferogram images and change in flow regime during heating of liquid and calculated critical value of Rayleigh's Ra_c number in flow transition regime determined. Conduction regime ranged from 0 to 65 seconds and density of strips gradually increased. After 65 seconds convection regime started, which also reflected on the shape of interference strips (Fig. 5d). Here we can see transition regime (transient) from conduction regime to convective, for calculated $Ra_c = 1036$. Consequently, it is in convection regime at $t = 130$ s started to form Bénard's cells (Fig. 5e, 5f).

Practical applications of studed problem are seen in solar ponds represents a large scale solar thermal collector with storage of heated water. Water cooling of electronic equipment also uses the principle of Rayleigh-Bénard´s problem of thermal instability.

REFERENCES

BÉNARD, H., 1901. Les Tourbillons Cellulaires dans une Nappe Liquide Transportant de la Chaleur par Convection en Régime Permanent. *Ann. Chim. Phys*. (1901), 23:62–144.

CERISIER, P., RAHAL, S., CORDONNIER, J., LEBON, G., 1998. Thermal Influence of Boundaries on the Onset of Rayleigh-Bénard Convection. *Int. J. Heat Mass Transfer* (1998), 41:3309–3320. DOI: 10.1016/S0017-9310(97)00364-5.

DOMARADZKI, J.A., 1989. Heat Transfer Enhancement in Rayleigh-Bénard Convection. *Int. J. Heat Mass Transfer* (1989), 32(12):2475–2483. DOI: 10.1016/0017-9310(89)90206-8.

DRAZIN, P. G., REID, W. H., 2004. *Hydrodynamic Stability.* Cambridge University Press, 2004. ISBN 9780511616938.

CHANDRASEKKAR, S., 1961. *Hydrodynamic and Hydromagnetic Stability*. Oxford, Clarendon Press, 1961. ISBN 9780486640716.

DZURŇÁK, R., KIZEK, J., JABLONSKÝ, G, 2017. Influence of oxygen on heat transfer by convection in the experimental device. AIP Conference Proceedings 1889(1):020007. DOI: 10.1063/1.5004341.

KOLEDA, P., BARCÍK, Š., VANČO, M., 2017. Effect of thermal treatment and grinding on surface color change of selected wood spicies. *Acta facultatis technicae,* (2017), 22(2):47–61.

KOLEDA, P., KOLEDA, P., 2014. Special picture analysis dependent on the light intensity. *Acta facultatis technicae* (2014), 19(1):53–60.

KOLEDA, P., KOLEDA, P., GRÚBEL, S., 2016. Analysis of temperatures in the mould area during the process of engine cylinder heads casting. *Acta facultatis technicae* (2016), 21(1):31–40.

KOTŠMÍD, S., MARIENČÍK, J., BEŇO, P., MINÁRIK, M., 2015. Accuracy of a deflection computation at the step shaft by the method of diameter reduction. *Acta facultatis technicae* (2015), 20(1):43–54.

KOZANOGLU, B., 1993. El Principio de la Convección en una Capa con un Fondo Cuerpo Negro Calentado desde Arriba. *Información Tecnológica* (1993), 4(5):60–65.

KOZANOGLU, B., CRUZ, J. A., 2003. Transient natural convection in a horizontal fluid layer, with a blackbody bottom; heated from above by radiation. *Latin American Applied Research* (2003), 33:39–44.

LAUTRUP, B., 2011. *Physics of Continuous Matter: Exotic and everyday phenomena in the macroscopic world.* CRC Press, 2003, 696 p. ISBN 9781420077001.

NEMEC, P., MALCHO, M., HOLUBCIK, M., 2016. Heat transport through the contact area of electric element and aluminium block of loop heat pipe evaporator. In *Energy and Clean Technologies Conference Proceedings*, SGEM 2016, Albena, Bulgaria, 2016, pp. 397–402. ISSN 1314-2704.

PRAKASH, A., KOSTER, J.N., 1996. Steady Rayleigh-Bénard Convection in a Two-Layer System of Immiscible Liquids. *Journal of Heat transfer-Transactions of ASME* (1996), 118: 366–373. DOI: 10.1115/1.2825853.

RAYLEIGH, L., 1916. On convection Currents in a Horizontal Layer of Fluid when the Higher Temperature is on the other Side. *Philos. Mag.* (1916), 32:529–43.

TRITTON, D. J., 1988. *Physical Fluid Dynamics.* Oxford University Press, 1988. ISBN 978-0442301316.

Contribution has been prepared within the solving of scientific grant project VEGA 1/0086/18 "Researching Temperature Fields in a Set of Shaped Heat Transfer Surfaces" and grant project KEGA 001TU Z-4/2016 "Support of Teaching for Heat and Mass Transfer in Technical Education."

Corresponding author:
Zuzana Brodnianská, Ing., PhD., tel.: 00421455206678, e-mail: zuzana.brodnianska@tuzvo.sk

DETECTING OF PARTICAL DIMENSIONS USING PICTURE ANALYSIS

ZISŤOVANIE ROZMEROV ČASTÍC POMOCOU OBRAZOVEJ ANALÝZY

Pavol Koleda, Mária Hrčková

Department of Manufacturing and Automation Technology, Faculty of Environmental and Manufacturing Technology, Technical University in Zvolen, Študentská 26, 960 53 Zvolen, pavol.koleda@tuzvo.sk, hrckova@tuzvo.sk

ABSTRACT: This papers deals with the design of applications to measure the dimensions of objects and particles in a digital image. Particle size measurement is an important part of any industry sector, whether by checking the manufactured parts, by checking the shape of the goods or by the presence of an insignificant element in the production apparatus. This application, apart from the basic area dimensions, also detects the circumference and the contents of the objects as well as the rotation of the individual objects in the image.

Key words: Dimensions, picture analyse, digital picture, Matlab.

ABSTRAKT: Článok sa zaoberá návrhom aplikácie pre meranie rozmerov objektov a častíc v digitálnom obraze. Meranie rozmerov častíc je dôležitou súčasťou každej oblasti priemyslu, či už kontrola vyrobených dielov, kontrola tvarov tovarov alebo prítomnosť nežiadúceho prvku vo výrobnom aparáte. Táto aplikácia bude okrem základných plošných rozmerov zisťovať tiež obvod a obsah objektov, ako aj natočenie jednotlivých objektov v obraze.

Kľúčové slová: Rozmery, obrazová analýza, digitálny obraz, Matlab.

INTRODUCTION

Today maximum effort is made to search for and use of energy saving solutions in every industry (Kováč, 2014). Measurement of sawdust and wood dust dimensions is an important part of the woodworking industry. Such an analysis allows to evaluate the characteristics of the machines used in woodcutting and optimizes the selection of a suitable separating device for contingent sorting of sawdust from the dust. The measurement evaluation informs about the potential emissivity of the working environment and the health risks at working in such environment, since small wood dust may have negative effects on the human body, even it was found that oak sawdust is carcinogenic (Irša, 2006). Appropriate selection of the tool can affect the proportion of the fine fraction of particles. (Očkajová, 2006).

The article deals with the small particles and dust size measurement using the optical method. This is one of the most advanced methods of fractal particles analyzing. It allows, getting more information about the measured particles.

MATERIAL AND METHODS

For particle size measurements, was proposed an application in Matlab (figure 1).

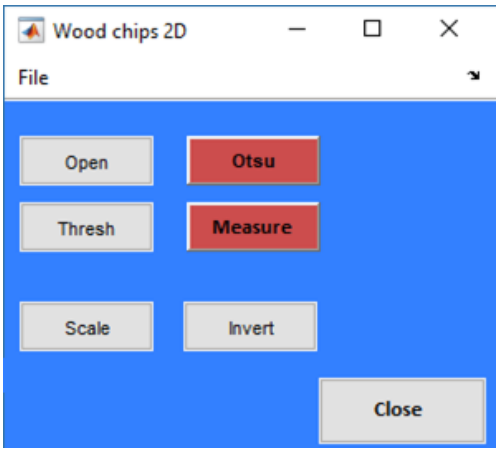

Fig. 1 Appearance of the proposed application window
Obr. 1 Vzhľad okna navrhnutej aplikácie

There is an image with measured objects open. In our experiment it is the sawdust of the common spruce (*Picea abies*) (figure 2). Sawdust are scanned using a digital camera Nikon D5300 with a tripod. For accurate particle identification, these were shot on a contrasting black background. When scanning other objects, select the appropriate background color to correctly identify of particles (Brodnianská, 2018, Koleda, 2014).

Fig. 2 Scanned particles – wood chips
Obr. 2 Zosnímané častice – piliny

In the process of image signal obtaining, its transfer, processing and evaluation, variable unexpected effects are imported into image. Every of them can unpredictable affect the image quality and subsequence operations proceeded with this image. The image can obtain information reducing its quality already at the image formation. If those effects have to be minimalized or supressed, it is necessary to apply a number of operations called image preprocessing. By application of image preprocessing there is not obtained any new information, only some information in image signal (important) is emphasized and other (not important and errors) are supressed. Preprocessing allows besides elimination of errors information to extract information from the image that is directive for its understanding on the base of predefined requirements. Before the measurement it is necessary to modify obtained images with measured objects. During this operations the perspective and spherical distortion of camera are removed (Hrčková, 2012; Jesenák, 2008).

The input image contains objects that are bad lighted, or casts a shadow. The reasons can be, that simple thresholding methods are fail. The solution are local (adaptive) thresholding methods (Koleda, 2013). Then are found objects in the image in two steps. Using Otsu algorithm is first found the optimal threshold value for image thresholding (figure 3). As an input to this algorithm, the image was adjusted to gray level by equation 1.

$$0.2989 * R + 0.5870 * G + 0.1140 * B \quad (1)$$

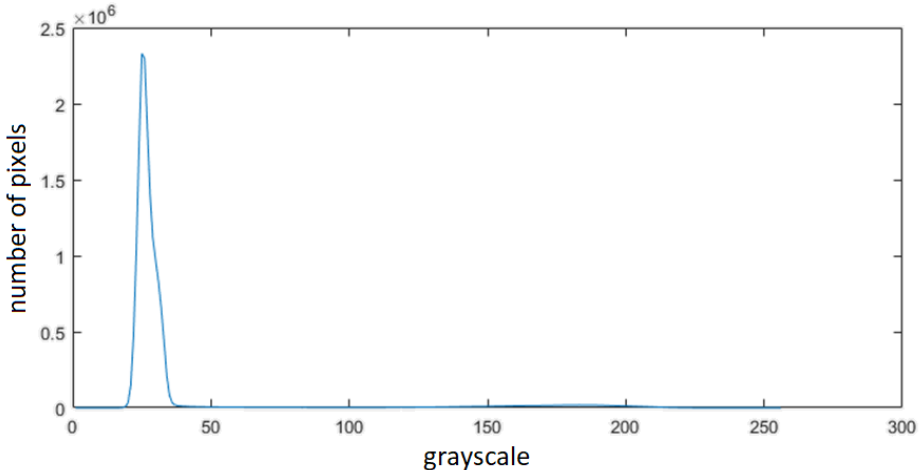

Fig. 3 Histogram of grayscale in the processed image
Obr. 3 Histogram úrovní šedi v spracúvanom obraze

In the second step, the image is threshold with the found threshold (figure 4). There are a several thresholding techniques, for our experiment was the most effective global threshold (Singh. 2014, Koleda, 2016). Global thresholding is based on the assumption that the image has a bimodal histogram and, therefore, the object can be extracted from the background by a simple operation that compares image values with a threshold value *T*. The object and background pixels have grey levels grouped into two dominant modes. One obvious way to extract the object from the background is to select a threshold *T* that

separates these modes (Bankman, 2008; Kučerka, 2014; Koleda, 2018). The threshold image $g(x, y)$ is defined by equation 2.

$$g(x,y) = \begin{cases} 1 \ \text{ if } (x,y) > T \\ 0 \ \text{ if } (x,y) < T \end{cases} \tag{2}$$

where g is pixel in input picture,
x, y are cartesian coordinates,
T is treshold value.

Fig. 4 Thresholded image
Obr. 4 Prahovaný obraz

In this binary image, where the objects are white and the background, are all objects in the image found using the function "bwboundaries" (Mathworks, 1994).

$$[B, L, N, A] = \text{bwboundaries}(Ig, \text{'noholes'}); \tag{3}$$

where B is cell array of boundary pixel locations [-],
L is label matrix, where objects and holes are labeled [-],
N is number of objects found [-],
A is adjacency matrix [-],
Ig is input binary image [-],
'noholes' is specification to not include the boundaries of holes inside other objects.

This function traces the exterior boundaries of objects, as well as boundaries of holes inside these objects, in the binary image Ig. bwboundaries also descends into the outermost objects (parents) and traces their children (objects completely enclosed by the parents).

The desired parameters are found in the founded objects, in this case was detected the perimeter, area, largest and smallest dimension of each particle.

RESULTS

The particle parameters described in the previous section are interpreted in a different way. To determine the particle size, 8 endpoints of each particle are found (figure 5). Of these the smallest and largest dimension is calculated.

Fig. 5 Found extreme points of wood chips
Obr. 5 Nájdené krajné body pilín

The detected perimeters and areas are represented by a histogram (figure 6).

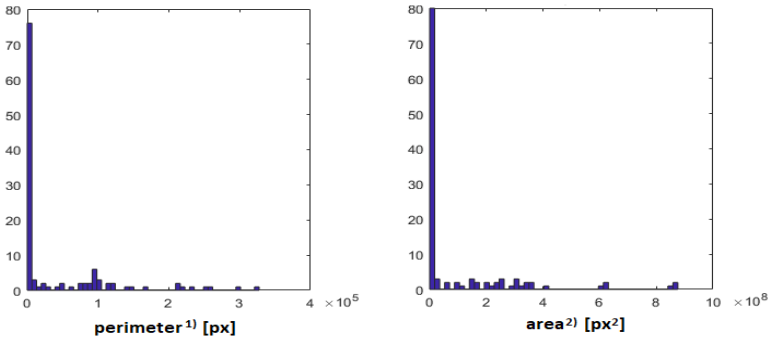

Fig. 6 Histograms of perimeters and areas
Obr. 6 Histogramy obvodov a obsahov
[1)] obvod, [2)] obsah

All measured parameters are also written in the Excel sheet, where it is possible to continue working with them. Particle sizes are detected in pixels. To determine dimensions in metric rates, you need to specify a conversion ratio for conversion from pixels to millimeters. This ratio is entered in such a way that together with the measured particles is recorded on one photo the known dimension, for example ruler. Selecting of two points in this ruler is then converted to a ratio.

CONCLUSION

The designed application allows to measure the dimensions of various objects such as sawdust or products after the production process to meet dimensional requirements. For correct identification of objects, is necessary to ensure that these objects are captured on a contrasting background. Compared to other methods, this allows to measure particle sizes that are brittle or unsuitable for sieve analysis. It is also possible to get more information about sample, even for each single particle. The weak side of this method is, the scanned particles must not overlap. Then the overlapping particles are identified as one.

LITERATURE

AL-THYABAT, S., MILES, N. J., 2006. *An improved estimation of size distribution from particle profile measurements*. Powder Technology 166(3): 152-160.

BANKMAN, I. N., 2008. *Handbook of Medical Image Processing and Analysis*. Elsevier Inc. ISBN: 978-0-12-381904-9, 1000 pp.

BRODNIANSKÁ, Z. 2018. The research of influence of gap and airflow between trapezoidal heat transfer surfaces. *In JP journal of heat and mass transfer*. 2018. no. 3, p. 579-596. ISSN 0973-5763.

ČERNECKÝ, J., BRODNIANSKÁ, Z., KONIAR, J., 2015. Intensification of heat transfer between heat exchange surfaces at low RE values. In *Chemical and Process Engineering - Inzynieria Chemiczna i Procesowa*. 2015. no. 3, p. 331-344. ISSN 0208-6425.

HRČKOVÁ, M., 2012. *Influence of preprocessing on the special image analysis*. Acta facultatis technicae 17(2): 35-43.

JESENÁK, K., 2008. *Analýza veľkosti častíc*. 2008. ISBN 978-80-223-2464-9.

KOVÁČ, J., KRILEK, J., KUČERA, M., BARCÍK, Š., 2014. *The impact of design parameters of a horizontal wood splitter on splitting force*. Drvna industrija 65(4): 263-271.

KOLEDA, P., BARCÍK, Š., NOCIAROVÁ, A. 2018. Effect of technological parameters of machining on energy efficiency in face milling of heat-treated oak wood. In *BioResources*. 2018. no. 3, s. 6133-6146.

KOLEDA, P.; KOLEDA, P., 2013. Optimal light intensity determination at optical analysis of fractional particles. Technológia Europea, Hradec Králové. Pp 5-12.

KOLEDA, P., KOLEDA, P., 2016. *Optical measurements of sawdust dimensions Optical measurements of sawdust dimensions*. In Wood research. 2016. no. 3 , p. 505-511. ISSN 1336-4561 .WOS, SCOPUS.

KOLEDA, P., KOLEDA, P., 2014. *Závislosť analýzy špeciálneho obrazu na intenzite osvetlenia*. In Acta facultatis technicae: vedecký časopis Fakulty environmentálnej a výrobnej techniky. 2014. č. 1 , s. 53-60. ISSN 1336-4472.

KUČERKA, M., OČKAJOVÁ, A., 2014. Particle size analysis of sawdust rising in the process of sawn dry spruce and oak wood. In: IX. International scientific conference Chip and chipless woodworking processes. Pp 105-110.

MATHWORKS, 1994. Product documentation (online). http://www.mathworks.com/help/ techdoc/ ref/ image_props.htm. First published 1994.
OČKAJOVÁ, A., LUČIĆ, B., ČAVLOVIĆ, A., TEREŇOVÁ, J., 2006. Reduction of dustiness in sawing wood by universal circular saw. Drvna industija 57(3): 119-126.
PIVARČIOVÁ, E., BOŽEK, P., 2014. Industrial production surety factor increasing by a system of fingerprint verification. In: ISEEE 2014: Proceedings. International conference on Information Science, Electronics and Electrical Engineering. April 26–28, 2014, Sapporo City, Hokkaido, Japan. Beijing: IEEE. Pp 493-497.
SINGH, T. R., ROY, S., SINGH, O. I., SINAM, T., SINGH, K. M., 2011. A new local adaptive thresholding technique in binarization. International Journal of Computer Science Issues, vol. 8, Issue 6, No 2, ISSN 1694-0814.
SUJOVÁ, E., SEMANOVÁ, P., KOLEDA, P., 2014. Particle size distribution analysis of metal-working fluid aerosols during turning process. Acta facultatis technicae 19(1): 135-144.
ŠURIANSKY, J., HRČKOVÁ, M., 2010. Influence of light source spectre on digital image of wood texture. Acta facultatis technicae 15(1): 113-122.

This paper was supported by VEGA Grant No. 1/0315/17 "Investigation of the relevant properties of thermally modified wood in contact phenomena in the machining process with the prediction of obtaining an optimal surface" and VEGA Grant No. 1/0725/16 "Prediction of the quality of the generated surface during milling solid wood by razor end mills using CNC milling machines."

Corresponding author:
Pavol Koleda, +421 45 520 6570, e-mail: pavol.koleda@tuzvo.sk

INFLUENCE OF FEED RATE AND CUTTING SPEED ON FINAL SURFACE QUALITY AFTER PLANE PLAIN MILLING OF OAK WOOD

VPLYV POSUVNEJ A REZNEJ RÝCHLOSTI NA KVALITU VÝSLEDNÉHO POVRCHU PO ROVINNOM VALCOVOM FRÉZOVANÍ DUBOVÉHO DREVA

Michal Korčok, Marek Vančo, Peter Koleda, Štefan Barcík

Katedra výrobnej a automatizačnej techniky, Fakulta environmentálnej a výrobnej techniky, Technická univerzita vo Zvolene, Študentská 26, 960 53 Zvolen, Slovenská republika, e-mail: korcokmichal@gmail.com, mvanco87@gmail.com, peter.koleda@tuzvo.sk, barcik@tuzvo.sk

ABSTRACT: The article deals with examination the influence of feed rate and cutting speed on final surface quality of natural and temperature modified oak wood when plain milling. Experiment part focuses on evaluation of equipment impact (angle geometry – γ = 15°, 20°, 30°) of material (of natural and temperature modified oak wood at temperatures of 160 °C, 180 °C, 210 °C, 240 °C) and technology factors (such as: cutting speed – v_c = 20 m.s^{-1}, 40 m.s^{-1}, 60 m.s^{-1}) adjustable feed rate – v_f = 6 m.min^{-1}, 10 m.min^{-1}, 15 m.min^{-1}) on quality of surface (Ra – medium arithmetic deviation of surface). The final quality of surface was measured using contactless method with help of device LPM 4, which works on a principle of laser profilometry. The best data of surface quality after wood working were measured at feed rate of 10 m.min^{-1} at temperature treatment of 160 °C. The worst measured data were at the wood in natural state at feed rate of 15m.min^{-1}. At cutting speed the lowest surface roughness was measured at untreated sample at cutting speed of 40m.s^{-1}, the worst surface quality was measured at cutting speed of 60 m.s^{-1} and temperature treatment of 210 °C.

Key words: plane milling, feed rate, cutting speed, ThermoWood®, thermal modification, surface quality

ABSTRAKT: Príspevok sa zaoberá posúdením vplyvov reznej a posuvnej rýchlosti na výslednú kvalitu opracovania prírodného a tepelne upraveného dubového dreva pri rovinnom frézovaní na spodnej vretenovej frézke. Samotný experiment sa zameriava na hodnotenie nástrojových vplyvov (uhlová geometria – γ = 15°, 20°, 30°) materiálu (v prírodnom a tepelne modifikovanom pri teplotách T: 160 °C, 180 °C, 210 °C, 240 °C) a technologických faktorov (rezná rýchlosť – v_c = 20 m.s^{-1}, 40 m.s^{-1}, 60 m.s^{-1}, posuvna rýchlosť – v_f = 6 m.min^{-1}, 10 m.min^{-1}, 15 m.min^{-1}) na kvalitu opracovania povrchu (Ra – stredná aritmetická odchýlka povrchu). Spracovanie vyhodnotených údajov sa realizovalo bezkontaktnou metódou, pomocou laserového profilometra LMP 4. Najlepšie namerané údaje pri opracovaní povrchu sa dostali pri posuvnej rýchlosti 10 m.min^{-1} s tepelnou úpravou 160 °C naopak najhoršie namerané údaje boli pri rastlom dreve s posuvnou rýchlosťou 15 m.min^{-1}.

Najnižšia drsnosť povrchu sa dosiahla pri neupravenej vzorke frézovanej reznou rýchlosťou 40 $m.s^{-1}$ naopak najhoršia kvalitu povrchu sa dosiahla pri reznej rýchlosti 60 $m.s^{-1}$ a tepelnej úprave 210 °C.

Kľúčové slová: Rovinné frézovanie, posuvná rýchlosť, rezná rýchlosť, ThermoWood®, tepelná úprava, kvalita povrchu

INTRODUCTION

Wood as a raw material is widely used by human in exteriors and interiors for over thousands of years. Nowadays wood used in outdoor has to comply with specific quality requirements – outdoor factors, which is exposed to. These factors affect the mechanical and aesthetical properties of wood. The wood exposed in this manner must show high dimensional stability, high resistance and good aesthetical characteristics during use (Kokutse et al. 2006, Kaplan et al. 2018). Even though the nature of wooden materials is valued, a great deal of disadvantages does exist. These harmful aspects were studied with aim to improve dimensional stability and to prolong the life span of material. Because of that, wood can be modified with new and with already established methods. In this connection, number of new methods were considered, which are in accordance with statutory rules, which forbid use of toxic chemicals (Jebrane et al. 2018).

From different processes of thermal modification of wood, ThermoWood® is most widespread, commercially attainable in two standard classes of treatment, Thermo – S and Thermo – D. With first approach the modification is being done with lower temperatures and it is designated mainly for indoor use, at which the letter S in its name stands for stability of shape and the dimension. The second approach of modification is at higher temperatures and by it the durability of material increases. Both approaches however, can be applied on soft as well as on hard species of wood, although as for Thermo – D, it is being applied only on hard wood, if darker colour is needed (Umit AYATA et al. 2017).

In the past the roughness of surface has mostly been detected by visual and by tactile checks, because these methods were fast and economic. However, these methods provided only subjective and qualitative estimate, but they didn't ensure adequate quality of goods or of processes (Sedlecký et al. 2017). Because of that, during any machining process on the machined place, certain anomalies of surface appear in disregard of if they are in natural state or in thermally modified state. That's why it is needed, to give attention to quality of surface and acknowledge different combinations of technical and of production parameters (Kvietková et al. 2015).

During machining high quality surface, cutting wedge must be well sharpened. The formation of wood cracks have to be eliminated. They are constantly forming across fibbers when machining at the beginning and the end of cut, where the cutting wedge comes in and out the cut (Lisičan, 1996). Milling is a process of machining wood with help of rotary tools, during which nominal thickness of chips is changing according to removal of material, from minimal to maximal value during conventional milling processes. The width or the shape of machined wood is also changing (Barcík et al. 2014).

MATERIALS AND METHODS

Making samples

During this experiment, the species of English Oak from area of Vlci Jarok (Budča, Slovak Republic, 440 m.a.s.l.) were used. After counting annual rings on round timber, average age was around 96 years. Sawn edgings with dimensions of 350 – 400 mm were carried out by School Woodland Enterprise for experimental measuring. Individual wood samples were produced by machining wood logs. Processing of round logs itself took place at workshop of Technical University, were we have on log band saw by cutting logs received sawn wood with thickness of 25 mm. Processed sawn wood has been placed in a kiln and dried too moisture content of 10 %. After drying, we have by cutting been able to gain side tangential timber with width of 110 mm.

Thermal modification of samples

Wood samples were heat treated in town Yoshkar – Ola in Russia at Volga State University of Technology according to times and temperatures in the Fig. 1.

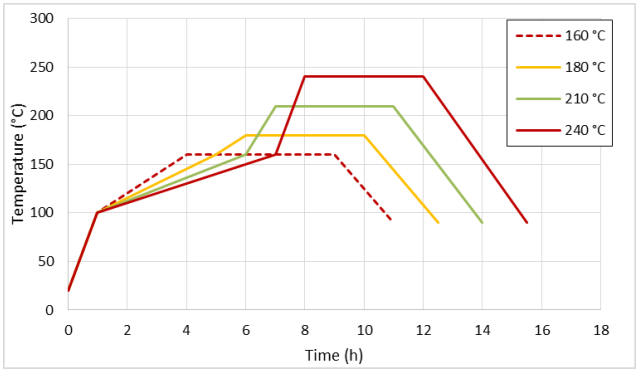

Fig. 1 Graphical progress of thermal modification of samples
Obr. 1 Priebeh termickej modifikácie vzoriek

Before experimental measuring heat-treated samples had the moisture content of 3 ÷ 6 %. One sample was left in natural state and other four were treated at given temperatures.

Table 1 Times intervals of individual heat treatments
Tabuľka 1 Časové intervaly fáz termickej modifikácie

Temperature [°C]	Phase 1 [h]	Phase 2 [h]	Phase 3 [h]
160	4	5	2
180	5	5	2.5
210	6	5	3
240	7	5	3.5

Determining wood density

The density of wood samples was determined according to STN 49 0108 standard for natural and thermally modified wood. Dimensions of 5 samples for density measuring were 20 x 20 x 30 mm (width x length x height). During individual treatments was 16 samples for processing of average value. All samples were measured by the adjustable digital caliper with accuracy of 0,01 mm and weighted by digital laboratory scales with accuracy of 0,01 g. The wood density was calculated by the equation:

$$\rho = \frac{m}{V}, \tag{1}$$

where ρ is the density of material [kg.m^{-3}],
m is the mass of material [kg],
V is the volume of material [m^{-3}].

Calculated values are in the Tab. 2, where percentage changes of heat-treated wood are compared to natural Oak wood.

Table 2 Measured English oak density values
Tabuľka 2 Namerané hodnoty objemovej hmotnosti duba letného

Thermal modification [°C]	ρ **[kg·m^{-3}]**	**Percentage change [%]**
N	639	–
160	622	2.73
180	619	3.23
210	588	8.67
240	571	11.90

Description and characterization of the machinery

For experimental measuring, the lower spindle milling machine FVS (Ligmet, Hradec Kralove, Czech Republic) was used with cylinder feeding system FROMMIA (Fig. 2). Basic parameters of machinery are in the Tab. 3.

Table 3 Basic parameters machine
Tabuľka 3. Základné parametre použitého strojového vybavenia

Lower spindle milling machine FVS		**Feeding device Frommia**	
Supply voltage	360, 220 (V)	**Type**	ZMD 252 / 137
Cutting speed	20, 40, 60 (m·min^{-1})	**Feed rate**	2.5;10; 15; 20; 30 (m·min^{-1})
Input power	4 (kW)	**Motor**	360 (V), 2 800 (m·min^{-1})

Fig. 2 Lower Spindle Milling Machine with attached Feeder
Obr. 2. Spodná vretenová frézka s upevneným podávacím mechanizmom

Characteristics and description of milling head

Three milling heads STANON (SZT – machinery Turany) for wood with changeable knives were used for plain milling. They are displayed in the Fig. 3 and their main parameters are in Tab. 4. The changeable cutting blades FH 45 were made of steel Special 55: 1985/5 with hardness of 64 HRC (WOOD – B, Nové Zámky, Slovakia). In each milling head, two knives were mounted, only one was in the cut, the second balanced the milling head. The depth of cut was 1mm.

Fig. 3 Milling heads with rake angle of 15°, 20° and 30°
Obr. 3 Frézovacie hlavy s uhlom čela 15°, 20° a 30°

Table 4 Milling heads parameters
Tabuľka 4. Parametre frézovacích hláv

Parameters of the milling head	
Diameter of the milling head with knife	130 (mm)
Diameter of the milling head	125 (mm)
Thickness of the milling head	45 (mm)
Number of knives	2
Cutting geometry	$\beta = 45°$; $\gamma = 15°, 20°, 30°$

Experimental milling

Experimental conventional milling (Fig. 4) was realised continually at cutting conditions displayed in the Table 5 at Development workshop of Technical University in Zvolen.

Table 5 Cutting conditions for experiment
Tabuľka 5 Rezné podmienky experimentu

Cutting conditions		**Value**
Feed rate v_f (m·min^{-1})		6, 10 15
Cutting speed v_c (m·s^{-1})		20, 40, 60
Tool geometry (°)	**Wedge angle**	β = 45°
	Rake angle	γ = 15°, 20°, 30°
Depth of cut a_p (mm)		1
Temperature of thermal modification T (°C)		N
		160
		180
		210
		240

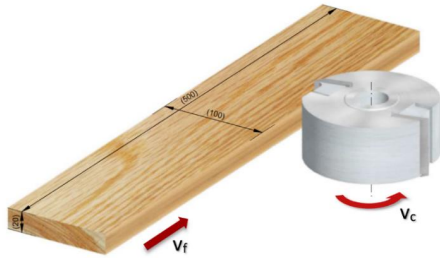

Fig. 4 Real 3D principle of conventional milling samples
Obr. 4 Princíp protibežného frézovania vzoriek

Measuring roughness of surface

The heat treated samples had the moisture of 3 ÷ 6 % before experimental measuring. With help of contactless laser profilometer LMP – 4, which is displayed on the Picture 5, the roughness of machined samples was measured. The principle of roughness measuring is based on laser profilometry. Roughness measuring was realized on the length of 40 mm, during which the measuring equipment measured in four paths from side edge of wood sample. Length between individual paths was 4 mm. The technical parameters of measuring equipment are displayed in Tab. 6.

Fig. 5 Laser profilometer LMP – 4
Obr. 5 Laserový profilometer LPM – 4

Table 6 Technical parameters of laser profilometer LMP – 4
Tabuľka 6 Technické parametre laserového profilometra LPM – 4

Technical parameters LMP – 4	
Measuring range in axis z (vertical)	420 mm to 470 mm
Measuring range in axis z	± 0.15 mm
Measuring range in axis x (transverse)	200 mm
Number of samples in axis x	1350
Processing speed	25 prof./s
Dispersed laser angle	30°
Roughness parameters	R_p, R_v, R_z, R_a, R_q, R_c
Waviness parameters	W_p, W_v, W_z, W_a, W_q, W_c

The result values were displayed graphically in program LPMWiew, which evaluates roughness of surface and at the same time evaluates surface waviness of the profile. The output values were saved in program EXCEL and prepared for data evaluation in STATISTICA 10 (StatSoft CR s. r. o., Prague, Czech Republic). With help of this program, one factor analysis (as well called single-factor analysis) and multifactor analysis of variance with graphs selected dependencies were implemented.

RESULTS AND DISCUSSION

Influence of feeding rate on surface roughness

The multifactor analysis of variance of dependence of surface roughness on feed rate is displayed in the Fig. 6 and one way ANOVA in graphs in the Fig. 7. From multifactor analysis we can see, that the highest roughness of surface was reached with natural wood, with feed rate of 15 m.min^{-1}. By contrast the best quality of surface has been reached with thermal modification of 160 °C with feed rate of 10 m.min^{-1}.

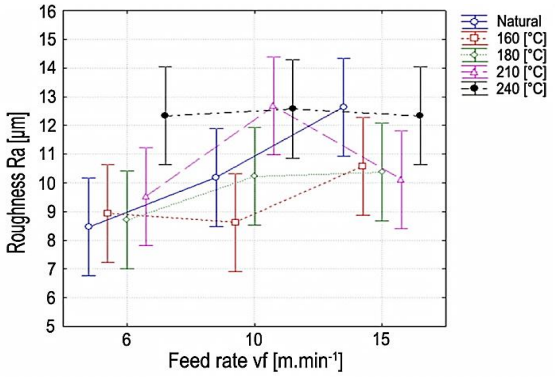

Fig. 6 Multifactor analysis of variance for the dependence of surface roughness on feed rate
Obr. 6 Viacfaktorová analýza rozptylu závislosti drsnosti povrchu na posuvnej rýchlosti

The basic statistic values of dependence of surface roughness on feed rate at different variants of cutting speed, thermal treatment and rake angle 15, 20 and 30° are displayed in the tab. 7. On basis of this table statistically important results worked out to be those of natural wood and of thermally modified wood, modified under temperature of 210 °C, with variants rake angle 15°. For rake angle 20° was statistical data significant with thermal modification 240 °C.

Table 7 View dispersal and the likelihood of dependence of surface roughness on feed speed at different variants of cutting speed, thermal treatment and rake angle 15, 20 and 30°
Tabuľka 7 Rozptyl a pravdepodobnosť podobnosti závislosti drsnosti povrchu na posuvnej rýchlosti pri rôznych rezných rýchlostiach, termickej modifikácii a uhloch čela 15, 20 a 30°

Cutting geometry γ [°]	Effect	SS	Degr. Of Freedom	MS	F	p
15	Native	205,256	4	51,314	3,83	0,014
	160 °C	105,878	4	26,470	2,01	0,121
	180 °C	16,744	4	4,186	1,36	0,272
	210 °C	1306,548	4	326,637	4,28	0,008
	240 °C	89,300	4	22,325	0,65	0,634
20	Native	137,882	4	34,471	2,70	0,052
	160 °C	35,175	4	8,794	0,55	0,699
	180 °C	9,585	4	2,396	0,57	0,688
	210 °C	84,256	4	21,064	2,52	0,064
	240 °C	99,868	4	24,967	5,95	0,001
30	Native	22,817	4	5,704	0,72	0,588
	160 °C	17,920	4	4,480	0,33	0,856
	180 °C	3,283	4	0,821	0,28	0,891
	210 °C	49,640	4	12,410	0,98	0,437
	240 °C	63,565	4	15,891	1,23	0,322

From analysis of variance it is visible, that with increasing feed rate the surface roughness increased. On contrary the worst quality of wood machining was gained at the use of natural wood with feed rate of 15 m.min^{-1}. During wood machining of all samples, the best values appeared to be at feed rate of 6 m.min^{-1}.

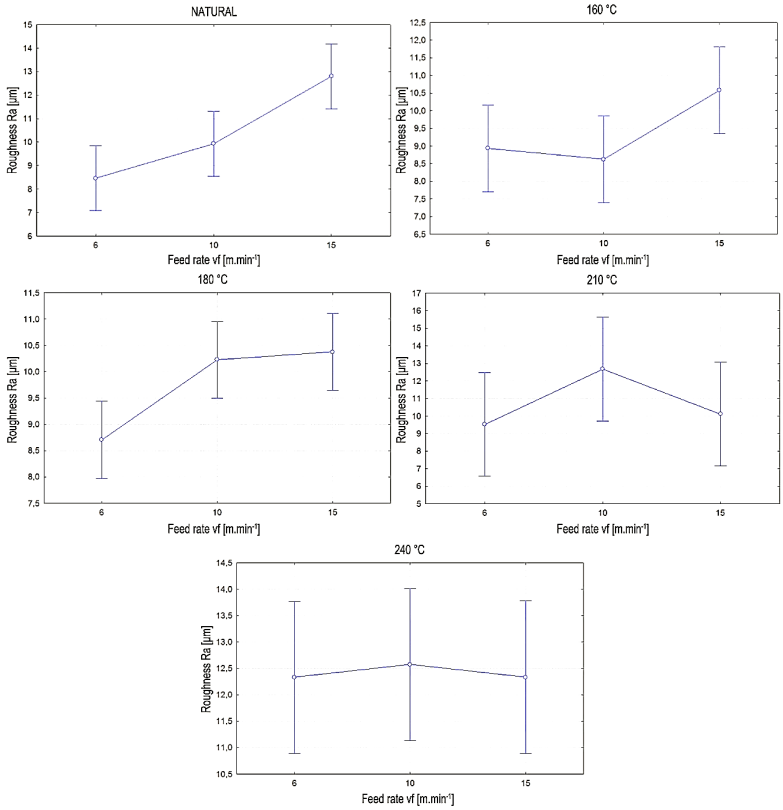

Fig. 7 Analysis of variance for the dependence of surface roughness on the feed rate
Obr. 7 Analýza rozptylu závislosti drsnosti povrchu na posuvnej rýchlosti

Influence of cutting speed on surface roughness

In the Fig. 8 the multifactor analysis of variance of surface roughness on cutting speed is displayed. Analysis of variance of dependence of surface roughness on cutting speed is displayed in the Fig. 9. From these analyses it is visible, that the best quality is at the sample with thermal treatment of 160 °C. At this sample it is visible, that at cutting speeds 40 and 60 m.s^{-1} the values of surface roughness are almost the same. The worst quality of wood machining was reached at the sample with thermal treatment of 210 °C with cutting speed of 60 m.s^{-1}.

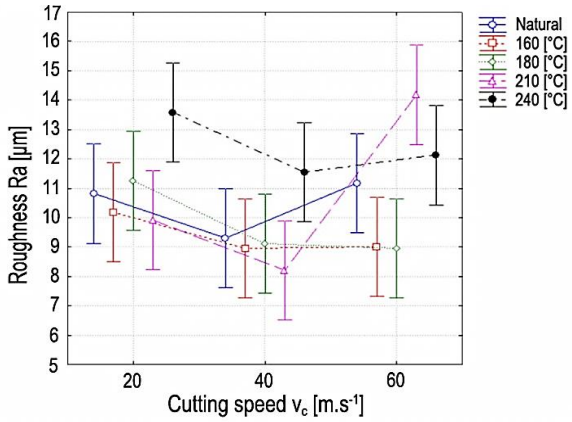

Fig. 8 Multifactor analysis of variance for the dependence of surface roughness on cutting speed
Obr. 8 Viacfaktorová analýza rozptylu závislosti drsnosti povrchu na reznej rýchlosti

Table 8 shows the variance and probability of similarity of dependence of surface roughness on cutting speed at different variants of rake angle, thermal treatment and feed rates of 6, 10 and 15 m.min^{-1}. Statistically important values are at feed rate of 10 m.min^{-1} at thermal treatment of 210 °C and at feed rate of 15 m.min^{-1} at native wood and heat treated wood at 210 °C.

Tab. 8 Basic statistical analysis of dependence of surface roughness on cutting speed at different variants of rake angle, thermal treatment and feed rates of 6, 10 and 15 m.min^{-1}
Tabuľka 8 Základná štatistická analýza závislosti drsnosti povrchu na reznej rýchlosti pri rôznych uhloch čela, termickej modifikácii a posuvných rýchlostiach 6, 10 a 15 m.min^{-1}

Feed speed v_f [m.min^{-1}]	Effect	SS	Degr. Of Freedom	MS	F	p
6	Native	31,608	4	7,902	1,36	0,273
	160 °C	30,929	4	7,732	0,47	0,756
	180 °C	12,020	4	3,005	1,09	0,383
	210 °C	207,520	4	51,880	1,71	0,177
	240 °C	67,854	4	16,963	1,47	0,239
10	Native	57,327	4	14,332	1,29	0,298
	160 °C	37,442	4	9,360	0,85	0,505
	180 °C	20,173	4	5,043	1,10	0,378
	210 °C	2392,780	4	598,195	11,07	0,000
	240 °C	78,340	4	19,585	0,66	0,626
15	Native	248,325	4	62,081	3,60	0,018
	160 °C	81,575	4	20,394	1,33	0,284
	180 °C	1,099	4	0,275	0,09	0,983
	210 °C	161,688	4	40,422	3,10	0,032
	240 °C	70,956	4	17,739	1,71	0,178

From worked out analysis it is visible, that with increasing cutting speed the surface roughness decreased. Different values are at the sample with thermal treatment of 210 °C, where with increasing cutting speed the surface roughness increased. A steady progress in dependence of surface roughness on cutting speed is displayed at thermal treatment of 180 °C, where at smallest cutting speed of 20 $m.s^{-1}$ and by its individual increasing the roughness of surface also decreased. The worst quality of surface was gained at thermal treatment of 210 °C and cutting speed of 60 $m.s^{-1}$. The best measured values were at untreated sample with cutting speed of 40 $m.s^{-1}$.

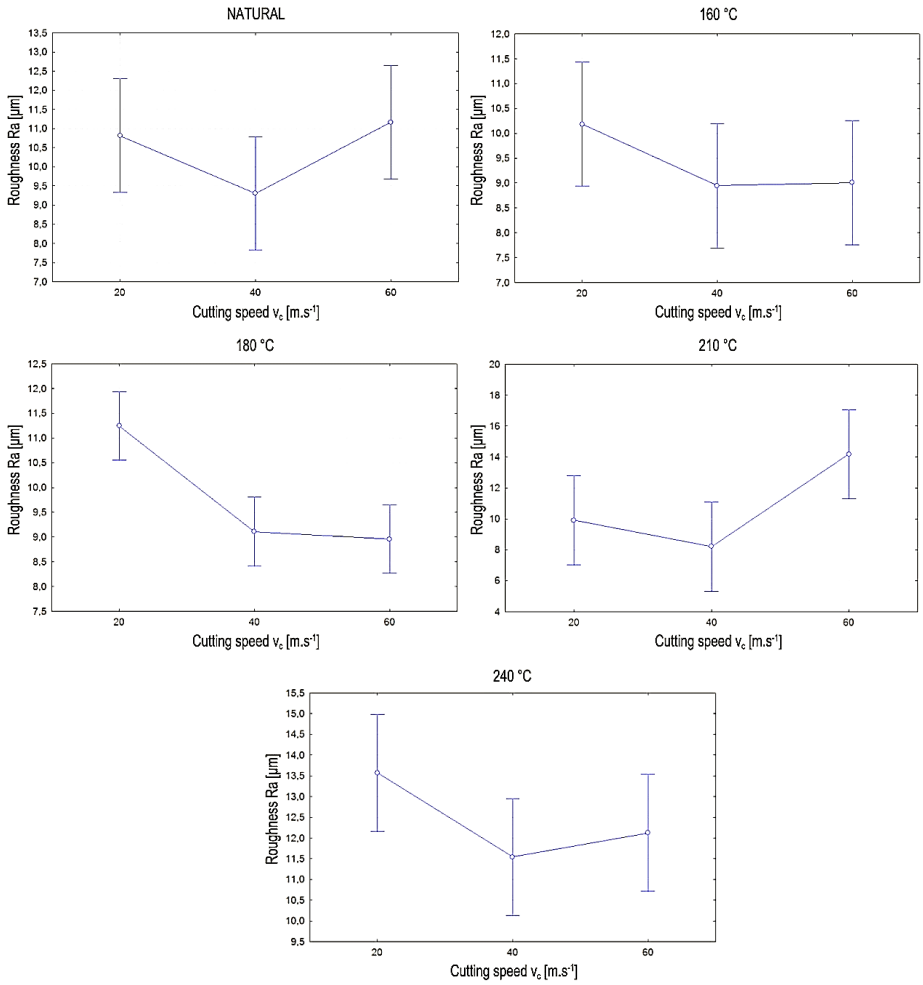

Fig. 9 Analysis of variance for the dependence of surface roughness on the cutting speed
Obr. 9 Analýza rozptylu závislosti drsnosti povrchu na reznej rýchlosti

On basis of experiments, which were published in this report, research was focused on dependence parameter – surface roughness, on independent technical and tool para-

meters after plain milling thermally modified and natural oak wood. With the same issue, which is roughness of thermally modified wood, it is possible to compare presented work with authors such as Kaplan et al. 2018 and Vančo et al. 2017, which in their works dealt with oak wood and beech wood. During their experiments authors evaluated roughness of surface by contact method (Kaplan et al., 2018) and by contactless method (Vančo et al., 2017). In the first and in the second report authors also confirmed a claim, that by influence of increasing feed rate the quality of wood machined surface is worsening and by increasing cutting speed the quality of machined surface is improving. Vančo had the same specified conditions and Kaplan was working in his experiments with different cutting speed and different feeding rate.

CONCLUSIONS

By experimental measuring it has been confirmed, that with gradual increase in feed rate the roughness of machined surface is increased. Whole progress of graphics was clear except for processes, where at heat treatment at 210 °C and 240 °C the adverse progress was observed. At feed rate of 10 $m.min^{-1}$ the biggest growth in roughness of machined surface always occurred.

On basis of experimental measuring of the samples the rule has been confirmed, that with increasing cutting speed the better quality finish with smaller roughness of surface can be reached. The rule has only confirmed itself with thermally treated samples at temperatures of 160 °C, 180 °C and 240 °C. With the others samples, which reached the opposite progress a problem could arise by improper machining the surface. The best quality value during surface wood machining was being reached with cutting speed of 40 $m.s^{-1}$.

REFERENCES

AYATA, U., GURLEYEN, L., ESTEVES, B., (2017). "EFFECT OF HEAT TREATMENT ON THE SURFACE OF SELECTED EXOTIC WOOD SPECIES" 60(199), 105-116, DOI: 10.12841/wood.1644-3985.198.08

BARCÍK, Š., GAŠPARÍK, M., (2014) "Effect of Tool and Milling Parameters on the Size Distribution of Splinters of Planed Native and Thermally Modified Beech Wood" *BioResources* 9(1), 1346-1360

BENDIKIENE, R.; KETURAKIS, G., (2016). "The effect of tool wear and planning parameters on birch wood surface roughness." *Wood research*. roč. 61, č. 5, s. 791-798. ISSN 1336-4561.

BENGTSOON, C., JERMER, J., CLANG, A., AND EK-OLAUSSON, B. (2003). "Investigation of Some Technical Properties of Heat-treated Wood," International Research Group on Wood Protection, Brisbane, Australia

GAFF, M., KVIETKOVÁ, M., GAŠPARÍK, M., KAPLAN, L., AND BARCÍK, Š. (2015). "Effect of selected parameters on the surface waviness in plane milling of thermally modified birch wood," *BioResources* 10(4), 7618-7626. DOI: 10.15376/biores.10.4.7618-7626

GANDELOVÁ, L., ŠLEZINGEROVÁ, J., HORÁČEK, P. 2009. Nauka o dřevě [Wood Science], Mendel University, Brno, Czech Republic, pp. 176.

HENDARTO, B.; SHAYAN, E.; OZARSKA, B.; CARR, R. "Analysis of roughness of a sanded wood surface." *The International Journal of Advanced Manufacturing Technology*. 2006, roč. 28, č. 7-8, s. 775-780. ISSN 1433-3015.

JEBRANE, M., POCKRANDT, M., CUCUI, I., ALLEGRETTI, O., UETIMANE, E., TERZIEV, N. (2018). "Comparative Study of Two Softwood Species Industrially Modified by Thermowood (R) and Thermo-Vacuum Process" *BioResources* 13(1), 715-728, DOI: 10.15376/biores.13.1.715-728

KAČÍKOVÁ, D., KAČÍK, F. 2011. Chemické a mechanické zmeny dreva při termickej úprave [Chemical and Mechanical Changes During Thermal Treatment of Wood], Technical University in Zvolen, Zvolen, Slovakia

KAPLAN, L., KVIETKOVÁ, MS., SIKORA, A., SEDLECKY, M. (2018). "Evaluation of the effect of individual paramaters of oak wood machining and their impact on the values of waviness measured by a laser profilometer" *WoodResearch* 63(1), 127-140

KVIETKOVÁ, M., GAŠPARÍK, M., GAFF, M. 2015. "Effect of thermal treatment on surface quality of beech wood after plane milling," BioResources 10(3), 4226-4238. DOI: 10.15376/biores.10.3.4226-4238

LISIČAN, J. et al. (1996). Teória a Technika Spracovania Dreva [Theory and technique of wood processing], Matcentrum, Zvolen (in Slovak).

POŽGAJ, A., CHOVANEC, D., KURJATKO, S., BABIAK, M. 1997. Štruktúra a Vlastnosti Dreva [Structure and Properties of Wood], Príroda a. s., Bratislava, Slovakia (in Slovak)

SEDLECKÝ, M. (2017). "Surface Roughness of Medium-Density Fiberboard (MDF) and Edge-Glued Panel (EGP) After Edge Milling" *BioResources* 12(4), 8119-8133, DOI: 10.15376/biores.12.4.8119-8133

SIKLIENKA, M., KMINIAK, R. 2013. Delenie a obrábanie dreva [Cutting and Wood Machining], Technical University in Zvolen, Zvolen, Slovakia

The paper was written within the projects: VEGA 1/0315/17 „Research of relevant properties of thermally modified wood at a contact effects in the machining process with the prediction of obtaining an optimal surface," and VEGA 1/0315/17 „Research of relevant properties of thermally modified wood at a contact effects in the machining process with the prediction of obtaining an optimal surface".

Corresponding author:
Michal Korčok, +421907 950 774, xkorcokm@is.tuzvo.sk

DEVELOPMENT OF PHOTOMETRIC AND SIZE CALIBRATION FACTORS FOR REAL-TIME AEROSOL MONITORING INSTRUMENT

STANOVENIE FOTOMETRICKÉHO A VEĽKOSTNÉHO KALIBRAČNÉHO FAKTORA PRE PRÍSTROJ NA MONITOROVANIE AEROSÓLOV V REÁLNOM ČASE

Lucia Mikušová, Miroslav Dado

Faculty of Environmental and Manufacturing Technology, Technical University in Zvolen, Študentská 26, 960 53 Zvolen. Slovak republic. E-mail: lulumikusova@gmail.com, dado@tuzvo.sk

ABSTRACT: DustTrak™ DRX aerosol monitor combines a photometric measurement to cover the mass concentration range and a single particle detection measurement to be able to size discriminate the sampled aerosol. To improve the accuracy of the mass concentration measurement, the instrument can be calibrated with gravimetric sample by conducting side-by-side comparisons. The goal of this study was to investigate the relationship between sanding dust mass concentrations recorded by DustTrak™ DRX aerosol monitor and sanding dust mass concentrations measured by the standard gravimetric method using IOM sampler. Results of this study indicate that it is reasonable to determine a both calibration factors. If size calibration factor is not determined, monitor will assign particles an incorrect size, which result in incorrect size segregated mass concentrations.

Key words: aerosol monitor, calibration factors, sanding, dust, beech

ABSTRAKT: Monitor aerosólu DustTrak™ DRX kombinuje fotometrické meranie pre zistenie rozsahu hmotnostnej koncentrácie a detekciu jednotlivých častíc tak, aby bol schopný rozlišovať veľkostnú distribúciu vzorky aerosólu. Z dôvodu zlepšenia presnosti merania hmotnostnej koncentrácie, prístroj je možné kalibrovať na základe porovnania s gravimetrickou vzorkou. Cieľom tejto štúdie bolo zistiť vzťah medzi hmotnostnou koncentráciou brúsneho prachu nameranej pomocou monitora aerosólu DustTrak™ DRX a štandardnou gravimetrickou metódou pomocou IOM vzorkovača za účelom stanovenia fotometrického a veľkostného kalibračného faktora. Výsledky tejto štúdie indikujú, že je potrebné určiť obidva kalibračné faktory. Ak nie je stanovený veľkostný kalibračný faktor, monitor priradí časticiam nesprávnu veľkosť, čo vedie k nekorektnej segregácii hmotnostnej koncentrácie z hľadiska distribučného rozdelenia častíc.

Kľúčové slová: aerosól monitor, kalibračné faktory, brúsenie, prach, buk

INTRODUCTION

At present, several measuring instruments are commercially available which enable real-time determination of the mass concentration or size distribution of solid aerosols in

the working atmosphere. Most of them work on one of the following principles – optical, electrical, mechanical, molecular and nuclear (Vincent 2007).

Photometers are portable real-time instruments for the measurement at high temporal resolution of mass concentration of particulate matter (PM). These instruments have in common that they are optical instruments that use a sheet of laser light formed from a laser diode and light-scattering by the cloud of particles detected in the chamber by a photo detector. Their accuracy is impacted by the fact that every light-scattering measurement is sensitive to particle size distribution, shape and composition (including density) as scattering per unit mass is a strong function of particle size and refractive index (Hinds 1999).

DustTrak DRX aerosol monitor differs from other photometers in that sense that it combines the photometric measurement of the group of particles in the measurement chamber with the optical sizing of single particles in one optical system, thus reporting concentrations for different size fractions (Wang et al. 2009). Relationship between gravimetric mass and DustTrak DRX measurements would not be consistent across environments affected by very different sources. For consistent biases, a statistical adjustment with an on-site photometric correction factor (PCF) obtained by comparison with the reference gravimetric measurements can be used to correct concentrations. This is actually recommended by the manufacturer as the factory calibration made with the standard ISO 12103–1, A1 test dust ("Arizona Road Dust") is only representative for PM of very similar properties (TSI Inc. 2014). For this reason the DustTrak DRX is fitted with a 37-mm filter cassette in-line with the aerosol flow, allowing for a gravimetric analysis of the same aerosol as measured optically (Rivas et al. 2017).

The objective of the experimental measurements is to determine the adequate value of the calibration factor for beech dust from the sanding process and to compare differences in the response of the monitor using different values of the photometric and size calibration factors.

MATERIAL AND METHODS

The DustTrak DRX aerosol monitor uses the principle of light scattering and combines the functions of two types of measuring instruments the photometer and the optical particle counter. The principle of the monitor's operation is illustrated in Fig. 1. According to the manufacturer's technical specification (TSI Inc. 2017), the device can determine a mass concentration of aerosol in the range of 0,001 $mg.m^{-3}$ to 150 $mg.m^{-3}$ for particles in the range 0,1 μm to 15 μm simultaneously in the PM1, PM2,5, PM4, PM10 and TSP fractions.

Experimental measurements were carried out in a homemade dust chamber sized 1180 mm x 520 mm x 760 mm (w x l x h). Dust was introduced manually into the chamber through entrance pipe and its dispersion into the dust chamber was provided by the fan (Fig. 2). Temperature and air humidity in the dust chamber were not regulated, but during the experiment they reached a relatively constant value in the range of 22-23 °C, respectively 35-36%. The average airflow rate in the dust chamber was determined in the range of values ranging from 0,17 $m.s^{-1}$ to 0,2 $m.s^{-1}$ using a thermo-anemometer (Testo 480, Testo).

The tested dust was produced in laboratory by sanding a plank of beech using an orbital sander (PSS 250 AE, Bosch) fitted with 80 grade sanding paper.

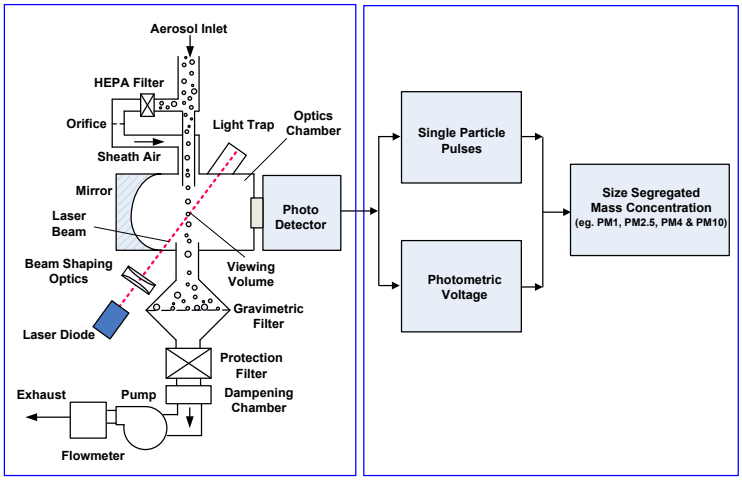

Fig. 1 DustTrak DRX – principle of operation (TSI Inc. 2012)
Obr. 1 DustTrak DRX – princíp činnosti (TSI Inc. 2012)

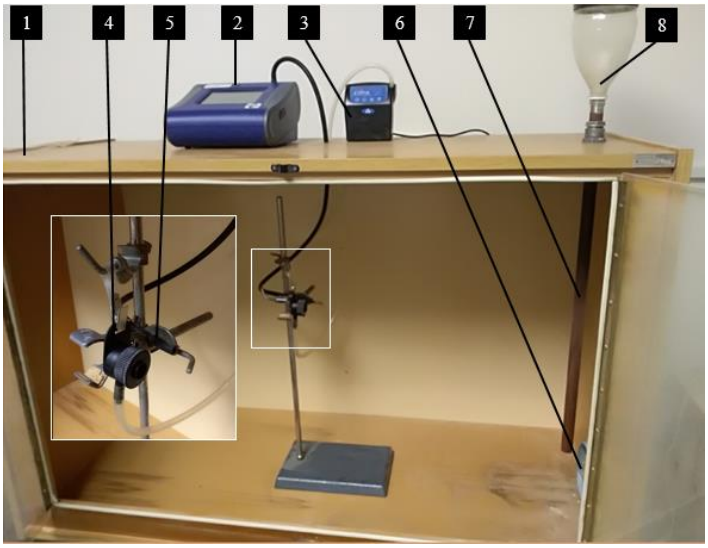

Fig. 2 Calibration dust chamber
1 – dust chamber, 2 – aerosol monitor, 3 – flow pump, 4 – IOM sampler,
5 – conductive tubing, 6 – fan, 7 – inlet tube, 8 – dust tray
Obr. 2 Kalibračná prachová komora
1– prachová komora, 2 – monitor aerosólu, 3 – prietokové čerpadlo, 4 – IOM vzorkovač,
5 – hadička, 6 – ventilátor, 7 – prívodná rúrka, 8 – zásobník prachu

Reference values of the mass concentration of dust were determined by the gravimetric method. Sampler for the inhalable fraction (IOM, SKC) was connected by tygon tubing to the flow pump (L-4, A. P. Buck), which was set to an airflow rate of 2 l min $^{-1}$. The indicated flow rate was before and after each sampling checked by a rotameter (320-4A5, SKC). Glass fibre filters of 25 mm diameter (GF 50 025, Albet) were pre-conditioned for at least 12 hours in the desiccator and weighed on analytical scales (XA 110, Radwag). Sampling time was 10 minutes.

To determine photometric calibration factor we used preweighed 37 mm gravimetric filter cassette loaded into DustTrak DRX monitor. Filter cassette was loaded with glass fibre filters (GF 50 027, Albet), which were conditioned and weighed on analytical scales (XA 110, Radwag) before and after exposure. The flow rate used to compute the mass concentration was 2 l min^{-1}. Sampling time was 5 minutes. Before each measurement, zero aerosol monitor calibration was performed.

To determine the size calibration factor (SCF), the procedure that the manufacturer directly programmed into the monitor was used: after selecting the *Size Correction* feature, the device automatically activated the sampling of the tested aerosol for 120 seconds. Subsequently, the PM2.5 impactor was installed and the instrument re-activated sampling for 120 seconds. Upon sampling, the device automatically calculates the SCF value.

RESULTS

Comparing the monitor response (set values of PCF = SCF = 1) to wood dust with the result of gravimetric analysis is shown in Fig. 3. The inverse value of the regression coefficient (regression line directive) is the average value of the calibration factor.

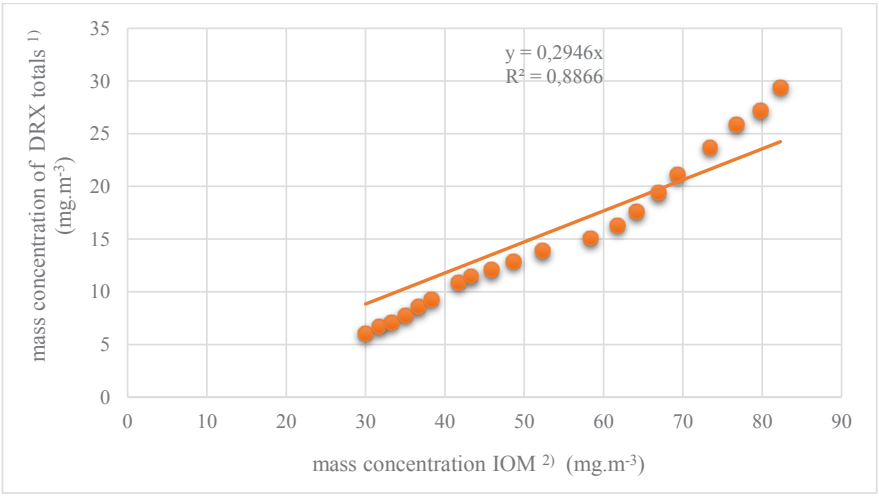

Fig. 3 The monitor response (PCF = SCF = 1) to the mass concentration of the inhalable fraction determined by the reference method

Obr. 3 Odozva monitoru (PCF=SCF=1) k hmotnostnej koncentrácii vdychovateľnej frakcie stanovenej referenčnou metódou

[1)] hmotnostná koncentrácia DRX celk., [2)] hmotnostná koncentrácia IOM

The results of determination the photometric calibration factor and the size calibration factor of aerosol monitor are given in Table 1.

Table 1. The results of determining the PCF and SCF
Tabuľka 1. Výsledky stanovenia PCF a SCF

	Number of Measurements *n*	Arithmetic Mean $\bar{x}$	Standard Deviation *SD*	Coefficient of Variation *CV (%)*
PCF	15	13.913	3.675	28.5
SCF	15	0.718	0.183	31.7

Comparing the monitor response (PCF = 13.913; SCF = 0.718) to wood dust with the result of gravimetric analysis is shown in Fig. 4.

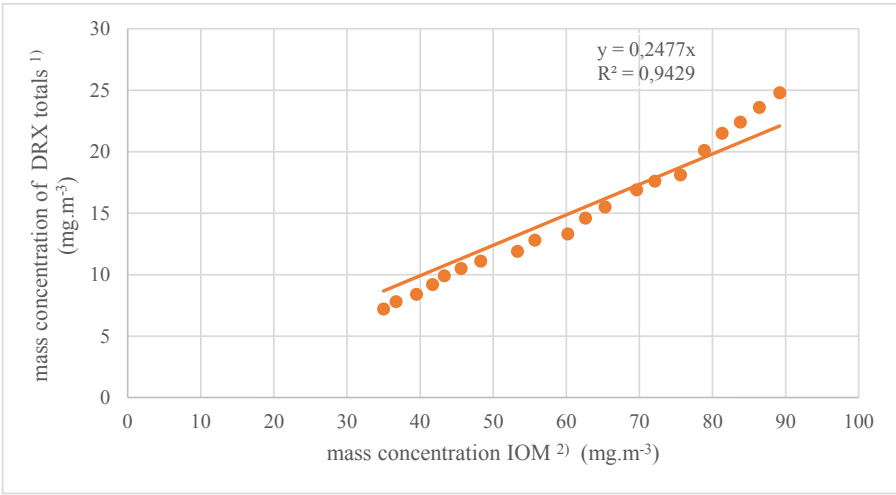

Fig. 4 The monitor response (PCF = 13.913; SCF = 0.718) versus the mass concentration of the inhalable fraction determined by the reference method
Obr. 4 Odozva monitoru (PCF=13,913; SCF=0,718) verzus hmotnostná koncentrácia vdychovateľnej frakcie stanovená referenčnou metódou
[1)] hmotnostná koncentrácia DRX celk., [2)] hmotnostná koncentrácia IOM

DISCUSSION AND CONCLUSION

The real-time measurement of mass concentration of solid aerosols is influenced by several factors and the correct calibration of the measuring instrument is a prerequisite for obtaining rational data (Lukáčová et al. 2009; Bodnárová & Lukáčová 2012; Lukáčová et. al 2014). In order to obtain an accurate measure of airborne particle concentration, the aerosol monitor should always be compared to a reference gravimetric dust sampler placed alongside and adjusted accordingly. Unless they are properly calibrated for the aerosol

being measured, photometers can significantly overestimate or underestimate the "true" concentration of the respirable fraction of aerosol (CEN 2012).

There have been various studies on determining correction factors for numerous photometer-type dust monitors. Torpe (2007) investigated the performance of five portable direct-reading dust monitors in a wind tunel for a range of industrial dusts to mainly determine their suitability for measuring the inhalable fraction of airborne dust in workplaces. The instruments tested were Split 2 (SKC Ltd), Sidepak (TSI Inc.), Dataram (Thermo Electron Ltd), PDS-2 (Sibata Scientific Technology Ltd) and Respicon (Hund Ltd). The instruments's responses were compared with reference dust samplers. These were the IOM sampler for the inhalable fraction and the Casella cyclon sampler for the respirable fraction. Each monitor greatly understimated the measurement of inhalable concentration for all the dust tested, although the linearity was good over a wide range of concentrations for any particular size distribution of dust. However, their calibration factors, defined as the ratio of reference inhalable concentration to monitor concentration, were especially sensitive to changes in particle size as the response of the instruments decreased rapidly with increasing particle size. The monitors generally overestimated the measurement of respirable dust concentration by up to a factor of about 2, apart from the PDS-2, which understimated it by a factor of up to 3.

Thorpe and Walsh (2013) assessed how these dust monitors behave when challenged with airborne dust containing particles in the inhalable size range and also to investigate alternative dust monitors whose response might not be as prone to variations in particle size or that could be adapted to measure inhalable dust concentration. Several photometer--type dust monitors and a Respicon, tapered element oscillating microbalance (TEOM) personal dust monitor (PDM) 3600, TEOM 1400, and Dustrak DRX were assessed for the measurement of airborne inhalable dust during laboratory and field trials. Laboratory results showed that the Respicon, modified PDM, and TEOM 1400 observed good linearity for all types of dust when compared with measurements made with a reference IOM sampler; the photometer-type dust monitors on the other hand showed little correlation. The Respicon also accurately measured the inhalable concentration, whereas the modified PDM underestimated it by ~27%. Photometer responses varied considerably with changing particle size, which resulted in appreciable errors in airborne inhalable dust concentration measurements. Similar trends were also observed during field trials.

Wang et al. (2016) used several real-time and filter-based aerosol instruments to measure PM2.5 levels in a high-rise residential green building in the Northeastern US and compared performance of those instruments. Results of this study suggest that accuracy of aerosol mass concentrations from direct-reading instruments in indoor environments depends on the instrument, and that correction factors can be used to reduce biases of these real-time monitors in residential green buildings with similar aerosol properties.

Dado et al. (2017) conducted controlled experiments to compare the performance of two photometer-based direct-reading aerosol monitors (Microdust Pro CEL 712 and HAZ--DUST IV) with gravimetric reference sampler positioned alongside, based on determination of the correction factor. Both monitors showed good linearity when compared with reference IOM respirable concentration, indicated by high coefficient of determination

values. Results of this study confirmed that determining of correction factor should be an essential part of any aerosol photometer using.

Pahler et al. (2018) investigated the relationship between particulate matter (PM) concentrations recorded by real-time monitors and respirable crystalline silica, in the form of quartz, (RCS) concentrations measured by the standard NIOSH 7500 method using an aluminum cyclone attached to a filter-cassette. Two DustTrak DRX monitors were used to collect area samples of PM1, PM2.5, PM4, PM10 and PMtotal, and two SidePak AM510 monitors were used to collect personal samples of PM2.5. Calculated r-squared (R^2) values analyzed how well paired data from real-time monitors and filter-based methods fit a line of regression, and how well real-time monitor measurements predicted RCS concentrations. Results of this study indicate that it is reasonable to determine a calibration factor for DRX direct-read monitors, enabling them to estimate concentrations of RCS in real-time.

Results of this study are consistent with above mentioned results of previous studies. When measuring the mass concentration of the beech sanding dust through the DustTrak DRX aerosol monitor, there is a reasonable assumption that by determining the appropriate photometric and size calibration factor increases the accuracy of the measurement. Contrary to expectations, based on the comparison of the experimentally determined average values of the calibration factors (see Fig. 3 – CF = 3,394 and Fig. 4 – CF = 4,037), the above assumption was not fulfilled. We think there are several possible reasons. It is most important to consider the fact that, in determining the average values of the calibration factors, the inhalable fraction of the aerosol, which the monitor obviously underestimates, was evaluated in the reference method.

Based on of the experience gained, we plan to assess the respirable aerosol fraction in the following experiments in determining the average values of the calibration factors within the reference method and sieve analysis to determine the particle size distribution of the tested wood dust.

REFERENCES

BODNÁROVÁ, A., LUKÁČOVÁ, K. 2012. Porovnanie vybraných zariadení pre odber respirabilnej frakcie pevných aerosólov. In *Fyzikálne faktory prostredia*. Roč. 2, č. Október (2012), s. 69-72.

CEN/TR 16013-3:2012. *Workplace exposure. Guide for the use of direct-reading instruments for aerosol monitoring*. Part 3: Evaluation of airborne particle concentrations using photometers.

DADO, M., MIKUŠOVÁ, L., HNILICA, R., OČKAJOVÁ, A. 2017. *Calibration of Photometer--Based Direct-Reading aerosol Monitors.* MM Science Journal 2017. Dostupné na: http://www.mmscience.eu/content/file/archives/MM_Science_201788.pdf

HINDS, W.C., 1999. *Aerosol Technology: Properties, Behavior, and Measurement of Air-borne Particles*. Second ed. John Wiley & Sons, New York. Dostupné na: https://www.amazon.com/Aerosol-Technology-Properties-Measurement-Particles/dp/0471194107#reader_0471194107

LUKÁČOVÁ, K., BADIDA, M., LUMNITZER, E., LIPTAI, P. 2009. Concentration of solid aerosols in working environment. In *Proceedings from MMA 2009* , *Novi Sad, 9.-10.10.2009*. Novi Sad : FTS, 2009, pp. 262-265. ISBN 9788678922237.

LUKÁČOVÁ, K., LIPTAI, P., LUMNITZER, E., MORAVEC, M. 2014. Possibilities of utilization of equipment using ir principles for monitoring solid aerosols in real conditions. In *Proceedings from SGEM 2014,17-26, June, 2014, Albena, Bulgaria*. Sofia : STEF92 Technology, 2014, pp. 515-518. ISBN 978-619-7105-17-9.

PAHLER, L.F., MCKENZIE-SMITH, D.D., HANDY, R.G., SLEETH, D.K. 2018. *Development of custom calibration factors for respirable silica using standard methods compared to photometric monitoring data.* Journal of Chemical Health and Safety Volume 25, Issue 1, January–February 2018, pp. 27-35.

RIVAS, I., et al.. 2017. *Identification of technical problems affecting performance of DustTrak DRX aerosol monitors*. Science of the Total Environment (2017). Dostupné na: http://dx.doi.org/10.1016/j.scitotenv.2017.01.129.

Thorpe, A. 2007. *Assessment of personal direct-reading dust monitors for the measurement of airborne inhalable dust*. Annals of Occupational Hygiene, 2007, Vol. 51(1), pp 97-112.

Thorpe, A. and Walsh, P. T. 2013. *Direct-Reading Inhalable Dust Monitzoring – An Assessment of Current Measurement Methods*. Annals of Occupational Hygiene, 2013, Vol. 57, No. 7, pp 824-841.

TSI Incorporated, 2012. DustTrak™ DRX aerosol monitor theory of operation. Application note EXPMN-002. Dostupné na: http://www.tsi.com/uploadedFiles/_Site_Root/Products/Literature/Application_Notes/EXPMN-002_DustTrak_DRX_Theory_of_Operation.pdf

TSI Incorporated, 2014. DustTrak™ DRX aerosol monitor*. Operation and Service Manual, DustTrak DRX Aerosol Monitor, Revision L, P/N 6001898.* Dostupné n: https://www.manualslib.com/manual/1218827/Tsi-Incorporated-Dusttrak-Drx-8533.html?page=2#manual

TSI Incorporated, 2017. DustTrak™ DRX aerosol monitor. Operation and Service Manual. P/N 6001898, Revision M. Dostupné na:
http://www.tsi.com/uploadedFiles/_Site_Root/Products/Literature/Manuals/8533-8534-DustTrak_DRX-6001898-web.pdf

VINCENT, J. H. 2007. *Aerosol Sampling: Science, Standards, Instrumentation and Application.* John Willey & Sons, 636 p., ISBN 978-0-470-02725-7.

WANG, X., HASE, A., OLSON, G., SREENATH, A., AGARWAL, J. 2009. Response of the DustTrak DRX to Aerosols of Different Materials. Dostupné na: http://www.gaef.de/eac2009/EAC2009abstracts/T09%20Instrumentation/T092A06.pdf

WANG, Z., CALDERÓN, L., PATTON, A.P., SORENSEN ALACCI, M., SENICK, J., WENER, R., ANDREWS C.J., MAINELIS, G. 2016. Comparison of real-time instruments and gravimetric method when measuring particulate matter in a residential building. J Air Waste Manag Assoc. 2016 Nov;66(11):1109-1120.

This paper is based on work performed under research contracts KEGA 008TU Z-4/2016 which support is gratefully acknowledged.

Corresponding author:
Ing. Lucia Mikušová, tel. – 045 52 0**6 026**, e-mail: lulumikusova@gmail.com

EFFECT OF TECHNOLOGICAL, MATERIAL AND TOOL FACTORS ON THE QUALITY OF FINISHED SURFACE WHEN PLANE MILLING OF THERMALLY TREATED SESSILE OAK WOOD

VPLYV TECHNOLOGICKÝCH, MATERIÁLOVÝCH A NÁSTROJOVÝCH FAKTOROV NA KVALITU OBROBENEJ PLOCHY PO FRÉZOVANÍ TEPELNE MOFIFIKOVANÉHO DUBOVÉHO DREVA

Marek Vančo, Michal Korčok, Peter Koleda, Štefan Barcík

Technical University in Zvolen, Faculty of Environmental and Manufacturing Technology, Department of Manufacturing and Automation Technology, 26 Studentska str., 960 53 Zvolen, Slovak Republic

ABSTRACT: The paper deals with the experimental examination of the temperature influence of heat treated sessile oak (*Quercus petraea*) wood in terms of quality of the machined surface as well as with the analysis of the impact of monitored independent parameters: cutting speed, feed rate, material, angular geometry of the tool, on dependent parameters representing machined surface quality (Ra - mean arithmetic roughness, Rz - maximum roughness) when plane milling of thermally modified oak wood (T = 160, 180, 200 and 220 °C), and their comparison with native wood. The roughness measurement was carried out by non-contact method. Based on experimental measurements, the effect of the observed factors on surface quality was determined in this order: thermal modification, cutting speed, feed speed, rake angle.

Key words: surface roughness, plane milling, ThermoWood®, quality of machining

ABSTRAKT: Tento príspevok sa zaoberá experimentálnym skúmaním vplyvu teploty tepelne upraveného dubového dreva z pohľadu kvality obrobeného povrchu, ako aj analýzou vplyvu sledovaných nezávislých parametrov: rezná rýchlosť, rýchlosť posuvu, materiál, uhlová geometria nástroja, na závislé parametre reprezentujúce kvalitu opracovania povrchu (Ra – stredná aritmetická drsnosť, Rz – maximálna drsnosť,) pri rovinnom frézovaní tepelne upraveného (T = 160, 180, 200 a 220 °C) dubového dreva a ich porovnanie s natívnym drevom. Meranie drsnosti bolo realizované bezkontaktnou metódou. Na základe experimentálnych meraní bol zistený vplyv sledovaných faktorov na kvalitu povrchu v tomto poradí: tepelná úprava, rezná rýchlosť, rýchlosť posuvu, uhol čela.

Kľúčové slová: Drsnosť povrchu, rovinné frézovanie, ThermoWood®, kvalita opracovania

INTRODUCTION

At present research of wood utilization is focused on different species of wood for the heat treatment process. Heat-treated wood can be machined with the same technical and technological procedures as natural wood (Janda et al. 2013). Recently, the interest in heat treated wood, which has been used in different areas, has increased. The increase in consumption of heat treated wood is also related to its subsequent machining and the related surface quality problems (Lisičan et al., 1996; Požgaj et al. 1997; Siklienka et al., 2013).

One of the main tasks of thermal modification is to increase the resistance of less durable woods to various biological and abiotic factors (Niemz et al., 2010). The issues of pricing of the treated wood and the eco-toxicology are equally important - so that the heat-treated wood does not load the environment more than natural wood (Boonstra et al., 2007; Horáček et al., 1998; Kačíková at al. 2011; Reinprecht et al. 2007; Sikora et al., 2018). Unlike chemical protection, wood is not treated with a toxic biocide, what is particularly important from an ecological point of view. On the basis of these facts, the heat protection of wood is more widely used in practice (Bekhta et al. 2003).

This paper deals with research of the influence of selected factors (temperature of heat treatment, cutting speed, feed rate, angular geometry of tool) on the quality of machined surface when flat milling of heat treated wood with the aim of pointing out the difference between the heat treated and the natural, thermally untreated material.

MATERIAL AND METHODS

As a material for the samples the log of *Quercus petraea* was used from Vlčí járok locality (Budča), 440 m a.s.l. The boards 25 mm thick were made from logs according to Fig. 1. This operation was carried out using the MEBOR HZT 1000 band saw band (Mebor d.o.o., Železniki, Slovenia).

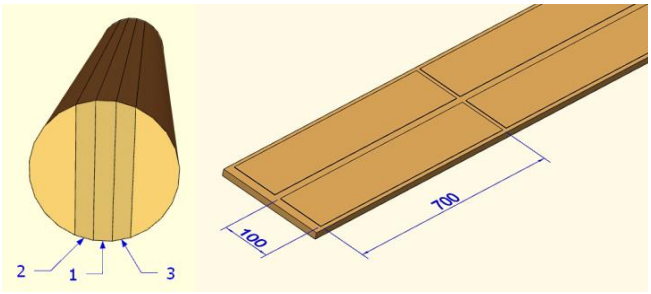

Fig. 1 Sample preparation
Obr. 1 Príprava vzoriek

The final sample sizes were 700 mm long, 100 mm wide and 20 mm thick. One set of samples (10pcs) was not heat treated while remaining in the natural state. The other four sets of samples were designed for heat treatment that was carried out at Arboretum FLD

(ČZU Praha) in Kostelec nad Černými lesy using the S400/03 chamber (LAC Ltd., Czech Republic), which is intended for heat treatment of wood by ThermoWood technology. The heat treatment process was computer controlled using the program by Katres spol. Ltd.

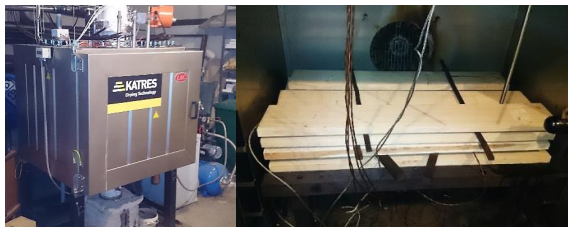

Fig. 2 Chamber S400/03 and samples prepared for thermal modification
Obr. 2 Komora S400/03 a pripravené vzorky na tepelnú úpravu

The time duration and temperature course of heat treatment are displayed in the fig. 3. After heat treatment, the samples were packaged in plastic film to minimize environmental impact.

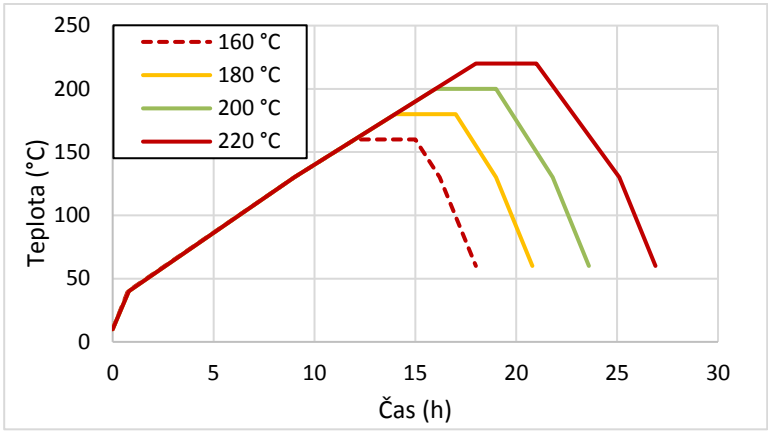

Fig. 3 Graphical representation of thermal modification
Obr. 3 Grafické zobrazenie tepelnej úpravy

All of the experimental millings were performed at a workshop at the Technical University in Zvolen, Slovakia by means of a lower spindle milling machine (Model FVS, Czechoslovakia Music Instruments, Hradec Králové, Czech Republic, 1976) and feeding mechanism (ZMD 252 / 137, Frommia, Fellbach, Germany, 1972) with the technical parameters that are shown in the Table 1.

Fig. 4 Lower spindle milling machine FVS and feeder Frommia ZMD 252/137
Obr. 4 Spodná vretenová frézka FVS s podávacím zariadením Frommia ZMD 252/137

Table 1 Technical parameters of FVS miller and feeder Frommia ZMD 252/137
Tabuľka 1 Technické parametre frézky FVS a podávacieho zariadenia Frommia ZMD 252/137

FVS	
Input power[1)] [kW]	4
Voltage system[2)] [V]	360/220
Frequency[3)] [Hz]	50
Year[4)]	1976

ZMD 252/137	
Feed range[5)] [m.min^{-1}]	2,5;10;15;20;30
Engine[6)]	380 V; 2800 min^{-1}
Year[4)]	1972

[1)]Príkon, [2)]Napäťový systém, [3)]Frekvencia, [4)]Rok, [5)]Rozsah posuvu, [6)]Motor

The change of cutting speed was realised by frequency converter UNIFREM 400 VONSCH s r. o., Brezno, Slovensko). Revolutions for each cutting speed were determined according to equation [1] and measured by speedometer DT-1236L (Lutron Electronics Inc., Coopersburg, USA).

$$n = \frac{v_c \cdot 1000}{\pi \cdot D} \ [\text{min}^{-1}] \tag{1}$$

v_c – cutting speed [m.s^{-1}], D – cutter head diameter [mm]

Miller heads for wood FH 45 Staton (SZT machines Turany, Slovakia) were used in experiments (Table 2).

Table 2 Parameter of used milling heads
Tabuľka 2 Parametre použitých frézovacích hláv

Diameter of the milling head body[1)] [mm]	125
Diameter of the milling head body with knives[2)] [mm]	130
Thickness of the milling head body[3)] [mm]	45
Number of knives[4)]	2
Rake angle[5)] [°]	γ = 15, 25, 30

[1)]Priemer tela frézy, [2)]Priemer tela frézy s nožmi, [3)]Hrúbka tela frézy, [4)]Počet nožov, [5)]Uhol čela

Fig. 5 Used milling heads
Obr. 5 Použité frézovacie hlavy

A double-bladed wood cutter with a rake angle (γ) of 15°, 20°, and 30° and interchangeable blades was used as the cutting tool for plane milling with a cutting depth of 1 mm (Fig. 5). The geometry of the cutting tool and the cutting conditions were the same as those used by Koleda et al. (2018), which were a cutting speed of 20 m/s, 40 m/s, and 60 m/s and a feed rate of 6 m/min, 10 m/min, and 15 m/min.

Table 3 Cutting conditions of experimental milling
Tabuľka 3 Rezné podmienky experimentálneho frézovania

Parameter		**Value**[8)]
Feed rate[1)] [m.min^{-1}]		6, 10, 15
Cutting speed[2)] [m.s^{-1}]		20, 40 , 60
Tool geometry[3)] [°]	Rake angle[6)]	γ =15; 25; 30
	Wedge angle[7)]	B = 45; 20; 10
Depth of cut[4)] [mm]		1
Temperature of thermal modification[5)] [°C]		N, 160, 180, 200, 220

[1)]Podávacia rýchlosť, [2)]Rezná rýchlosť, [3)]Geometria nástroja, [4)]Hĺbka rezu, [5)]Teplota termickej modifikácie, [6)]Uhol čela, [7)]Uhol chrbta, [8)]Hodnota

The surface roughness was measured using an LPM-4 laser profilometer (KVANT Ltd., Slovak Republic) (Fig. 6), and the basic parameters are given in Table 4. The measured values were processed and displayed on a computer using the LPMView 1.2 measuring software (KVANT Ltd., Slovak Republic) (Šustek, 2010). The evaluation of surface roughenss was carried out according to ISO 4287. Subsequently, the data was processed with STATISTICA 10 software (StatSoft CR s.r.o., Prague, Czech Republic). Using this program, the resulting graphs and dependencies were generated via a single-factor and multifactor analysis of variance (ANOVA).

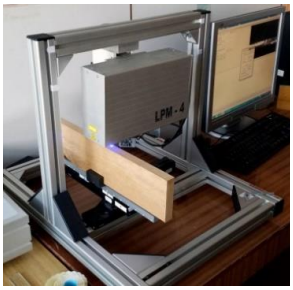

Fig. 6 Profilometer LPM – 4
Obr. 6 Profilometer LPM – 4

Table 4 Parameters of profilometer LPM – 4
Tabuľka 4 Parametre laserového profilometra LPM – 4

Measurement range in axis z (vertical)[1)] [mm]	420 – 470
Measurement range in axis y[2)] [mm]	± 0,15
Measurement range in axis x[3)] (transversal) [mm]	200
Number od samples in axis x [4)]	1350
Processing speed[5)] [prof.s^{-1}]	25
Type of laser diode[6)] [nm.mW^{-1}]	660/25
Scattering angle of laser[7)] [°]	30
Roughness parameters[8)]	Rp, Rv, Rz, Ra, Rq, Rc
Waviness parameters[9)]	Wp, Wv, Wz, Wa, Wq, Wc

[1)]Rozsah merania v osi z, [2)]Rozsah merania v osi y, [3)]Rozsah merania v osi x, [4)]Počet vzoriek v osi x, [5)]Rýchlosť spracovania, [6)]Typ laserovej diódy, [7)]Rozptyľový uhol, [8)]Parametre drsnosti, [9)]Parametre vlnitosti

RESULTS

The table below (Table 5) shows the measured density values according to STN 49 0108 for natural and heat treated samples, comparing the decrease in volume weight to natural samples.

Table 5 Measured values of density
Tabuľka 5 Namerané hodnoty hustoty

Sample[1)]	Density[2)] [kg.m^{-3}]	Change to Nat.[3)] [%]
Native[4)]	775,85	–
160	719,73	7,23
180	687,39	11,40
200	617,84	20,37
220	608,96	21,51

[1)]Vzorka, [2)]Hustota, [3)]Zmena k natívnemu, [4)]Natívne

In thermally treated samples, it was assumed that by increasing the temperature of the heat treatment, the density of wood is reduced. The not treated sample had a density of 775,85 kg.m^{-3}. At the temperature of 160 °C, the density dropped of 7,23 %, and the density of sample treated at 220 °C dropped of 21.51 % to the value of 608,96 kg.m^{-3}.

Effect of thermal treatment

The Fig. 7 represents the results measured for the impact of wood heat treatment on the resulting surface quality.

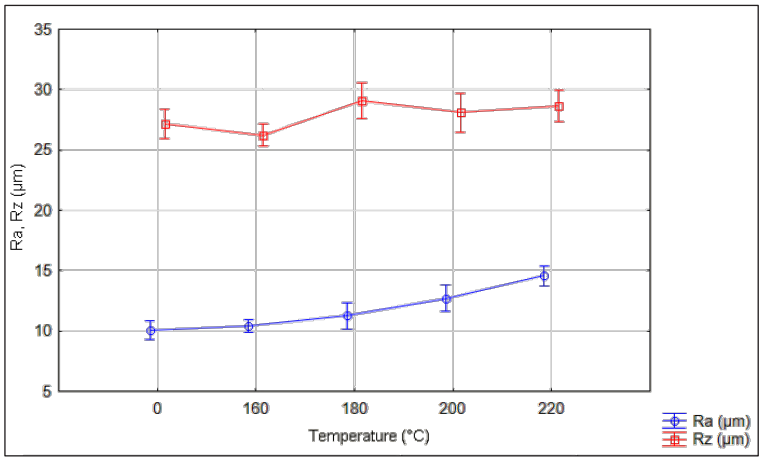

Fig. 7 Dependence of surface roughness on heat treatment of wood
Obr. 7 Závislosť drsnosti povrchu od tepelnej úpravy dreva

The increase in surface roughness was confirmed at the increasing temperature of the heat treatment of the samples, where the best surface quality was achieved at 160 °C (average Ra = 10,44 µm) and the worst surface quality at 220 °C (average Ra = 14,58 µm).

Effect of angular geometry

The Fig. 8 shows the analysis of variance for surface roughness (Ra and Rz) depending on the rake angle. It is clear that with the increasing rake angle, the surface quality improves, but this was not confirmed by the tool with the rake angle of 30°, with a thermal treatment at 200 °C, where a roughness increase was measured.

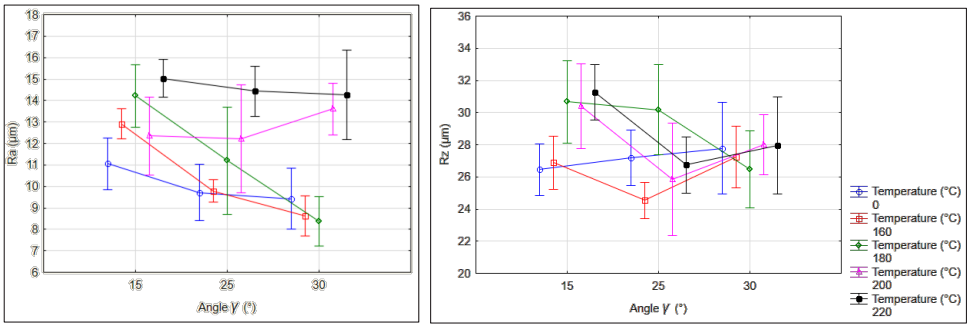

Fig. 8 Multifactor analysis of the influence of angular geometry on surface roughness
Obr. 8 Viacfaktorová analýza vplyvu uhlovej geometrie nástroja na drsnosť

For the angular geometry γ = 15°, the best results were obtained for the untreated sample (average Ra = 11,06 µm, Rz = 26,46 µm) and for the sample treated at 200 °C (average Ra = 12,35 µm, Rz = 30,38 µm). The worst results were obtained at 220 °C (average Ra = 15,04 µm, Rz = 31,08 µm). For the angular geometry γ = 25°, the best surface roughness values were measured at the untreated sample (average Ra = 9,71 µm, Rz = 27,2 µm) and at the sample treated at 160 °C (average Ra = 9, 79 µm, Rz 24,53 µm). The worst results were found in the heat-treated sample at 220 °C (average Ra = 14,43 µm, Rz = 26,74 µm). For rake angle γ = 30°, the best surface roughness values were measured at 180 °C (average Ra = 8,37 µm, Rz = 26,46 µm) and at temperature of 160 °C (average Ra = 8,62 µm, Rz = 27,25 µm). In this case, the worst results were also obtained at 220 °C (average Ra = 14,26 µm, Rz = 27,95 µm).

The table 6 shows the results of the weighted average values of surface roughness depending on the angular geometry of the tool. The minimal average Ra was measured at the angle of 30°, minimal Rz at 25°.

Table 6 Weighted means – effect of angular geometry
Tabuľka 6 Vážené priemery – vplyv uhlovej geometrie

γ (°)	Ra [µm] Average[1)]	Ra [µm] St. dev.	Ra [µm] -95,00%	Ra [µm] +95,00%	Rz [µm] Average[1)]	Rz [µm] St. dev.[2)]	Rz [µm] -95,00%	Rz [µm] +95,00%	N
15	13,11	0,30	12,53	13,70	29,13	0,48	28,19	30,08	180
25	11,47	0,41	10,66	12,28	26,90	0,53	25,86	27,94	180
30	10,86	0,36	10,14	11,57	27,49	0,54	26,43	28,54	180

[1)]Priemer, [2)]Smerodajná odchýlka

Effect of feed rate

The Fig. 9 displays the analysis of variance for dependence of surface roughness on feed rate

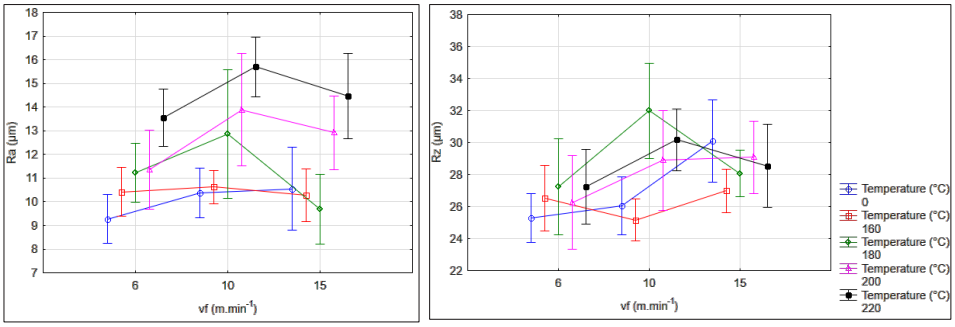

Fig. 9 Multifactor analysis of the influence of feed rate on surface roughness
Obr. 9 Viacfaktorová analýza vplyvu posuvnej rýchlosti na drsnosť

The best roughness of the surface at feed rate of 6 m.min^{-1} was measured at the untreated sample (Ra = 9,27 µm, Rz = 27,27 µm) and the samples treated at 160 °C (Ra = 10,42 µm, Rz = 26,08 µm) and 180 °C (Ra = 11,23 µm, Rz = 26,06 µm). The worst results were obtained at the sample treated at 220 °C (Ra = 13,55 µm, Rz = 27,24 µm). The best surface roughness at the feed rate of 10 m.min^{-1} was also obtained at the untreated sample (Ra = 10,38 µm, Rz = 28,17 µm). At the sample treated at 160 °C, the mean Ra was 10,63 µm and Rz 25,17 µm. The worst results were obtained at the temperature of 220 °C (Ra = 15,70 µm, Rz = 30,18 µm). The best surface quality at the feed rate of 15 m.min^{-1} was obtained at the temperature of 180 °C (Ra = 9,69 µm, Rz = 28,07 µm). At the sample treated at 160 °C, the average Ra value was 10,27 µm and the Rz 26,98 µm. The worst surface roughness results were again at 220 °C (Ra = 14,48 µm, Rz = 28,54 µm).

The table 7 shows the results of the weighted means of the surface roughness dependence on the feed rate. The minimal average Ra and Rz were measured at the rate of 6 m.min^{-1}.

Table 7 – Weighted means – effect of feed rate
Tabuľka 7 Vážené priemery – vplyv posuvnej rýchlosti

v_f [m.min^{-1}]	Ra [µm] Average[1)]	Ra [µm] St. dev.[2)]	Ra [µm] -95,00%	Ra [µm] +95,00%	Rz [µm] Average[1)]	Rz [µm] St. dev.[2)]	Rz [µm] -95,00%	Rz [µm] +95,00%	N
6	11,16	0,29	10,58	11,74	26,51	0,53	25,46	27,56	180
10	12,69	0,42	11,87	13,52	28,45	0,54	27,38	29,52	180
15	11,58	0,37	10,86	12,30	28,56	0,47	27,63	29,48	180

[1)]Priemer, [2)]Smerodajná odchýlka

Effect of cutting speed

The Fig. 10 shows the analysis of variance for dependence of surface roughness on cutting speed.

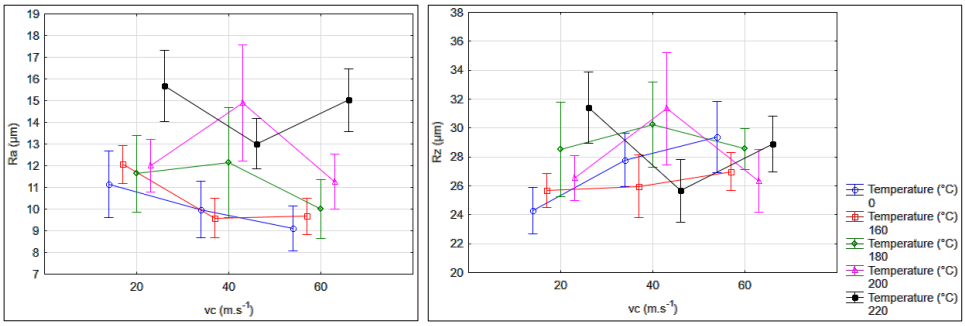

Fig. 10 Multifactor analysis of the influence of cutting speed on surface roughness
Obr. 10 Viacfaktorová analýza vplyvu reznej rýchlosti na drsnosť

The best surface roughness value at the cutting speed of 20 m.s^{-1} was measured at the untreated sample (Ra = 11,13 µm, Rz = 24,28 µm) and at the sample treated at 180 °C (Ra = 11,63 µm, Rz = 28,53 µm). The worst results were measured at the sample treated at 220 °C (Ra = 15,69 µm, Rz = 31,42 µm). The best surface roughness value at the cutting speed of 40 m.s^{-1} was measured at the sample treated at 160 °C (Ra = 9,59 µm, Rz = 25,97 µm). Higher surface roughness had the untreated sample (Ra = 9,97 µm, a Rz = 27,79 µm). The worst surface roughness results were measured at 200 °C (Ra = 14,9 µm, Rz = 31,34 µm). The best surface quality at the cutting speed of 60 m.s^{-1} was in the untreated sample (Ra = 9,09 µm, Rz = 29.37 µm). The second best quality appeared at 160 °C (Ra = 9,66 µm, Rz = 26.99 µm). At this cutting speed, the worst surface roughness was measured at 220 °C (Ra = 15,02 µm, Rz = 28,88 µm).

The table 8 shows the results of the weighted means of the surface roughness dependence on the cutting speed. The minimal average Ra was measured at the speed of 60 m.s^{-1}, minimal Rz at 20 m.s^{-1}.

Table 8 Weighted means – effect of cutting speed
Tabuľka 8 Vážené priemerov – vplyv reznej rýchlosti

v_c [m.s^{-1}]	Ra [µm] Average[1)]	Ra [µm] St. dev.	Ra [µm] -95,00%	Ra [µm] +95,00%	Rz [µm] Average[1)]	Rz [µm] St. dev.[2)]	Rz [µm] -95,00%	Rz [µm] +95,00%	N
20	12,50	0,34	11,84	13,17	27,29	0,50	26,30	28,28	180
40	11,93	0,43	11,07	12,78	28,20	0,61	26,99	29,41	180
60	11,01	0,31	10,40	11,62	28,03	0,42	27,19	28,87	180

[1)]Priemer, [2)]Smerodajná odchýlka

DISCUSSION

Barcík et al. (2014) (2009) also confirmed that increasing the cutting speed improves the surface quality and, on the contrary, by increasing the feed rate, the final surface quality deteriorates. The best results for angular geometry were achieved at the angle of 15°, which is inconsistent with our results. The best results of the surface finish were also

reached at the temperature of 160 °C, but the surface roughness dependence on the heat treatment was not clear. When comparing, it should be noted that natural and heat-treated pine wood was used in his experiments. Surface measurement was made by this method using a contact method. According to Kvietková et al. (2015), the heat treatment of the material did not have a significant effect on the resulting surface quality, and the best surface quality results were achieved at a temperature of 210 °C. In this case, it was natural and heat-treated birchwood. However, when increasing the cutting speed, the improvement of the surface quality was confirmed and, on the other hand, the deterioration at the increasing feed rate. Surface measurement was also carried out by the contact method in this experiment. Pinkowski et al. (2016), examined the quality of the machining of natural and heat treated pine wood, found out a decrease in surface roughness due to the increasing temperature of the heat treatment, which does not correspond to our results. However, at increasing cutting speeds, it also confirmed the improvement of surface quality and, on the contrary, deterioration in quality at increasing feed rate.

Rajko (2016) also confirmed the increase in surface roughness due to the increase in the temperature of the heat treatment and the best surface quality found in the heat treatment of 160 °C. Even in this case, the same dependencies for cutting speed and feed rate were confirmed. For his experimental measurement, he used three knife heads with rake angles of 15°, 20° and 30°. With angular geometry, he had the best results at the 15° angle, the worst results at the angle of 30°. In his experiment he used natural and heat-treated pine wood. According to Korčok (2017), who also examined English oak (*Quercus robur*) wood, there was also an increase in roughness of the surface with increasing heat treatment of wood. In this case, the best detected roughness values were again for heat treated wood at 160 °C. Even in this experiment the same dependencies for cutting speed and feed rate were confirmed. Korčok used three knife heads with rake angles $\gamma = 15°$, 20° and 30°, where the best results were reached at the angle of 30° and the worst at the angle of 15°, which coincides with the results found in our work.

CONCLUSION

Experimental measurements were focused on the difference in surface quality and the optimization of cutting conditions in order to achieve surface finish quality at the final product level. Surface roughness was measured using a non-contact (laser profilometer) method. Surface roughness results varied in some cases with the same combinations of milling conditions. These sample deviations could be affected by the structure of the sample wood, since in the case of each milling, every 1 mm of material was taken from the sample, which means another surface of the workpiece for each measurement.

In some measurement cases, the non-contact method could have insufficient laser focusing on the measured surface of the sample, or small dirt on the surface of the sample could occur, even in the form of fine dust from machining

- Heat treatment has a clear effect on final surface quality after milling. On the basis of the measured results, it was clearly confirmed that by increasing the treatment temperature the surface roughness (quality deteriorates) after milling.
- When examining the effect of the rake angle γ, the improvement of the surface quality with a larger angle of the face has been demonstrated.

– For the influence of the feed rate, the assumption of surface deterioration was confirmed in response to the increasing feed rate.
– The influence of cutting speed has been confirmed by the assumption of surface quality improvement depending on the increasing cutting speed.

LITERATURE

BARCÍK, Š., KVIETKOVÁ, M.; BOMBA, J., SIKLIENKA, M., 2013. Dřevoobráběcí nástroje - údržba a provozování. Praha: Powerprint, 2013. 355 s. ISBN 978-80-87415-80-1

BARCÍK, Š., ŘEHÁK, T., 2009. Vliv vybraných technicko – technologických a materiálových faktorů na energetickou náročnost při rovinném frézování. Praha, 2009. 84 s. Diplomová práca na České zemědělské univerzitě v Praze, fakultě lesnické a dřevařské.

BARCÍK, Š., GAŠPARÍK, M., HOUSKA, A., RAZUMOV, E. Y., SEDLECKÝ M., 2014. Vliv technologických faktorů na kvalitu opracování povrchu při frézováni termicky modifikovaného borovicového dřeva, In: Trieskové a beztrieskové obrábanie dreva 2014. Zborník prednášok 9(1): 11–22, 2014, ISSN 1339-8350

BEKHTA P., NIEMZ P.: Effect of high temperature on the changes in colour, dimensional stability and mechanical properties of spruce wood. Holzforsch, 2003, s. 539 – 546

BOONSTRA, M. J., VAN ACKER, J., PIZZI, A., 2007. "Anatomical and molecular reasons for property changes of wood after full-scale industrial heat-treatment," Proceedings of the Third European Conference on Wood Modification, 15-16th October, Cardiff, UK, pp. 343-358.

Finnforest, ThermoWood® Handbook, [online]. 2002 [cit.2017-02-11]. Dostupné na internete: <http://www.vandormaeltimber.com/TW%20handbook%20FF.pdf>.

HORÁČEK, P., 1998. Fyzikální a mechanické vlastnosti dřeva 1. vyd. Brno: Mendelova zemědělská a lesnícka univerzita, 1998, 128s. IBNS 80 – 7157 – 347 – 7

JANDA, P., KMINIAK, R., 2013. Vplyv spôsobu upnutia frézovacej hlavy na kvalitu vytvoreného povrchu pri frézovaní na štvorstrannej frézke. Acta facultatis xylologiae Zvolen : vedecký časopis Drevárskej fakulty. 2013. zv. Roč. 55, č. č. 2, s. 51--58. ISSN 1336-3824.

KAČÍKOVÁ, D., KAČÍK, F., 2011. Chemické a mechanické zmeny dreva pri termickej úprave. Zvolen: Technická univerzita vo Zvolene, 2011. 71s. ISBN 978-80-228-2249-7.

KOLEDA, P., BARCÍK, Š., NOCIAROVÁ, A., 2018. "Effect of Technological Parameters of Machining on Energy Efficiency in Face Milling of Heat-treated Oak Wood," *BioResources* (13)3, 6133-6146. DOI: 10.15376/biores.13.3.6133-6146

KORČOK, M., 2017. Vplyv technicko-technologických nezávislých parametrov na kvalitu opracovania povrchu pri rovinnom frézovaní termicky modifikovaného dubového dreva: Diplomová práca. Zvolen: Technická univerzita vo Zvolene. Fakulta environmentálnej a výrobnej techniky. 2017. 129 s.

KVANT [online]. 2008, LPM profilometer, [cit. 2018-01-02]. Dostupné na internete: <http://www.visionsystems.sk/sk/riesenia/lpm/>.

KVIETKOVÁ M., GAFF M., GAŠPARÍK, M., KAPLAN, L., BARCÍK, Š., 2015. Surface quality of milled birch wood after thermal treatment at various temperatures. BioResources 10(4), 6512-6521. DOI:10.15376/biores.10.4.6512-6521 ISSN: 1930-2126.

LISIČAN, J. et al. 1996. Teória a technika spracovania dreva. MAT-CENTRUM, 1996.

NIEMZ, P., HOFMANN, T., RÉTFALVI, T., 2010. "Investigation of chemical changes in the structure of thermally modified wood," Maderas. Ciencia y Tecnología 12(2), 69-78. DOI: 10.4067/so718-221x2010000200002

PINKOWSKI, G., KRAUSS, A., PIERNIK, M., SZYMANSKI, W., 2016. Effect of thermal treatment on the surface roughness of scots pine (Pinus sylvestris L.) wood after plane milling. 11. 5181-5189. 10.15376/biores.11.2.5181-5189.

POŽGAJ, A. et al. 1997. Štruktúra a vlastnosti dreva. Vydavateľstvo Príroda, Bratislava, ISBN 64-065-97.

RAJKO, Ľ. 2016. Vplyv vybraných technologických, nástrojových a materiálových faktorov na kvalitu opracovania povrchu pri rovinnom frézovaní termicky modifikovaného borovicového dreva: Diplomová práca. Zvolen: Technická univerzita vo Zvolene. Fakulta environmentálnej a výrobnej techniky.2016. 119 s.

REINPRECHT, L., VIDHOLDOVÁ, Z., 2008. Termodrevo – príprava, vlastnosti a aplikácie. Zvolen: Technická univerzita vo Zvolene, 2008. 89 s. ISBN 978-80-228-1920-6.

SIKLIENKA, M., KMINIAK, R., 2013. Delenie a obrábanie dreva. 1. vyd. Zvolen: Technická univerzita vo Zvolene, 207 s. ISBN 978-80- 228-2618- 1

SIKORA, A., KAČÍK, F., GAFF, M., VONDROVÁ, V., BUBENIKOVA, T., KUBOVSKÝ, I., 2018. Impact of thermal modification on color and chemical changes of spruce and oak wood. Journal of Wood Science. 10.1007/s10086-018-1721-0.

STN EN ISO 4287 – 1999. Geometrické špecifikácie výrobkov (GPS). Charakter povrchu. Profilová metóda – Termíny, definície a parametre charakteru povrchu.

STN 26 0070 – 1995. Klasifikácia a označovanie sypkých hmôt dopravovaných na dopravných zariadeniach.

ŠUSTEK J., 2010. Manuál ku kompaktnému profilometru LPM

Contribution has been prepared within the solving of scientific grant project VEGA 1/0315/17 „ Research of relevant properties of thermally modified wood at a contact effects in the machining process with the prediction of obtaining an optimal surface.“

Corresponding author:
Peter Koleda, peter.koleda@tuzvo.sk

MODIFICATION OF EXPERIMENTAL DEVICE TRIBOTESTOR M 06 ALLOWING THE HEATING OF THE SLIDING ELEMENTS

MODIFIKÁCIA SKÚŠOBNÉHO ZARIADENIA TRIBOTESTOR M 06 UMOŽŇUJÚCA OHREV POSUVNÝCH PRVKOV

Adam Fürstenzeller[1], Milan Kadnár[1], Marek Halenár[2], Peter Kuchar[2], Jozef Nosian[2]

Adam Fürstenzeller1, Milan Kadnár1, Marek Halenár2, Peter Kuchar2, Jozef Nosian2
[1]Department of Machine Design, Faculty of Engineering, Slovak University of Agriculture in Nitra, Tr. A. Hlinku 2, 949 76, Nitra, Slovakia, dtf@uniag.sk
[2]Department of Transport and Handling, Faculty of Engineering, Slovak University of Agriculture in Nitra, Tr. A. Hlinku 2, 949 76, Nitra, Slovakia, dtf@uniag.sk

ABSTRACT: The submitted article deals with issue of modification the testing device Tribotestor M06. The device was modified by heating unit, which was able to increase the temperature of sliding knot. The device consists of a PID controller, a spiral, a temperature sensor and an electronic relay. Proposed modification was tested on the testing device Tribotestor M06 during experimental measurements. Experiment itself was performed on sliding seating composed of pair sleeve – shaft. Sleeve was made from material B 60 and shaft was made from 16MnCr5 steel. Experimental tests were carried out in ecological oil Fuchs Plantohyd 45 S in two temperature ranges (without oil heating and with oil heating). Results of experimental tests were statistically processed and on basis of them were established relations between friction coefficient, temperature and the time of test duration.

Key words: modification of the Tribotestor M 06, heating unit, sliding knot

ABSTRAKT: Predložený vedecký príspevok sa zaoberá problematikou úpravy skúšobného zariadenia Tribotestor M 06. Zariadenie bolo modifikované pomocou ohrevnej jednotky, ktorou bolo možné zvyšovať teplotu klzného uzla. Zariadenie pozostáva z PID regulátora, špirály, snímača teploty a elektronického relé. Navrhnutá modifikácia bola otestovaná na skúšobnom zariadení Tribotestor M 06 počas experimentálnych meraní. Samotný experiment bol vykonaný na klznom uložení puzdra s označením B 60 a hriadeľa s kontaktnou plochou vyrobenou z ocele 16MnCr5. Experimentálne skúšky prebehli v prostredí mazanom ekologickým olejom Fuchs Plantohyd 45 S v dvoch teplotných rozsahoch (bez ohrevu a s ohrevom). Výsledky experimentálnych skúšok boli štatisticky spracované a na ich základe sa stanovil priebeh súčiniteľa trenia a teploty v závislosti od času trvania skúšky.

Kľúčové slová: modifikácia Tribotestora M 06, ohrevná jednotka, trecí uzol

INTRODUCTION

Gradual change of attitude towards the surrounding environment is reflected in all areas of social life. The rise of the use of ecological processes and resources is supported by the legislative changes at the national level, but especially at the international level. Agriculture, including agricultural production, is no exception. Improving environmental conditions leads to the substitution of mineral oils with biodegradable oils [13,19].

The market with ecological liquids is spreading significantly. One of the offered products are ecological oils used in hydraulic and transmission mechanisms [4,11]. We focused on this product group. During the experimental laboratory tests sliding elements were lubricated with Plantohyd 46 S ecological oil from Fuchs Lubricants (UK). The aim was to assess its tribological properties during limiting state. We focused on experimental tests carried out in temperature limit state of used ecological oil [3].

To achieve the oil temperature limit state, we modified the testing device Tribotestor M 06 using a heating unit consisting of a PID controller, a spiral, a temperature sensor and an electronic relay. Using the modification, we have identified how the load and elevated temperature influence tribological properties of the selected ecological lubricant.

In general, it is very important to know the limits of used lubricants, not just ecological ones. Therefore, various modifications of test devices are made or developed, for testing the lubricants. Determining the properties of lubricants during extreme loads helps to prevent operational failures and to prolong the life of machines and equipment. Therefore, it is very important to continue with research simulating these boundary conditions.

Lubricants are one of the main supporting components. The performance of the tribological node is influenced by the performance of the lubricant. Current research attempts to combinate knowledge about the modern techniques used in lubricating mechanisms with the development of lubricants. It is therefore extremely important to know the parameters and specifications of the lubricants under extreme conditions [22].

MATERIAL AND METHODS

For experimental tribological tests was used device Tribotestor M 06 (Fig. 1.). Tribotestor M 06 is an universal device for the rapid identification of tribological properties of sliding pairs. It allows to carry out the following types of tests:

a) boundary loading test (seizure test),
b) boundary speed test (speed seizure test),
c) load rating test for P-V diagram determination,
d) operating life test (durability).

The experimental device consists of three main parts:

a) testing part: power unit with rotational motion of samples, vertical load force and measuring head,
b) pneumatic circle and electronic devices,
c) controller unit: desktop PC allows starts, operating, management, data collecting and test evaluation.

Fig. 1. Measuring device Tribotestor M 06
Obr. 1. Meracie zariadenie Tribotestor M 06

Figure 2 shows a detailed view of the measuring head and test sample. Sliding knot is formed by a pair of solids, forming a surface contact by rotating shaft against friction bearing [21]. The B 60 sliding bearing is all-bronze, centrifugally cast with dimensions ϕ 30r7 x ϕ 25 F7 x 20 mm [2]. Sliding bearing is pressed onto measuring head. Testing shaft sleeve with outer diameter ϕ24,960 mm and length 25 mm was made of 14 220 (16MnCr5) steel and pressed onto the cylindrical portion of the support shaft [14,16].

The supporting shaft was attached to power unit with shrinking cone connection using tightening force through an internal wheel in the cone [17]. Lubrication of friction elements by the tested ecological oil was done by gravitational dropping through the measuring head upper part [18].

Fig. 2. Detail view of the measuring head and the test sample
Obr. 2. Detailný pohľad na meraciu hlavicu a skúšobnú vzorku

Before the experiment and starting the device Tribotestor M 06, a heating device (Fig. 3.) was installed on area of sliding pair, which served to heat the test head to the desired temperature. The heating device consisted of four parts:

a) simple PID controller,
b) temperature sensor J (Fe-CuNi),
c) electronic relay in industrial housing (SSR RS 230 V 10 A DC IP),
d) spiral.

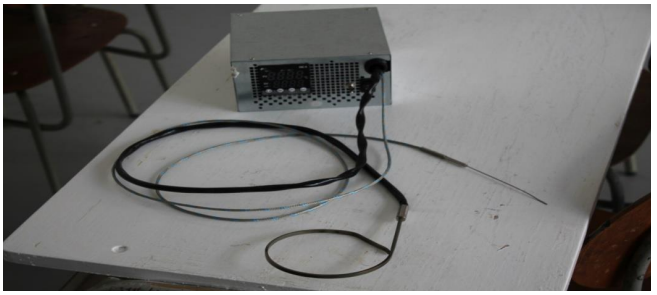

Fig. 3. Heating equipment
Obr. 3. Ohrevné zariadenie

The Fuji PXE4 PID controller (Fig. 4.) is a simple, economical controller equipped with precise control algorithms. It offers standard functions such as two-position, PID or fuzzy control, with automatic optimization of control parameters. The resistive temperature sensor or thermocouple can be connected to the measuring input. The control output can be a relay or SSR driver for switching solid state relay with direct input.

Fig. 4. PID controller Fuji PXE4
Obr. 4. PID regulátor Fuji PXE4

Table 1. Dimensions of PID controller Fuji PXE4
Tabuľka 1. Rozmery PID regulátora Fuji PXE4

Properties	Value
Front panel format[1)] [*DIN*]	1/16
Width[2)] [*mm*]	48
Height[3)] [*mm*]	48
Bult-in depth[4)] [*mm*]	60, 9
Panel thickness[5)] [*mm*]	1 ÷ 8

[1)]Formát čelného panela, [2)]Šírka, [3)]Výška, [4)]Vstavaná hĺbka, [5)]Hrúbka panelu

Table 2. Measuring input of PID controller Fuji PXE4
Tabuľka 2. Merací vstup PID regulátora Fuji PXE4

Properties	Values
Time constant of input filter[1] [*s*]	0,0 ÷ 120,0
Input impedance[2] [*M*Ω]	thermocouples: more than 1 MΩ
Input calibration[3] [*%*]	adjustable ± 10% of input range
Permissible input resistance[4] [Ω]	thermocouple: max. 100 Ω Pt100: resistance driven by max. 10 Ω

[1]Časová konštanta vstupného filtra, [2]Časová impedancia, [3]Kalibrácia vstupu, [4] Povolený vstupný odpor,

The M2-J1.5D100L-2U-150G is a simple temperature sensor of the M2 series, type J (Fe-CuNi), insulated from the sheath, material AISI 304, accuracy class 2, diameter 1,5 mm, with insulated fiberglass / fiberglass / metal braid.

Electronic relay CARLO GAVAZZI SSR RS 230V 10A DC IP (Figure 5) is a modern replacement for electromechanical relays. It is mostly produced in one or three phase designs. Inside, they are realized using different types of thyristors or modern IGBT transistors.

Fig. 5. Electronic relay CARLO GAVAZZI SSR RS 230V 10A DC IP
Obr. 5. Elektronické relé CARLO GAVAZZI SSR RS 230V 10A DC IP

Table 3. Technical parameters of CARLO GAVAZZI SSR RS 230V 10A DC IP
Tabuľka 3. Technické parametre CARLO GAVAZZI SSR RS 230V 10A DC IP

Properties	Values
Dimensions[1] [*mm*]	58x45x29
Rated voltage[2] [*V*]	230
Rated current[3] [*A*]	10
Minimum switching voltage[4] [*V*]	42
Working temperature[5] [˚C]	20 ÷ 70

[1]Rozmery, [2]Menovité napätie, [3]Menovitý prúd, [4]Minimálne spínacie napätie, [5]Pracovná teplota

The heating spiral FC4.2R2.2R315L200W is used to achieve high performance in a confined space or for uniform heating. Casing and connector are made of stainless steel. The Ni-CR (80-20) heating wire is isolated with magnesium oxide (MgO)
Table 3. Technical parameters of FC4.2R2.2R315L200W

Tabuľka 3. Technické parametre FC4.2R2.2R315L200W

Properties	Values
Cross section[1)] [mm^2]	4,2
Rated voltage[2)] [V]	230
Performance[3)] [W]	200
Total length[4)] [mm]	315
Heated length[5)] [mm]	250

[1)]Prierez, [2)]Menovité napätie, [3)]Výkon, [4)]Celková dĺžka, [5)]Výhrevné dĺžka

Tested product was biological oil Plantohyd 46 S from Fuchs Lubricants (UK) [12,15]. It is environmentally friendly, rapidly biodegradable, non-polluting hydraulic product based on synthetic HEES-type esters according to VDMA 24 568 standard. Plantohyd 46 S is compatible with materials commonly used in hydraulic systems. The base fluid and the additives used are toxicologically harmless. The liquid does not contain heavy metals and chlorine compounds, it is biodegradable up to more than 90% according to CEC-L--33-A-93. The scope of product usage is within the range -30 °C to 90 °C, with temperature peaks around 95 °C the usage of lubricant is allowable with respect to its boundary viscosity. Plantohyd 46 S is a universal oil used in all hydraulic and circulatory systems that require the use of ISO VG 46 grade oil. This product is suitable for mobile and stationary hydraulic systems. It is mainly used in installations operating in environments where there is a risk that leaking hydraulic fluids may endanger ground, groundwater or surface water. If oil leak occurs, the product is captured mainly in the upper layers of soil where it is rapidly biodegradable.

Table 4. Properties of PLANTOHYD 46 S
Tabuľka 4. Vlastnosti PLANTOHYD 46 S

Properties	Value	Test method
ISO VG [-]	46	DIN 51519
Kinematic viscosity at 40 °C[1)] [$mm^2.s^{-1}$]	48	DIN EN ISO 3104
Kinematic viscosity at 100 °C[2)] [$mm^2.s^{-1}$]	9,4	DIN EN ISO 3104
Viscosity index[3)] [-]	184	DIN ISO 2909
Density at 15 °C[4)] [$kg.m^3$]	920	DIN 51757
Colour[5)] [*ASTM*]	1.0	DIN ISO 2049
Flash point in open cup acc. to Cleveland[6)] [°C]	300	DIN ISO 2592
Pour point[7)] [°C]	-45	DIN ISO 3016
Neutralisation number[8)] [$mgKOH.g^{-1}$]	1.1	DIN 51558-1
Scuffing and scoring test, FZG A/8,3/90[9)] [*failure loadstage*]	12.	DIN ISO 14635-1

[1)]Kinematická viskozita pri 40 °C, [2)]Kinematická viskozita pri 100 °C, [3)]Viskózny index, [4)]Hustota pri 15 °C, [5)]Číslo farby, [6)]Bod vzplanutia podľa Clevelanda, [7)]Bod tuhnutia, [8)]Neutralizačné číslo, [9)]Mechanická záťažová skúška FZG A/8,3/90

During the experimental test shaft rotation was 180 rpm. in clockwise direction. The test time was set to 70 min. with 10 min. run-up phase and 60 min. test phase [6,8]. The load force in run-up phase was set in the range from 500 to 3000 N., where the load was

increased by 500 N step every 120 s. After run-up phase load was increased to 3000 N and remained constant for 60 min. [7,20]. In the first series of experimental tests were not used heating unit. The second series of experimental tests were differed by heating of the measuring head prior to the start of the experiment to 70 ° C, other parameters were consistent with the first series of experimental tests.

RESULTS AND DISCUSSION

The obtained results from experimental test of ecological oil Plantohyd 46 S on the device Tribotestor M 06 at both temperature ranges were statistically processed and assessed. Test results were graphically evaluated as course of the friction coefficient and temperature depending on time of test. Each curve is presented in a single coordinate system in both temperature variations. Curve showing the individual trends, whether friction coefficient or temperature depending on test time, is generated using the least squares method.

Figure 6 shows the course of friction coefficient value of the Plantohyd 46 S during both temperature modes, where immediately after test phase started from 600 s up to 700 s the values of the friction coefficient was increased. After this section, values gradually stabilized. Depending on the duration of the test, both curves have a decreasing character. The common coordinate system allows better comparison of curves coefficient of friction. In both cases, the dependence of the friction coefficient on the change in the load force is evident. The course of the friction coefficient in no-heating variation is balanced and be stabilized at about 0.01. In the heating variation of the sliding node is possible to see decrease from the higher values of the coefficient of friction to the final value of 0.04. From listed above is clear, that with the influence of increasing temperature the friction coefficient increases, what can occur e.g. during increased operational loading of equipment.

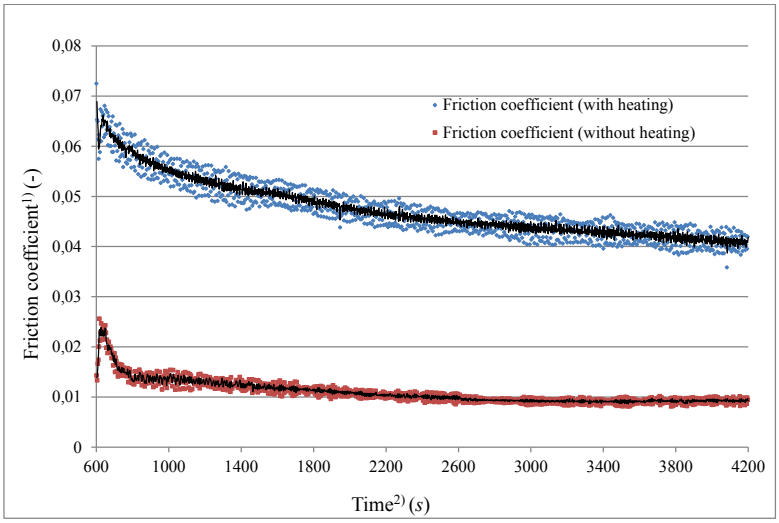

Fig. 6. Friction coefficient course of ecological oil Plantohyd 46 S
Obr. 6. Priebeh súčiniteľa trenia ekologického oleja Plantohyd 46 S
[1]Súčiniteľ trenia, [2]Čas

The course of the temperature depending on the duration of the test is shown in Figure 7, these values are shown as being indicative of the ability of heat dissipation by the organic liquid Plantohyd 46 In the area of the sliding knot.

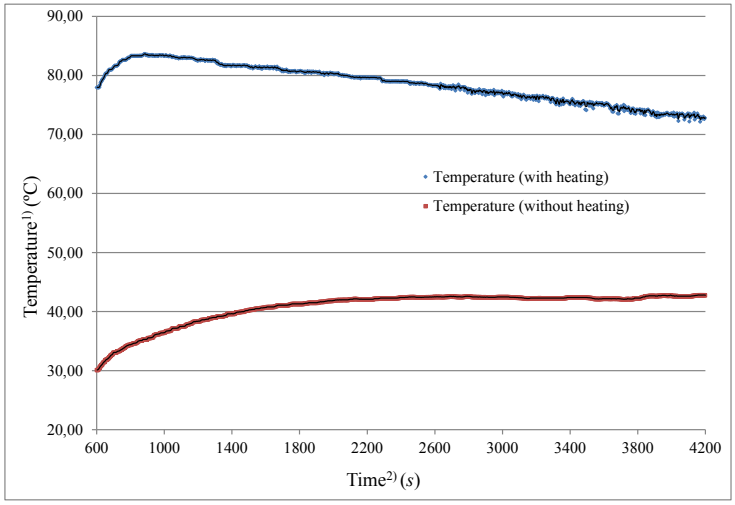

Fig. 7. Temperature course of the ecological oil Plantohyd 46 S
Obr. 7. Priebeh teploty ekologického oleja Plantohyd 46 S
[1)]Teplota, [2)]Čas

CONCLUSION

The main objective of submitted article was modification of experimental device Tribotestor M 06 by using heating unit. By using of proposed modification, we were able to move closer to limiting working conditions of ecological lubricant Plantohyd 46 S in a specified tribological sliding system. Specifically, the ambient temperatures of the contact point of two friction elements. We evaluated how load and increased temperature affect oil quality and tribological properties.

The course of the friction coefficient during the experimental test was declining in both temperature variants. Ecological oil Plantohyd 46 S achieved lower friction coefficients during non-heating experimental measurements, approximately 0,01. In the second variation with heating, the oil had a significantly higher level of friction coefficient. Decreasing trend of friction coefficient was stabilized at 0,04 before the end of the test.

Based on the above experiment, we have proved correct function of the proposed modification, tested in friction system lubricated by ecological lubricant Plantohyd 46 S.

By using of the modified device is possible to test the use lubricants throughout the whole thermal range in tribological systems in further research. In the forthcoming research, we will focus on the simulation of boundary conditions obtained from analyses from real operating conditions in tribological systems. We will also investigate the effect of PVD coatings on the final course of the friction coefficient and temperature.

LITERATURE

1. BOŠANSKÝ, M., VANYA, A., HUDÁKOVÁ M., MALÝ V., 2012. Tverdyje pokrytia kak vozmožnosť povyšenia nagruzočnoj sposobnosti vypuklo-vognytych zaceplenii vzaimodejstvujuščich s vio-masľanoj smaskoj. In: *Visnik nacionaľnovo techničnovo universitetu "XIII"*. Charkiv: Nacionaľnyj techničeskij univesitet, 2012, No. 35, pp. 16-24, ISSN 2079-0791
2. BHUSHAN, B., 2013, Introduction to Tribology, 2nd edition, New Jersey : John Wiley & Sons, Inc.. ISBN 978-1-119-94453-9
3. ČAVOJSKÝ, P., RUSNÁK, J., TÓTH, F., 2015, Možnosti využitia ekologického oleja Hydros UNI v definovanom tribologickom systéme. In: *Kvalita, technológie, diagnostika v technických systémoch*. Nitra : Slovak University of Agriculture, 2015, pp. 171-175, ISBN 978-80-552-1329-3
4. KADNÁR, M., RUSNÁK, J., KUČERA, M., MALÝ, V.,2010 Využitie tribologických skúšok v automobilovom priemysle. In: *51. medzinárodná vedecká konferencia katedier častí a mechanizmov strojov : Košice, 8.-10. 9. 2010*. Košice : C-Press, pp. 99-102, ISBN 978-80-970-294-1-8
5. KOPILÁKOVÁ, B., BOŠANSKÝ, M., PETRÁK, Ľ., 2016, Comparison HRC and C-C gearing for damage to pitting. In: *Visnik nacionaľnovo techničnovo universitetu „CHPI"*. 2016, pp. 77-81, ISSN 2079-0791
6. KOSTOLÁNI, P., KUČERA, M., TÓTH, F., 2011. Ovládací program zariadenia tribotestor. In: *Nové trendy v konštruovaní a v tvorbe technickej dokumentácie 2011 : pri príležitosti 42. výročia založenia Technickej fakulty SPU v Nitre a 18. Medzinárodného strojárskeho veľtrhu v Nitre : zborník vedeckých prác Nitra, 26. mája 2011*. Nitra : Slovak University of Agriculture in Nitra, 2011, pp. 33-38, ISBN 978-80-552-0585-4 Available in: <http://www.slpk.sk/eldo/2011/zborniky/16-11/kostolani.pdf>.
7. KOSTOLÁNI, P., KUČERA, M., TÓTH, F., 2013, Vplyv tribologického experimentu na opotrebenie prvkov trecej dvojice. In: *Nové trendy v konštruovaní a v tvorbe technickej dokumentácie 2013*. Nitra: Slovak University of Agriculture in Nitra, 2013, pp. 93-98, ISBN 978-80-552-1020-9, Available in: <http://www.slpk.sk/eldo/2013/zborniky/030-13/s2-Kostolani.pdf>.
8. KUČERA, M., HNILICOVÁ, M., 2015, Tribological evaluation of lubricants with a lower environmental impact using four-ball tribotester at different temperatures and loads. In: *XVII. Medzinárodná vedecká konferencia mladých 2015*. Zvolen : Technical university in Zvolen, 2015, pp. 108-112, ISBN 978-80-228-2781-2
9. KUČERA, M., HNILICOVÁ, M., ALEŠ, Z., 2014, Inspection of wear particles contaminating used engine oils. In: *Acta Facultatis Technicae Zvolen – Slovakia*, 2014, Vol. 19, No. 2, pp. 39-47.
10. LIČKOVÁ, M., HUJOVÁ, E., MAJERIK, J., TÓTH, F., TÖKÖLY, P., 2016, Evaluation of tribological properties of high-strength material with deposited CrN layer. In: *University Review*. 2016, Vol.10, No. 2, pp. 24-28, ISSN 1337-6047
11. MAJDAN, R., STANČÍK, B., TÓTH, F., VITÁZEK, I., ABRAHÁM, R., ŠTULAJTER, I., 2012, Hodnotenie vlastností ekologických kvapalín na základe opotrebenia súčiastok traktorových hydrogenerátorov. In: *Technika v technológiách agrosektora 2012*. Nitra : Slovak University of Agriculture, pp. 128-133, ISBN 978-80-552-0895-4
12. MAJDAN, R., TKÁČ, Z., TULÍK, J., KOSIBA, J., ZIGIŇ, P., BUREŠ, Ľ., 2010. Vyhodnotenie skúšky ekologickej hydraulickej kvapaliny na základe prietokovej účinnosti hydrogenerátora. In: *Acta technologica agriculturae*. 2010, Vol. 13, No. 3, pp. 61-64, ISSN 1335-2555
13. MAJDAN, R., TKÁČ, Z., TULÍK, J., VOZÁROVÁ, V., CHRASTINA, J., ŠIMOR, R., KOSIBA, J., 2010. The methods for smart inspection of biodegradable transmission oil of tractor: Metode za brzu kontrolu ekološkog transmisionog ulja traktora. In: *Savremena poljoprivredna tehnika*. 2010, Vol. 36, No. 3, pp. 276-284, ISSN 0350-2953

14. MANG, T., DRESEL, W., 2007, Lubricants and Lubrication. 2. ed. Weinheim: WILEY-VCH Verlag GmbH & Co. KGaA. ISBN 978-3527326709
15. RUSNÁK, J., KADNÁR, M., KUČERA, M., 2009, Biologicky odbúrateľné oleje z pohľadu ich tribologických vlastností : metódy, prístroje a interpretácia : monografia. 2009, Nitra: Slovak University of Agriculture in Nitra, ISBN 978-80-552-0166-5.
16. STACHOWIAK, W. G., 2005. *Engineering Tribology*. 3. vyd. Oxford: Elsevier Butterworth--Heinmann , 2005. 801 s. ISBN 0-7506-7836-4.
17. TÖKÖLY, P., BOŠANSKÝ, M., MALÝ, V., 2013. Metodika opredelenija zakalennogo sloja v nezvoľventnom zubčatom zeceplenii. In: *Visnik nacionaľnovo techničnovo universitetu "XIII"*. 2013, No. 41, pp. 148-153, ISSN 2079-0791
18. TÓTH, F., RUSNÁK, J., HAAS, P., PUKÁČ, M., 2015, Návrh koncepcie obehového systému mazania tribologického klzného uzla. In: *Vidiecke stavby v európskych regiónoch III*. Nitra : Slovak University of Agriculture, 2015, pp. 159-163, ISBN 978-8-552-1399-6
19. TÓTH, F., RUSNÁK, J., KUČERA, M., FILO, I., 2012. Porovnanie tribologických vlastností olejov Madit PP 80 a Mobil Mobilube SHC. In: *XIV. medzinárodná vedecká konferencia mladých 2012*. Zvolen: Technical university in Zvolen, 2012, pp. 292-296, ISBN 978-80-228-2342-5
20. TÓTH, F., RUSNÁK, J., KUČERA, M., LYŽIČIAR, P., 2013, Porovnanie tribologických vlastností olejov Mobil Mobilube SHC a Hydros UNI. In: *Nové trendy v konštruovaní a v tvorbe technickej dokumentácie 2013*. Nitra: Slovak University of Agriculture in Nitra, 2013, pp. 129-133, ISBN 978-80-552-1020-9, Available in: <http://www.slpk.sk/eldo/2013/zborniky/030-13/s2-Tothb.pdf>.
21. ZDRAVECKÁ, E.,2000, *Changes of surface layers at abrasive wear. Nadzemnaja* a *aerokosmičeskaja tribologija.* Sankt-Peterburg: Rossijskaja Akademija Nauk, pp.82 – 85. 2000. ISBN 588-8350-37-6
22. LUGT, P., 2016, Metodika opredelenija zakalennogo sloja v nezvoľventnom zubčatom zeceplenii. In: *Tribology International.* 2016, Vol. 97, pp. 467-477,

Corresponding author:
Adam Fürstenzeller, +421 911 110 292, e-mail: xfurstenzell@is.uniag.sk

EVALUATION OF HYDRAULIC FLUID DURING OF THE OPERATING TEST

HODNOTENIE HYDRAULICKEJ KVAPALINY POČAS PREVÁDZKY

Marek Halenár[1], Jozef Nosian[1], Peter Kuchar[1], Juraj Tulík[1], Adam Fürstenzeller[2]

[1]Department of Transport and Handling, Faculty of Engineering, Slovak University of Agriculture in Nitra, Tr. A. Hlinku 2, 949 76, Nitra, Slovakia, xhalenarm@is.uniag.sk
[2]Department of Machine Design, Faculty of Engineering, Slovak University of Agriculture in Nitra, Tr. A. Hlinku 2, 949 76, Nitra, Slovakia, xfurstenzell@is.uniag.sk

ABSTRACT: This paper presents the results of analyses of organic synthetic oil samples during the operating test. The fluid was assessed in terms of chemical elements contamination. Oil Operations Examination with Transport and Handling Department and Slovnaft LtD. was made. Analysis of ferrograpfy samples in the laboratory of the department was performed and other analyses by an accredited laboratory WAERCHECK Almásfüzitő, Hungary were performed. In the samples of oil after completing 900 engine hours are found large clusters of small wear particles and were foundling also large wear particles.

Key words: kinematic viscosity, viscosity index, ferrography

ABSTRAKT: Tento článok prezentuje výsledky analýz vzoriek organického syntetického oleja počas prevádzky. Hydraulická kvapalina bola hodnotená z hľadiska kontaminácie chemických prvkov. Hodnotenie kvapaliny vykonala Katedra dopravy a manipulácie v spolupráci so spoločnosťou Slovnaft LtD. V laboratóriu Katedry dopravy a manipulácie bola vykonaná analýza ferografických vzoriek, pričom ďalšie analýzy hydraulickej kvapaliny boli vykonané v akreditovanom laboratóriu WAERCHECK Almásfüzitő v Maďarsku. Vo vzorkách oleja po ukončení 900 hodín motora sa nachádzali veľké zhluky malých častíc opotrebovania, veľké častice opotrebenia.

Kľúčové slová: kinematická viskozita, viskózny index, ferografia

INTRODUCTION

The operating test of Mol Farm UTTO synthetic oil followed over laboratory tests conducted at the Department of Transport and Handling. Influence of exerted oil on the flow rate characteristics of UD 25 hydrostatic pump during laboratory test was investigated; simultaneously samples of oil were analyzed.

UD 25 hydrostatic pump is used at the Zetor Forterra 114 41 tractors. In the tractor gear-hydraulic circuit of exerted MOL Farm UTTO Synt was applied. In the range of work 450 engine hours (EH) and 900 (EH) samples of oil form tractor were detracted. These samples in an accredited laboratory WAERCHECK Almásfüzitő and in laboratory at the analysis of ferrography samples at the Department of Transport and Handling were analyzed.

At the present time, hydrostatic systems are widely dispersed in the industry. It provides the various types of motions. The power transmission is realized by hydraulic fluid. Hydraulic fluid needs service and observation of operating parameters (Majdan et al., 2008). Therefore, it is extremely important to replace mineral oils with vegetable oils or synthetic oils of plant-based (Tkáč, 2010 et al., Kosiba, 2016).

From utilization of hydraulic fluid in a machine point of view there is the most important to know the running properties of fluid i.e. to know the influence of fluid on technical state of parts in the hydraulic system (Tkáč, 2008 et al., Jablonický, 2007 et al.).

MATERIAL AND METHODS

The ecological fluid, which was used, is a newly developed ecological fluid, which is made with synthetic base fluid based on poly-alpha-olefins. We choose this fluid, because it has high chemical stability and miscibility with mineral fluids, which are currently used in tractors in Slovakia. During the test we used a new ecological fluid MOL Farm UTTO Synt, which is produced by MOL Group, Hungary. This fluid belongs to the group of universal transmission hydraulic fluid designed for tractors. The main specifications of fluid are: kinematics viscosity at 40 °C = 58,14 $mm^2 . s^{-1}$; kinematic viscosity at 100 °C = 10,22 $mm^2 . s^{-1}$; viscosity index = 165; pour point = (-42 °C).

Ferrography analysis of oil

The aim of ferrography study is to identify the quantity and size of wear particles in the oil samples. Were studied samples of the new oil, samples of oil after completing 450 engine hours and after completing 900 engine hours. Wear particles have a significant effect on the abrasive wear of friction pairs in the tractors gear-hydraulic circuits. These contaminants degrade the used hydraulic oil. (Angelovič, 2013, Tkáč, 2014)

Particle of pollution, despite located of oil filters in the tractor gear-hydraulic circuit should be during operating tests continued to grow. Particle of pollution during the test have tendencies agglutination and aggregation into larger particles (Kosiba, 2012). Technological progress of ferrography analysis in the laboratory of the Department of Transport and Handling, Faculty of Engineering, University of Agriculture in Nitra was carried out.

Analytical Ferrograph T^2FM and KAPA 6000 Microscope for the ferography analysis of samples oil was used. MOL Farm UTTO Synt was diluted before ferrography analysis in proportion 2:1 with tetrachlorethylene to better highlight of pollution particles in the oil.

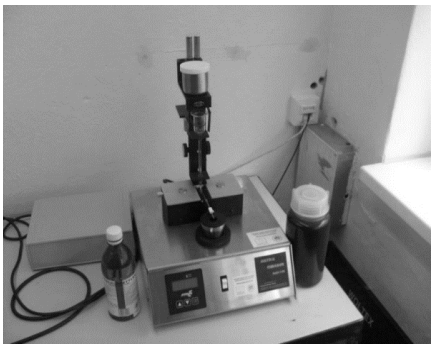

Fig. 1a. Analytical Ferrograph T²FM
Obr. 1a. Analytický Ferrograph T²FM

Fig. 1b. KAPA 6000 Microscope
Obr. 1b. KAPA 6000 Mikroskop

Physico-chemical propoerties of ecological fluid

For measuring of the total acid number (TAN), we used the test by which we neutralized the acids in the fluid by adding potassium hydroxide KOH. Amount of alkali

reagent, which is needs to achievement of neutralization point is a function of acid concentration in fluid.

When oxidizes the fluid, are produced organic acid which are collected in fluid and cause increase TAN. Like the kinematic viscosity and too total acid number reveals degraded fluid in which an occurred degradation processes and were more or less exhausted antioxidant additives. Of course, if the parameters ware not changed by another way e.g. admixture of foreign acid character substances with a lower or higher viscosity than the tested fluid (Majdan, 2012)

Kinematic viscosity is one of the parameters of fluids and the value can goes up during operation, but also decrease. In some case, during fluid aging fluid, the viscosity decrease and whereupon and as increase the oxidation products can begin grow. During the evaluation of kinematic viscosity therefore we assume from lower and upper limits that are not exceeded during operation.

Limit values are determined percentage depending on the fluid type. For example, if the kinematic viscosity of hydraulic fluid changed more than 20% compared with value of new fluid have to be replaced

Fluid viscosity varies with temperature. Rate of viscosity change with temperature is referred to viscosity index (VI). Viscosity index is an empirical value that is used to quantify changes in viscosity in respect of temperature. Viscosity of fluid whit high VI does not change quickly whit temperature as fluid whit low viscosity index (Exxon, 2009).

Water content was determined by coulometric method, which is one of the most advanced and accurate measurement of water since 5ppm. Water in fluid is undesirable it can enters into only as an external substance, for example leakage through the cooling circuits, improper seal on fluid systems, poor storage (rain), but also by the condensation of a longer shutdown device (Intertribodia, 2010).

Water can be characterized as a catalyst for degradation – fluid aging, it can wash from fluid some additives, increases the acid number and thus increases the possibility of corro-

sion in the device. When it is found that the amount of water exceeded the limit values can be take order – e.g. remove the water by filtration (Majdan, 2011, Kosiba, 2013).

FT-IR Spectroscopy

FT-IR stands for Fourier Transform Infrared, the preferred method of infrared spectroscopy. In infrared spectroscopy, IR radiation is passed through a sample. Some of the infrared radiation is absorbed by the sample and some of it is passed through (transmitted). The resulting spectrum represents the molecular absorption and transmission, creating a molecular fingerprint of the sample. Like a fingerprint no two unique molecular structures produce the same infrared spectrum. This makes infrared spectroscopy useful for several types of analysis (Thermonicolet, 2008).

Base of FT IR Spectroscopy is in interaction IR radiance whit analyzed material, which emits photons of material or to absorb them. FT-IR Spectroscopy can measured content of soft impurities (water, glycol.) as well as certain kinds of solid impurities (fibre, seal.) (Kučera, 2008, Majdán, 2014)

RESULTS AND DISCUSION

In the samples of unused MOL Farm UTTO Synt synthetic oil practically not be found particle of pollution. After completing 450 engine hours in samples of oil are wear particles, less than 10 mm. At the same time in these samples clusters of small wear particles that have not a negative impact on activity of gear-hydraulic circuit of Zetor Forterra 114 41 tractor. In the samples of oil after completing 900 engine hours are found large clusters of small wear particles and were foundling also large wear particles.

The ferrography images of synthetic oil were compared with a catalog wear particle. In comparison with the images in the catalog of wear particles we found that these are particle of adhesive wear.

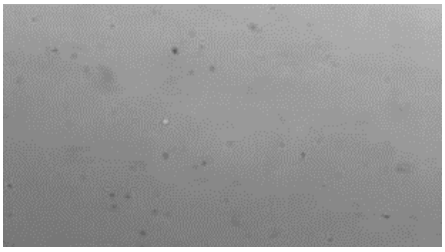

Fig. 2. Wear particles in a sample of new oil
Obr. 2. Častice opotrebenia vo vzorke nového oleja

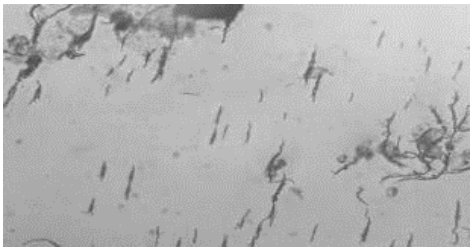

Fig. 3. Wear particles in the sample of oil after completing 450 engine hours
Obr. 3. Častice opotrebenia vo vzorke oleja po odpracovaní traktorom 450 motorhodín

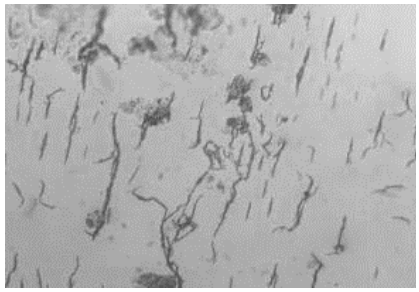

Fig. 4. Wear particles in the sample of oil after completing 900 engine hours
Obr. 4. Častice opotrebenia vo vzorke oleja po odpracovaní traktorom 900 motorhodín

During the test were evaluated the main physic-chemical properties of organic fluid which was tested. Samples were evaluated at an accredited laboratory WEARCHECK Almásfüzitő.

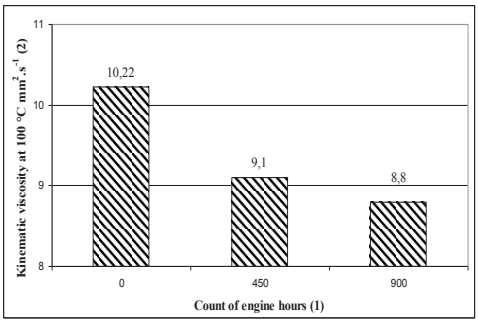

Fig. 5. Kinematic viscosity at 100 °C
Obr. 5. Kinematická viskozita pri 100 °C

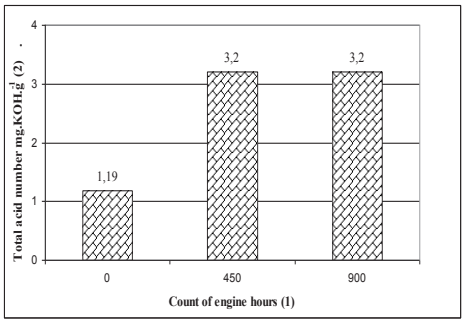

Fig. 6. Total acid number
Obr. 6. Číslo kyslosti

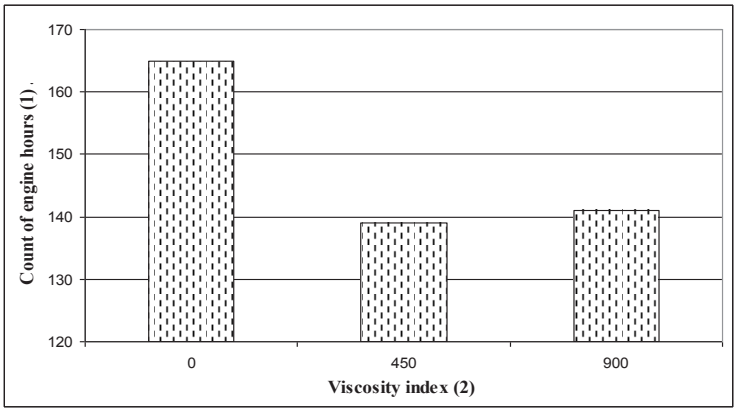

Fig. 7. Viscosity index
Obr. 7. Viskozitný index

The evaluation of kinematic viscosity is on the basis of manufacturers requirements, the value of kinematic viscosity have to not exceeded the tolerance of ± 10 %. The values obtained during the test of ecological fluid are in required tolerances, which means that the fluid is in terms of viscosity in good condition (Figure 5). Evaluation of TAN of fluid is important because the increases of acid amount is characteristic for the fluid aging process, thus directly determines the degree of fluid degradation. Measured values of TAN (Figure 6) had a slightly increasing trend up to 450 engine hour and then the TAN has not changed. Values are not exceeded the limits, the fluid thus meets. Water content in ecological synthetic fluid was so low that it can not be measured by device. The values of VI (Figure 7) during the test held the manufactures specified limits and also does not reason for the replacement of ecological fluid.

The fluid samples was performed FT-IR Spectroscopy. The infrared spectrum representatives the print whit absorption peaks, which corresponding to the frequency of vibrations between the bonds of atoms.

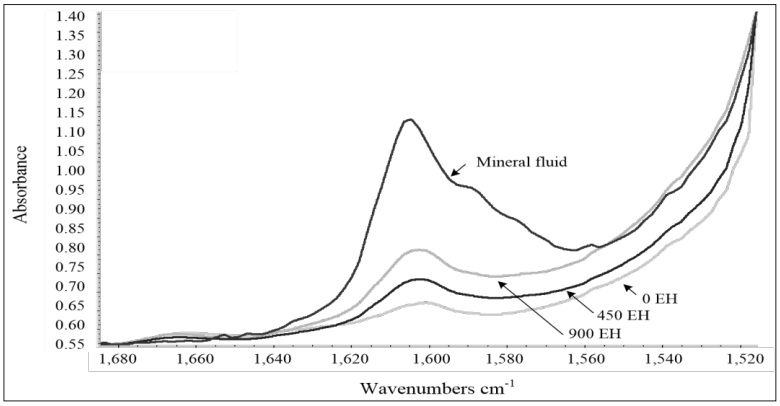

Fig. 8. IR Spectrum of ecological fluid
Obr. 8. IČ spektrum ekologickej kvapaliny

In Figure 8, we see the IR spectra of the studied ecological synthetic fluid. In the regions around 1 600 cm^{-1} can be seen the increases peak with the rise of engine hours. The change of peak size in this area is characteristic for the identity change of fluid. It follows that during the operation test in the fluid leaks foreign substance there has been mixing with other fluid. This peak change caused the mineral fluid, which was in additional devices. Also in fluid are resins, which are degradation products of mineral oil.

CONCLUSION

The paper is focused on the analysis of new ecological synthetic fluid marked as MOL Farm UTTO Synt. The fluid was applied to tractor Zetor Forterra 114 41.

Based on the analysis of ferrography images and comparing with a catalog of wear particles was found that the gear-hydraulic circuit of the Zetor Forterra 114 41 tractor is in the process of running wear. In FT-IR spectroscopy is based on the peaks accretion in char-

acteristic area for fluid identity, we discovered that there is a mixing of ecological fluid through additional device of tractor with mineral fluid. This was confirmed by the finding of resins as a typical product of mineral fluid degradation. The evaluation of physico-chemical properties during the operational test, it is possible to seen that not exceeding the limits specified by manufacturer and ecological synthetic fluid has good physical and chemical properties after 900 engine hours. In term of ferrography, we recommended the fluid for filtration due to extends its technical life. At the present time, therefore, at the Department of Transport and handling we propose a new filtration device.

LITERATURE

ANGELOVIČ, M., TULÍK, J., KOSIBA, J. 2013. Evaluation of pollution of newly developed biodegradable fluid during accelerated laboratory tests. *MendelNet 2013*. 1st ed. 1. 60(6): 417–424.

INTERTRIBODIA, 2010. Obsah vody coulometrický Karl Fisher [online]. Dostupné na internete: http://www.intertribodia.sk/coulometer.html [cit. 10. marec 2018].

JABLONICKÝ, J., ABRAHÁM, R., MAJDAN, R., CVÍČELA, P., 2007. Skúšky traktora s biologicky odbúrateľným olejom (Tests of the tractor with biodegradable oil). *In Assurance – quality – responsibility: 3. International Scientific conference – Košice: The Technical University, 2007*. ISBN 80-8073-258-2. S. 123-127

KOSIBA, J., TULÍK, J., 2012. Vyhodnotenie ferografických vzoriek z prevádzkovej skúšky syntetického oleja (Evaluation of ferrography samples from operating test of synthetic oil). In: XIV. International conference of young scientists 2012. Zvolen : Techical university in Zvolene, 2012. S. 182-186. ISBN 978-80-228-2342-5

KOSIBA, J., ČORŇÁK, Š., GLOS, J., JABLONICKÝ, J., VOZÁROVÁ, V., PETROVIĆ, A., CSILLAG, J. 2016. Monitoring oil degradation during operating test. *Agronomy Research*, 14(5): 1626–1634.

KOSIBA, J., TKÁČ, Z., HUJO, Ľ., TULÍK, J., ŠEVČÍK, P., ŠINSKÝ, V., RAŠO, M. 2013. Effect of ecological energy carriers on flow characteristics of tractor hydraulic pump. *Journal of Central European Agriculture* online, 14(4): 1415–1425.

KUČERA M., ROUSEK M. 2008. Evaluation of thermooxidation stability of biodegradable recycled rapeseed-based oil NAPRO-HO. *Research in Agricultural Engineering*, 54(4): 163–169

MAJDAN, R., ABRAHÁM, R., HUJO, Ľ., MOJŽIŠ, M., 2012. Fyzikálno chemické vlastnosti ekologického oleja. In Tribotechnika vol V, 2012 no. 2, p.s. 38-40. ISSN 1338-0524.

MAJDAN, R., CVÍČELA, P., BOHÁT, M., IVANIŠOVÁ, K,. 2008. The observation of hydrostatic pump deterioration during the durability test according to hydraulic fluids contamination *In X. International conference of young scientists 2008: Conference Proceedings, Czech Republic. – Prague: Czech University of Life Sciences Prague*, 2008. – ISBN 978-80-213-1812-0. – S. 147-153

MAJDAN, R., TKÁČ, Z., STANČÍK, B., ABARAHÁM, R., ŠTULAJTER, I., ŠEVČÍK, P., RAŠO M., 2014. Elimination of ecological fluids contamination in agricultural tractors. *Research in agricultural engineering*, 60(spec. issue): 9–15.

THERMONICOLET, 2008. Introduction to Fourier Transform Infared Spectrometry [on-line]. Dostupné na internete: http://mmrc.caltech.edu/FTIR/FTIRintro.pdf [cit. 10. marca 2018)

TKÁČ, Z., MAJDAN, R., DRABANT, Š., ABRAHÁM, R., VOZÁROVÁ, V., JABLONICKÝ, J., 2010. Hodnotenie vlastností hydraulických kvapalín na základe skúšok s použitím hydrogenerátora (Evaluation of the properties of hydraulic fluids based tests with using hydrostatic pump). Nitra: SPU in Nitra, 2010. 112 s. ISBN 978-80-552-0338-6

TKÁČ, Z., DRABANT, Š., MAJDAN, R., CVÍČELA, P., 2008. Testing Stands for Laboratory Tests of Hydrostatic Pump of Agricultural Machinery. Agricultural Engineering. *In Research in Agricultural Engineering,* 2008, Vol. 54: s.183-191.

TKÁČ, Z., KOSIBA, J., HUJO, Ľ., UHRINOVÁ, D., ŠTULAJTER, I. 2014. Hydraulic laboratory devices for testing of hydraulic pumps. *Advanced Materials Research,* 1059 (special. iss.): 111–117.

1/0155/18

Aplikovaný výskum využívania ekologických nositeľov energie v poľnohospodárskej, lesníckej a dopravnej technike

Corresponding author:
Marek Halenár, 0904 844 600, e-mail: xhalenarm@is.uniag.sk

USAGE OF DISTANCE OPERATORS FOR CREATING ENVIRONMENT DATA BY PRINCIPLE OF ICP ALGORITHM

VYUŽITIE OPERÁTOROV VZDIALENOSTÍ PRE VYTVÁRANIE ÚDAJOV PROSTREDIA PRINCÍPOM ALGORITMU ICP

Lukáš Vacho, Juraj Baláži, Dušan Hrubý, Marián Kišev, Patrik Kósa

Department of Electrical Engineering, Automation and Informatics, Faculty of Engineering, Slovak University of Agriculture in Nitra, Tr. A. Hlinku 2, 949 01, Nitra, Slovakia

ABSTRACT: The use of metric operators to determine similarity in data sets is one of used the techniques for simplicity. For this reason, it is appropriate to use these operators in ICP algorithm for creating environment maps. Environment maps are created from data that is mostly acquired by sensors. In our case, the Hokuyo URG04-LX laser scanner was used. The computational difficulty of the ICP algorithm depends on the type of metric operator used. The Euclidean operator was used to determine the similarity between the measured distances in data set. With this operator, the greater weight is placed on objects that are far apart. The shortest time in the calculation has the Manhattan operator, on the contrary, the largest time Mahalanobis type. The ICP algorithm compared data from the laser scanner. Reference data were compared with the data in transformation process by translation and rotation. The analyzed algorithm parameters were: iteration time, the number of iterations which lead algorithm to convergence and RMS - root mean square. The ICP algorithm is applied in the process of simultaneous localization and mapping (SLAM) for mobile robotics used in agriculture and forestry.

Key words: ICP algorithm, laser scanner, metric operators

ABSTRAKT: Využitie metrických operátorov k určovaniu podobnosti v súboroch dát patrí medzi využívané techniky z hľadiska jednoduchosti. Z toho dôvodu je pre potreby vytvárania máp prostredia pomocou algoritmu ICP vhodné tieto operátory využiť. Mapy o okolí sú vytvárané z údajov, ktoré sú zväčša získané snímačmi. V našom prípade bol použitý laserový skener Hokuyo URG04-LX. Výpočtová náročnosť ICP algoritmu závisí od typu použitého metrického operátora, kde v našom prípade bol využitý Euklidovský operátor pre určovanie podobnosti medzi nameranými vzdialenosťami v súboroch. Pri tomto operátore sa väčšia váha umiestňuje na objekty, ktoré sú od seba vzdialenejšie. Najkratší čas pri výpočte mal operátor typu Manhattan, naopak najdlhší typ Mahalanobis. Algoritmom ICP sa porovnávali údaje z laserového skenera. S referenčnými údajmi sa porovnávali údaje po transformácií posunutím a rotáciou. Skúmanými parametrami algoritmu boli: čas iterácie, počet iterácií vedúcich ku konvergencii algoritmu a RMS – stredná kvadratická odchýlka. Algorit-

mus ICP sa uplatňuje v procese simultánnej lokalizácie a mapovania (SLAM) pre oblasti mobilnej robotiky využívanej v podmienkach poľnohospodárstva a lesníctva.

Kľúčové slová: ICP algoritmus, laserový skener, metrické operátory

INTRODUCTION

Shape registration is a key stage in the process of reconstruction or acquisition of 2D or 3D surfaces so that it is considered a base in the fields of computational algorithm of data processing from scanned area. It is also a task of major importance in many other fields like 2D/3D model reconstruction from multiple range images (Armesto et al., 2010), computer aided interventions (Guo et al., 2016) quality control of manufactured pieces (Bispo & Fisher, 1996), and robotic applications ranging from full environment reconstruction for navigation to particular objects 2D/3D model creation and tracking (Belshaw & Greenspan, 2009). Sensors scanned scene where the result is information in the form of the points that represent the scanned scene. The aim is to reconstruct the scanned scene as accurately as possible, which is a ‹shape registration› process where multiple data sets obtained by the sensors are combined. Currently, the most popular method for 2D/3D rigid registration for the Robotics community is the Iterative Closest Point (ICP) algorithm (Besl, & McKay, 1992). This method estimates the relative transformation between two overlapping point clouds. The ICP algorithm can be divided into six stages (Mora et al., 2006): point selection, matching, pair weighting, outlier removal, error metric, and minimization. Function of ICP algorithm is based on the closest point criteria used for establishing the correspondences, so that the corresponding point for a source point is its closest one in the model (Besl, & McKay, 1992). Point cloud registration error and the number of iterations of the algorithm depend on the amount of data in the cluster of data. The computational difficulty of the algorithm also depends on the initial value of two point clouds (He, et al., 2017), (Rusinkiewicz, & Levoy, 2001).

The distances between the points are calculated by using the distance metric operators which define the closest point operator. There are many distance measures. Choosing the most appropriate metric is a key point to make the ICP algorithm fast. There are several types of metrics (Mora et al., 2016). The research efforts are mainly focused on selected parameter like a computational time of selected distance metric with variable datasets. Selected distance metric applicable in to ICP algorithm calculate distance between data set take from laser scanner. Distance metrics can be used in many areas where it is necessary to determine the distance between data with an acceptable error in dataset (Thanpattranon, et al., 2015). The data characterizes the tracked object. Using the Euclidean metric, it is possible to obtain an error rate ranging from 3 to 14 % for detect tree trunk diameter (Ringdahl, et al., 2013), (Zheng, et al., 2012). Result of ICP algorithm is shape registration of scanned interior area, where taken data. In robotics these techniques have been successfully applied to build local maps for indoor and outdoor navigation (Minguez et al., 2004), (Lacroix et al., 2002), (Montesano et al., 2005) where is used SLAM approaches. The potential of using the ICP algorithm can be applied in the field of image analysis (Tóth et al., 2017). In use of LIDAR sensor localization methods and ICP algorithm, an important factor in transformation methods is to determine their relative errors, where for translation

it can be δ = 3,15 % and error for rotation can reach δ = 0,45 %. These parameters are taken from dataset with selected distance and angle range (Konecny, et al., 2016).

Simultaneous Localization and Mapping (SLAM) is a well-defined problem in mobile robotics and has been extensively studied for indoor and outdoor environments. Many SLAM applications use ICP algorithm for estimates the transformation between two overlapping point clouds scanned with sensors. SLAM Method which implement algorithm ICP, can be uses in large or small environment (Tiar, Lakrouf & Azouaui, 2015) and applicable on mobile robotic device. In an outdoor environment is possible to use another navigation principle, like GPS, which in fusion by SLAM, creates a robust navigating system (Guivant, et al., 2002).

Described principles give basics solution for localization and navigation algorithm in mobile robotics.

MATERIAL AND METHODS

A distance metric ϱ is defined as function in a set X so that $\varrho : \boldsymbol{X} \times \boldsymbol{X}$, being $\mathbb{R}$ the set of real numbers. This function describes the distance between points, for example $x_r y_s$ of the $\boldsymbol{X}$ set. Number must meet the following conditions:

$$\varrho\left(\boldsymbol{x_r}\,;\,\boldsymbol{x_s}\right) = \varrho\left(\boldsymbol{x_s}\,;\,\boldsymbol{x_r}\right) \tag{1}$$

$$\boldsymbol{x_r} \neq \boldsymbol{x_s} \Leftrightarrow \varrho\left(\boldsymbol{x_r}\,;\,\boldsymbol{x_s}\right) > 0 \tag{2}$$

$$\boldsymbol{x_r} = \boldsymbol{x_s} \Leftrightarrow \varrho\left(\boldsymbol{x_r}\,;\,\boldsymbol{x_s}\right) = 0 \tag{3}$$

$$\varrho\left(\boldsymbol{x_r}\,;\,\boldsymbol{x_s}\right) \leq \varrho\left(\boldsymbol{x_r}\,;\,\boldsymbol{x_h}\right) + \varrho\left(\boldsymbol{x_h}\,;\,\boldsymbol{x_s}\right) \tag{4}$$

When the concept of distance metric has been defined, we can address the formulation of the proposed distance metrics as candidates for the reduction of the computational value.

Euclidean distance

The Euclidean distance between the point x_r and x_s is defined as the length of the segment which connects these segments. If we use Cartesian coordinate, $x_r = (x_{r1,}\, x_{r2,..,}\, x_{rn})$ and $x_s = (x_{s1,}\, x_{s2,..,}\, x_{sn})$ are two points in Euclidean space, then their distance $\varrho_E(x_r\,;\, x_s)$ is :

$$\varrho_E\left(x_r\,;x_s\right) = \sqrt{\sum_{i=1}^{n}(x_{ri}-x_{si})^2} \tag{5}$$

When using the Euclidean metric to determine the distance between the data in set, it is necessary to know that the type of metric does not take into account the correlation of the individual characters in data set. As a result, data may be distorted (Mora et al., 2016), (Minguez et al., 2006).

Mahalanobis distance

The common way of dealing with correlation and differential weighting of variables in many multivariate techniques is through the Mahalanobis distance (Cerioli, 2010).

The Mahalanobis distance has the major advantage of taking correlations into account when S – correlation matrix, is not diagonal.

Manhattan distance

The Manhattan or City block distance between the points: x_r and x_s is defined as the sum of the absolute values of the differences of their coordinates. Then the Manhattan distance of two n-dimensional points is described by (Mora et al., 2016):

ICP – Iterative Closest Point algorithm

Given a reference scan S_{ref}, the new scan S_{new} and a rough estimation q_0 of the relative displacement of the sensor between the scans, the objective is to estimate the real displacement $q = (x; y; \mu)$ between them**.** The ICP algorithm addresses this problem with an iterative process in two steps. At each iteration k, there is a search of correspondences between the points of both scans. Then the estimation of relative displacement q_k is improved through a minimization process. The process is repeated until convergence.

First let place each point p'_i of Snew in the system of reference S_{ref} using the estimation q_k, $p''_i = q_k(p'_i)$. Then, due to the discrete nature of the data, it is assumed a local structure in S_{ref} between successive points $(p_i; p_{i+1})$ of S_{ref}. Thus, the correspondent point to p''_j is the closest point p_j belonging to one of th segments $[p_i\, p_{i+1}]$ (Minguez et al., 2006):

$$\min\left\{d\left(p_j^{\cdot},\left[p_i\ p_{i+1}\right]\right)\right\} \tag{8}$$

Result is a set C of n correspondence (p_j , p''_j).

Compute the displacement estimation q_{min} that minimize the mean square error between pairs of C. The Criterion to minimize is q:

$$E_{dist}(q) = \sum_{i=1}^{n} d\left(q\left(p_j\right), p_j^{''}\right)^2 \tag{9}$$

If there is convergence the estimation is q_{min}, otherwise we iterate again with $q_{k+1} = q_{min}$.

A detailed description of the ICP algorithm we use is given in the first original ICP method (Besl & McKay, 1992), (Ouadah et al., 2013). According to the original ICP algorithm, the data are tested in the experiment in the Matlab - MathWorks® environment simulation.

Laser range finder

Laser scanner or laser range finder are becoming a common sensing device to aid the steering device to avoid obstacles, and im mapping environments for use in robotics and

agricultural applications (Jiménez et al., 1999), (Lee & Ehsani, 2008). For measure distance in area we use laser range finder Hokuyo URG 04LX. This uses semiconductor laser beam of 745 nm to measure distance. It has a fixed scanning range of 240° with 0, 36° angular resolution. Maximum measurement distance reach 4500 mm, when measureable object is white paper. These conditions are tested by manufacturer. The scanner and device for data collector communicate via RS232 port with set up baud rate of 19, 2 – 750 Kbps or USB port with a baud rate 9 Mbps.

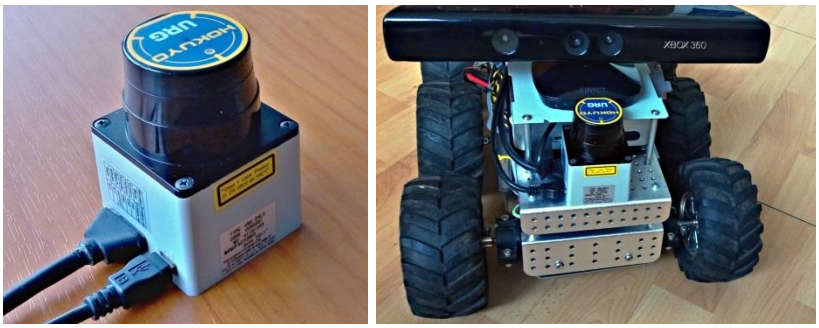

Fig. 1. Laser range finder Hokuyo URG 04LX and their application on the mobile robotic platform
Obr. 1. Laserový skener Hokuyo URG 04LX na mobilnej robotickej platforme

Max. range [1] [*mm*]	4500
Resolution[2] [*mm*]	1
Scan rate [3] [*scans/sec*]	10
Power voltage [4] [*V*]	5 ± 5%
Current [5] [m*A*]	500
Measurement error [6] [%]	±2

[1]Maximálny rozsah, [2]Rozlíšenie, [3]Rýchlosť skenovania, [4]napájacie napätie, [5]Odoberaný prúd, [6]chyba merania

RESULTS

Data collection for experimental purposes was performed under laboratory conditions. By the laser scanner, the selected interior area was scanned when individual distances in the scanning range were obtained. In experiments, the laser scanner was placed in the designated location in area. For data processing, images were created as basic without transformation as well as transformation in the form of displacement and rotation.

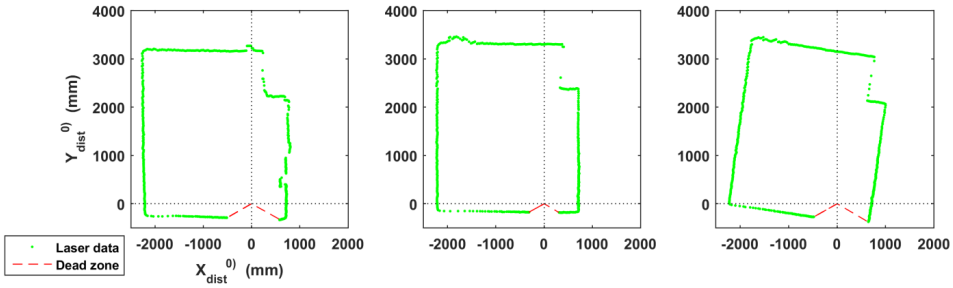

Fig. 2. Visualised data taken with Laser range finder Hokuyo URG 04LX, in interior area. First scan (from left to right) is reference scan, second translate and third rotate.
Obr. 2. Vizualizácia údajov nasnímaných laserovým skenerom Hokuyo URG 04LX, v interiérovom priestore. Prvý scan (zľava doprava) je referenčný scan, druhý posunutý a tretí pootočený. [0)] Súradnice vzdialenosti v smere osi X a Y

Figure 2 shows a visualization of measured data by a laser scanner, where the first visualization is a reference data set. The second set consists of shifting a laser scan in the measuring plane by a distance of 170 mm. A third set of data is created by rotating the laser scanner by 30 degrees in a plane perpendicular to the plane of measurement.

The sets of data obtained are metrics and are also intended as input data to the ICP algorithm. The maximum range of measured data for each set is 682, which is the number of measurement steps in the laser range of the laser scanner. Each element of the set can acquire the maximum value given by the distance measure of laser scanner.

Table 2. Elapsed time for metrics with different number of data set
Tabuľka 2. Výpočtový čas pre jednotlivé metriky pri rôznych počtoch údajov v množine

Count of data / **Elapsed time for metric**	**21**	**43**	**85**	**171**	**341**	**682**
Euclidean [1)] [*ms*]	0,14484	0,14821	0,26851	0,435	0,88492	4,97
Mahalanobis [2)] [*ms*]	0,48841	0,40998	0,73863	1,1385	1,6697	6,22
Manhattan [3)] [*ms*]	0,14725	0,10586	0,19873	0,28246	0,45425	1,54

[1)]Euklidovská metrika, [2)]Mahalanobisova metrika, [3)]Manhattanská metrika

Three types of most commonly used metrics were measured in experimental measurements. Since the ICP algorithm consists of the several steps described above, it is necessary to know the calculation time when processing the data. A key step in the algorithm is to evaluate the distance between data set using metrics. Based on this, the ICP algorithm determines the correspondence between the points of the reference data and the comparison data.

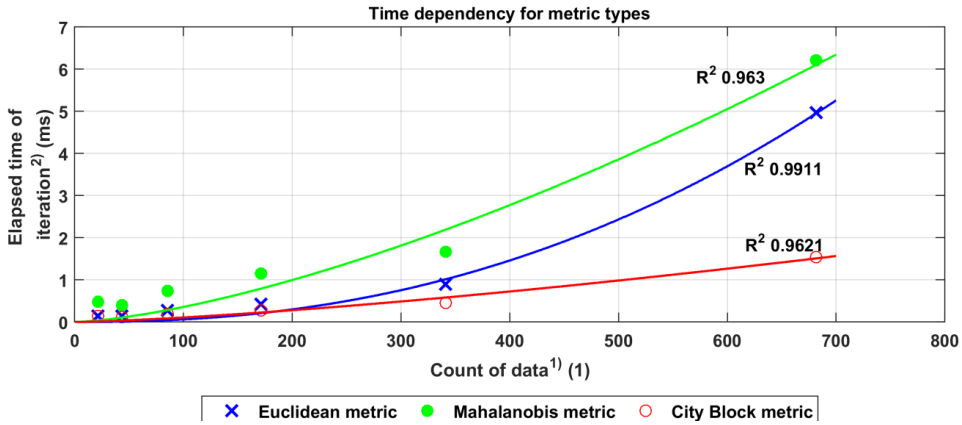

Fig. 3. Calculation time dependence on the number of data in a set for different metrics
Obr. 3. Závislosť výpočtového času od počtu dát v množine pre rôzne metriky
[1)]Počet údajov, [2)]Výpočtový čas iterácie

In experiments, it was found that the largest computational time has the Mahalanobis type, while the smallest calculation time has a Manhattan-type metric. When comparing dependencies, we see the similarity of the Mahalanobis and Euklidean metrics. The calculating time of the Mahalanobis metric is the largest because of the covariance between the data in set. The dependence of the calculation time on the number of data in a set is exponential for all cases. The ICP algorithm with Euclidean metrics was applied to a set data scanned by a laser scanner. The input data was the reference laser data and the data of the scanner shifted from the basic position by 170 mm. The algorithm, by calculating the distance between the data and the minimization of the error quantity, gradually converges to a minimum, thereby achieving a solution search and match of reference data with displacement data.

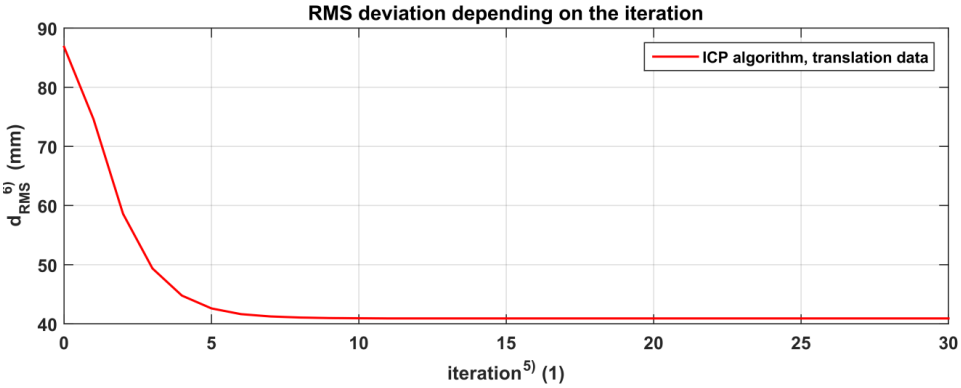

Fig. 4. Root-mean-square error depending on the number of iterations of the ICP algorithm
Obr. 4. Stredná kvadratická chyba v závislosti od počtu iterácií ICP algoritmu
[5)]Iterácia , [6)]Root-mean-square error

By increasing the number of iterations in the ICP algorithm, the Root-mean-square error decreases, finding the right solution. The right solution is to match the laser scanner reference data to the current scanned data. When creating an area map with a laser scanner for the needs of mobile robot where the SLAM algorithm is applied in the process, the rotation of both the robot and the scanning device occurs in addition to the displacement. For this reason, it is also necessary to use the ICP algorithm to consider the pointer scene, and take into account the data generated by it and to compare it with the reference data, which are not rotated. In algorithm is using Euclidean metrics. The algorithm was applied to a set data scanned by a laser scanner. The input data was the reference laser data and the data of the scanner rotated from the basic position by 30 degree.

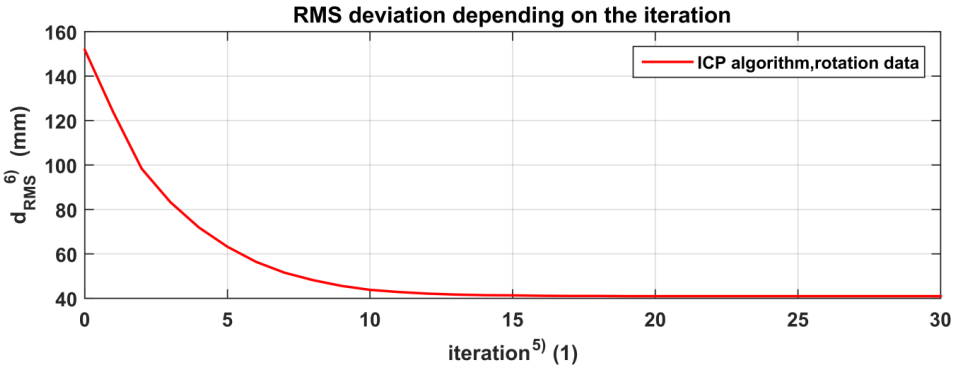

Fig. 5. Root-mean-square error depending on the number of iterations of the ICP algorithm
Obr. 5. Stredná kvadratická chyba v závislosti od počtu iterácií ICP algoritmu
[5)]Iterácia , [6)]Root-mean-square error

As in the case of translation using an ICP algorithm for measured data and for data processing with rotation, a certain number of iterations are required until the algorithm converges to a minimum.

DISCUSSION

The use of metrics or metric spaces is very widespread in areas where it is necessary to determine the similarity of data in the files to be scanned. These data can be written into vectors, thereby creating one or more multidimensional matrices. Then the data is processed using mathematical matrix apparatus. In computational algorithms, emphasis is placed on the complexity of computational computations as well as on the time required for data processing.

From amongst the metrics that can be applicable to the ICP algorithm, Mahalanobis metric has the greatest performance and time requirements. On the other hand, the smallest demand has a Manhattan metric (Mora et al., 2016). In many cases, the Euclidean metric is used (Minguez et al., 2006). For its simplicity and relatively low computational demands, the Euclidean metric is also used in ICP algorithms where it is necessary to determine the consistency of the data obtained by the laser scanner in the mapping process (Lakrouf & Azouaoui, 2015).

In our case, using the ICP algorithm for scanned data when shifting even when rotated, it confirmed the convergence of the algorithm in both cases. The results show that a certain number of iterations are needed to arrive at the correct solution, which, when overtaken, the root-mean-square error remains the same, but the computation time increases. For this reason, it is necessary to determine the number of iterations appropriately. In our case, if the scanner is able to scan 682 data in a single data set, the ICP algorithm is enough to determine the correct solution for 10 ÷ 15 iterations.

CONCLUSION

This article dealt with the issue of selected metrics for determining the similarity of data in individual datasets. The selection was based on three types of metrics, such as the Euclidean, Mahalanobis and Manhattan metrics. Their parameters have been compared with respect to the calculation time, depending on the number of data in the set. When navigating mobile robots in the process mapping process, the ICP algorithm has been recently expanded. In this algorithm, the Euclidean metric is used in our case. RMS was tracked based on the number of iterations in order to get the right solution. Algorithm convergence to the correct solution was confirmed, using data from the Hokuyo URG 04LX laser scanner.

The assumption of using the ICP algorithm along with various metrics is in the field of agriculture for environment mapping and metric map creation around the environment. In the future work, the ICP algorithm and SLAM algorithm are expected to be used as well as the results of this work to create a mobile robotic navigation system. When navigating and localizing, the characteristics of the environment, such as the size or shape of objects in the fields of agriculture and forestry, will be used.

LITERATURE

ARMESTO, L., MINGUES, J., MONTESANO, L., 2010. A generalization of the metric-based Iterative Closest Point technique for 3D scanmatching. In: *International Conference on Robotics and Automation (ICRA) 2010:* Anchorage, 2010.

BELSHAW, MS., GREENSPAN, MA., 2009. A high speed iterative closest point tracker on an FPGA platform. In: *International Conference on Computer Vision Workshops 2009:* Zurich, 2009.

BESL, PJ., McKAY, ND., 1992. A method for registration of 3-D shapes. In: *IEEE Transactions on Pattern Analysis and Machine Intelligence 1992:* USA, 1992.

BISPO, EM., FISHER, RB., 1996. Free - Form Surface Matching for Surface Inspection. In: Mulineiux, G. (ed.): *6. IMA Conference on the Mathematics of Surfaces*. Brunel University UK, 1996.

CERIOLI, A., 2005. K – Means Cluster Analysis and Mahalanobis Metrics: A problematic Match or An novel Overlooked Opportunity?. *Statistica Application* 17(1), pp 61-73.

HE, Y., LIANG, B., LI, S., HE, J. An Iterative Closest Points Algorithm for Registration of 3D Laser Scanner Point Clouds with Geometric Features. *Sensor* 17(8), pp 1862. DOI: 10.3390/s17081862.

GUIVANT, J. E., MASSON, R. F., NEBOT, M. E., 2002. Simultaneous Localization and Map Building Using Natural Features and Absolute Information. *Robotics and Autonomous Systems*

2(3), pp 79-90. DOI: doi.org/10.1016/S0921-8890(02)00233-6
GUO, H., WANG, G., HUANG, L., HU, Y., YUAN, C., LI, R., 2016. A Robust and Accurate Two-Step Auto-Labeling Condition alI Iterative Closest Points (TACICP) Algorithm for Three-Dimensional Multi-Modal Carotid Image Registration. *PlosOne* 11(2), pp 1-22. DOI: doi.org/10.1371/journal.pone.0148783.
JIMÉNEZ, A.R., JAIN, A.K., CERES, R., PONS, J.L., 1999. Automatic fruit recognition: a survey and new results using Range/Attenuation images. *Pattern Recognition* 32(10), pp 1719-1736. DOI: doi.org/10.1016/S0031-3203 (98)00170-8.
KONECNY, J., PRAUZEK, M., HLAVICA, J., 2016. ICP Algorithm in Mobile Robot Navigation: Analysis of Computational Demands in Embedded Solutions. *IFAC-PapersOnline* 49(25), pp 396-400. DOI: doi.org/10.1016/j.ifacol.2016.12.079.
KYEONG-HAWN, L., ESHANI, R., 2008. Comparison of two 2D laser scanners for sensing object distances, shapes, and surfacepatterns. *Computers and Electronics in Agriculture* 60(2), pp 250-262. DOI: doi.org/10.1016/j.compag.2007.08.007.
LACROIX, S., MALLET, A., BONNAFOUS, D., BAUZIL G., FLEURY, S., HERB, M., CHATILA, R., 2002. Autonomous rover navigation on unknown terrains: Functions and integration. *International Journal of Robotics Research* 21(10-11), pp 917-942.
MINGUEZ, J., MONTESANO, L., LAMIRAUX, L., 2006. Metric-based iterative closest point scan matching for sensor displacement estimation. In: *IEEE Transactions on Robotics 2006:* USA, 2006.
MINGUEZ, J., MONTESANO, L., MONTANO, L., 2004. An architecture for sensor-based navigation in realistic dynamic and trouble some scenarios. In: *IEEE Int. Conf. on Intelligent Robot and Systems 2004:* Japan, 2004.
MONTESANO, L., MINGUEZ, J., MONTANO, L., 2005. Modeling the static and the dynamic parts of the environment to improve sensor-based navigation. In: *Insubmitted to the IEEE International Conference on Robotics and Automation (ICRA):* Spain, 2005.
MORA, H., MORA-PASCUAL, H., GARCõÂA-CHAMIZO JM., JIMENO-MORENILA A., 2006. Real-time arithmetic unit. In: *Real-Time Systems:* 34(1), pp 53-79
MORA, H., MORA-PASCUAL, J., GARCõÂA-CHAMIZO A., MARTõÂNEZ P., 2016. Computational Analysis of Distance Operators for the Iterative Closest Point Algorithm. In: *PLoS ONE:* 11(10), pp 1-19. DOI: 10.1371/journal.pone.0164694.
RINGDAHL, O., HOHNLOSER, P., HELLSTROM T., HOLMGREN J., LINDROOS O 2013. Enhanced Algorithms for Estimating Tree Trunk Diameter Using 2D Laser Scanner. In: *Remote Sensing:* 5(10), pp 4839-7856. DOI: https:// doi.org/10.3390/rs5104839.
RUSINKIEWICZ, S., LEVOY, M. 2001. Efficient Variants of ICP Algorithm. In: *Proceedings Third International Conference on 3-D Digital Imaging and Modeling:* Canada, 2001.
THANPATTRANON, P., AHAMED, T., TAKIGAWA T. 2015. Navigation of an Autonomous Tractor for a Row-Type Tree Plantation Using a Laser Range Finder—Development of a Point-to-Go Algorithm. In: *Robotics:* 4(3), pp 341-364. DOI: https://doi.org/10.3390/robotics4030341.
TIAR, R., LAKROUF, O., AZOUAOUI, O., 2015. Fast ICP-SLAM for a Bi-steerable Mobile Robot in Large Environments. In: *2015 Inernational Conference on Advanced Robotics:* Turkey, 2015.
TÓTH, L., HRUBÝ, D., CVIKLOVIČ, V., OLEJÁR, M., 2017, *Algorithms of Autonomous Mobile Robots*. Nitra: SUA Nitra, 2017. pp 136. ISBN 978-80-552-1681-2.
ZHENG, Y., LIU, J., WANG D., YANG R. 2012. Laser Scanning Measurements on Trees for Logging Harvesting Operations. In: *Sensor:* 12(7), pp 9273-9285. DOI: https:// 10.3390/s120709273.

Corresponding author:
Ing. Lukáš Vacho, +421 37 641 4763, e-mail: xvacho@is.uniag.sk

TOOTH CONTACT ANALYSIS OF SPUR GEAR PAIRS HAVING NORMAL STRAIGHT TEETH IN THE FUNCTION OF THE MODULE

KONTAKTNÁ ANALÝZA ZUBU DVOJICE ČELNÝCH OZUBENÝCH KOLIES S PRIAMYMI ZUBMI VO FUNKCII MODULU

Sándor Bodzás

Department of Machanical Engineering, Faculty of Engineering, University of Debrecen, Debrecen, Ótemető str. 2-4, 4028, email: bodzassandor@eng.unideb.hu

ABSTRACT: The aim of this publication is analysis of the normal stress, the normal elastic strain and the normal directional deformation of spur gear pairs having normal straight profile in the function of the module. A computer aided program was worked out to design of many types of gear pairs. After the designing the three dimensional computer aided model could be generated by a designer software. Beside the same loads and boundary conditions tooth contact analysis (TCA) could be done on the tooth connection zone. The distribution of the analysed TCA parameters on the tooth surfaces has to be analysed.

Key words: module, TCA, stress, strain, deformation

ABSTRAKT: Cieľom tejto publikácie je analýza normálového napätia, normálovej elastickej deformácie a normálovej smerovej deformácie párov čelných ozubených kolies, ktoré majú rovnobežný profil vo funkcii modulu. Počítačový program bol vypracovaný na návrh mnohých typov dvojíc kolies. Po navrhovaní trojrozmerného počítačového modelu by mohol byť generovaný návrhárskym softvérom. Popri rovnakých zaťaženiach a hraničných podmienkach by sa mohla vykonať analýza kontaktu zuba (TCA) v mieste pripojenia zuba. Malo by sa realizovať rozloženie analyzovaných TCA parametrov na povrchu plochy zuba.

Kľúčové slová: aerosól monitor, kalibračné faktory, brúsenie, prach, buk

INTRODUCTION

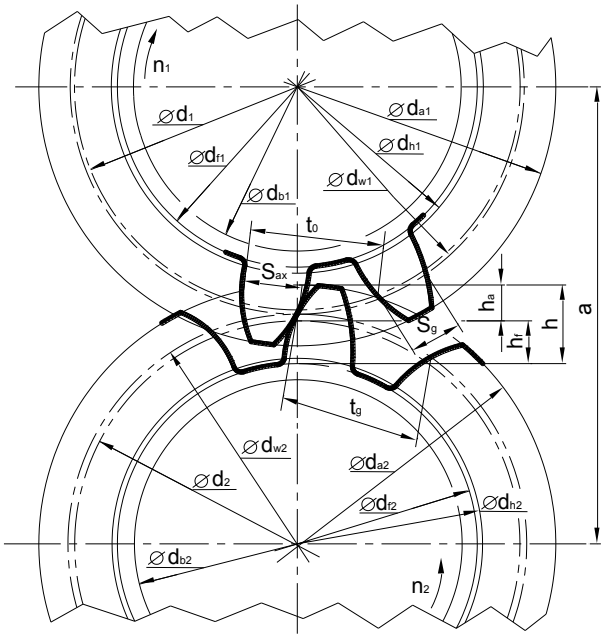

Figure 1. The parameters of the spur gear pair having normal straight teeth
Obr. 1. Parametre kolies s čelným ozubením s priamymi zubmi

The spur gear pairs having normal straight profile is widely used on the field of medical equipments, vehicles, measuring devices, etc. That is why the finding of optimum shape of the gear pairs is important in aspects of load and life [DUDÁS, ERNEY, LITVIN, TERPLÁN].

The main parameters of a spur gear pair having normal straight profile could be seen on Figure 1.

Table 1. Main parameters of the spur gear pair having normal straight
Tabuľka 1. Hlavné parameter čelných ozubených kolies

Notation	Nomination	Notation	Nomination
d_1, d_2	Pitch circle diameter	h_f	Dedendum
d_{f1}, d_{f2}	Root circle diameter	h_a	Addendum
d_{a1}, d_{a2}	Tip circle diameter	h	Whole depth
d_{h1}, d_{h2}	Base circle diameter	t_0	Circular pitch
d_{w1}, d_{w2}	Rolling circle diameter	S_{ax}	Tooth thickness
c	Bottom clearance	m	Module
h_w	Working depth	z	Number of teeth
a_1	Centre distance	j_s	Backlash
d_{b1}, d_{b2}	Involute base circle diameter	α_0	Base profile angle
t_g	Circular pitch along working pitch circle	S_g	Tooth thickness along working pitch circle

Addendum modification is applied on the contact gears for designing the spur gear pair having normal straight tooth. In this case the meshing of the tooth of the mating gears is not along the pitch circle but along the rolling circle. That is why addendum modification is used which could be positive or negative in the function of the tool setting (±xm) (Figure 2) [ERNEY, LITVIN, TERPLÁN].

DESIGNING OF SPUR GEARS HAVING NORMAL STRAIGHT TEETH

There are many parameters which are needed to determine for the designing of this gear pairs. For the comperative TCA analysis many types of spur gear have to be designed. We have worked out a computer program for easing of the designing calculations. The main input parameters are the module (m), the number of teeth (z_1 and z_2), the bottom clearance factor (c^*), the base profile angle (α_0) and the angle of contact (α_g).

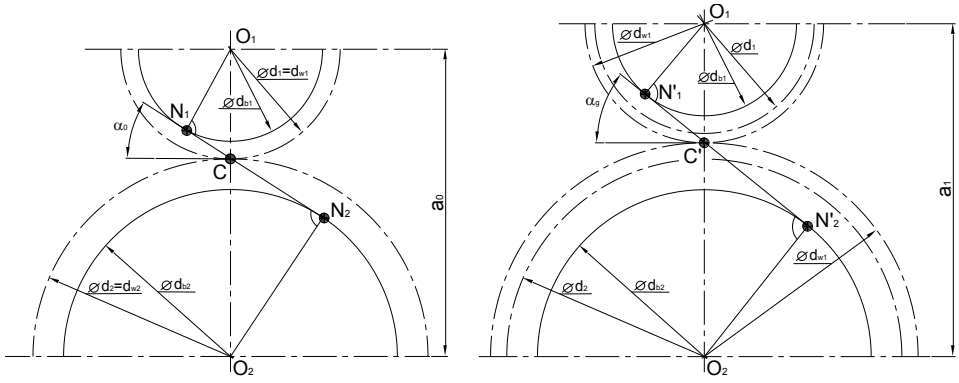

a) x-zero gear drive b) spur gear drive having normal straight

Figure 2. The definition of the base profile angle (α_0) and the angle of contact (α_g)
Obr. 2. Definícia základného uhla profilu a uhla záberu

Five spur gear drives having normal straight teeth and different modules are designed for the analysis (Table 2). Beside the constancy of other parameters only the modules are changed. The formula of the sum of the addendum modifications is [TERPLÁN]

$$\sum x = x_1 + x_2 = \frac{z_1 + z_2}{2} \cdot \frac{inv\alpha_g - inv\alpha_0}{tg\alpha_0} \tag{1}$$

Table 2. The parameters of the designed spur gear drive pairs having normal straight teeth
Tabuľka 2. Parametre navrhnutého čelného ozubenia s rovnými zubami

Parameters	Gear drive I.	Gear drive II.	Gear drive III.	Gear drive IV.	Gear drive V.
Axial module (m) [mm]	5	10	15	20	25
Number of tooth of the driving gear (z_1)	25	25	25	25	25
Number of tooth of the driven gear (z_2)	35	35	35	35	35
Centre distance (a_1) [mm]	153.126	306.253	459.380	612.506	765.633
Elementary centre distance (a_0) [mm]	150	300	450	600	750
Addendum (h_a) [mm]	4.885	9.770	14.655	19.540	24.425
Bottom clearance (c) [mm]	1	2	3	4	5
Dedendum (h_f) [mm]	5.885	11.770	17.655	23.540	29.425
Circular pitch (t_0) [mm]	15.708	31.415	47.123	62.831	78.539
Circular pitch along the working circle (t_g) [mm]	16.035	32.070	48.106	64.141	80.177
Backlash (j_s) [mm]	0.801	1.603	2.405	3.207	4.008
Whole depth (h) [mm]	10.770	21.540	32.310	43.080	53.850
Working depth (h_w) [mm]	9.770	19.540	29.310	39.080	48.850
Tooth thickness (S_{ax1}) [mm]	8.802	17.604	26.407	35.209	44.011
Pitch circle diameter of the driving gear (d_1) [mm]	125	250	375	500	625
Tip circle diameter of the driving gear (d_{a1}) [mm]	137.375	274.751	412.127	549.502	686.878
Root circle diameter of the driving gear (d_{f1}) [mm]	115.835	231.671	347.506	463.342	579.177
Basic circle diameter of the driving gear (d_{ak1}) [mm]	117.461	234.923	352.384	469.846	587.307
Working pitch circle diameter (d_{w1}) [mm]	127.605	255.211	382.816	510.422	638.028
Tooth thickness (S_{ax2}) [mm]	9.349	18.698	28.047	37.396	46.745
Pitch circle diameter of the driven gear (d_2) [mm]	175	350	525	700	875
Tip circle diameter of the driven gear (d_{a2}) [mm]	188.418	376.835	565.253	753.671	942.089
Root circle diameter of the driven gear (d_{f2}) [mm]	166.877	333.755	500.633	667.510	834.388
Basic circle diameter of the driven gear (d_{ak2}) [mm]	164.446	328.892	493.338	657.784	822.231
Working pitch circle diameter (d_{w2}) [mm]	178.647	357.295	535.943	714.591	893.239
The x_1 addendum modification [mm]	0.260	0.260	0.260	0.260	0.260
The x_2 addendum modification [mm]	0.410	0.410	0.410	0.410	0.410
The sum of the addendum modifications () [mm]	0.671	0.671	0.671	0.671	0.671
Specific centre distance increment (y) [mm]	0.625	0.625	0.625	0.625	0.625
Transmission ratio (i)	1.4	1.4	1.4	1.4	1.4
Base profile angle (α_0) [°]	20	20	20	20	20
Angle of contact (α_g) [°]	23	23	23	23	23

The geometry of the spur gear is drown by our developed computer program. Based on the involute profile point and the calculated parameters the computer aided model (CAD) could be prepared by SolidWorks Designer Software (Figure 3) [BODZÁS, TERPLÁN]. The outside diameters of the gears were adopted proportional:

$$d_{hole1} = 12 \cdot m \tag{2}$$

$$d_{hole1} = 18 \cdot m \tag{3}$$

The tooth length of the gears was chosen to be each.

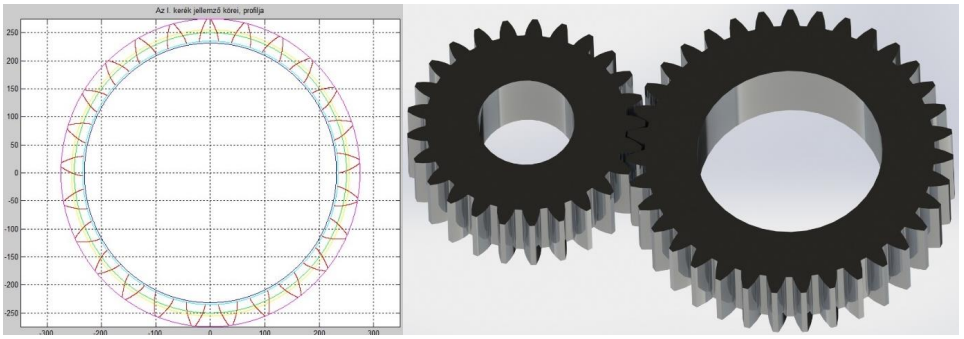

Figure 3. Designing of the CAD model of the spur gear having normal straight teeth
Obr. 3. Návrh CAD modelu čelného ozubenia

MAKING THE MESH OF FEM ANALYSIS

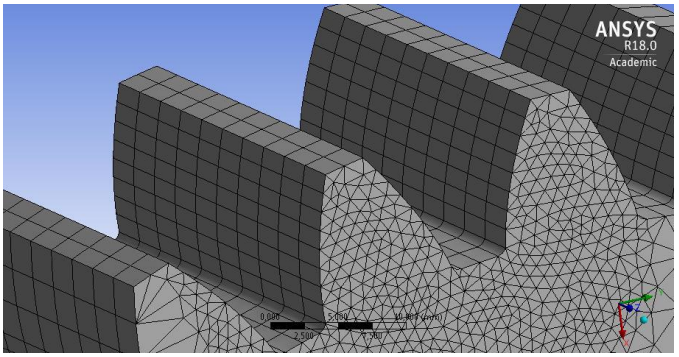

Figure 4. Application of the mesh of FEM
Obr. 4 Aplikácia siete MKP

For the analysis of the contact points, Ansys R18.0 Finite Element Modeling (FEM) software was used. In the tooth contact zone, 0.15 frictional factor was applied.

During the calculations tetrahedron meshing was applied on the face surfaces, while tooth lengths were divided into 10 equal parts [GONZALES 2015,2017, LITVIN, PÁC-ZELT]. The density of the meshing was automatic outside the tooth contact zone. Inside the tooth contact zone 1 mm density meshing was applied (Figure 4).

SETTING THE LOADS AND BOUNDARY CONDITIONS

During the analysis, the material of the drive pairs was structural steel (Table 2). The driving cog wheel ($z_1 = 25$) was loaded by 100 Nm torque (Figure 5).

Table 3. Parameters of the material
Tabuľka 3. Parametre materiálu

Density	7850 kg/m^3
Yield limit	250 MPa
Ultimate strength	460 MPa

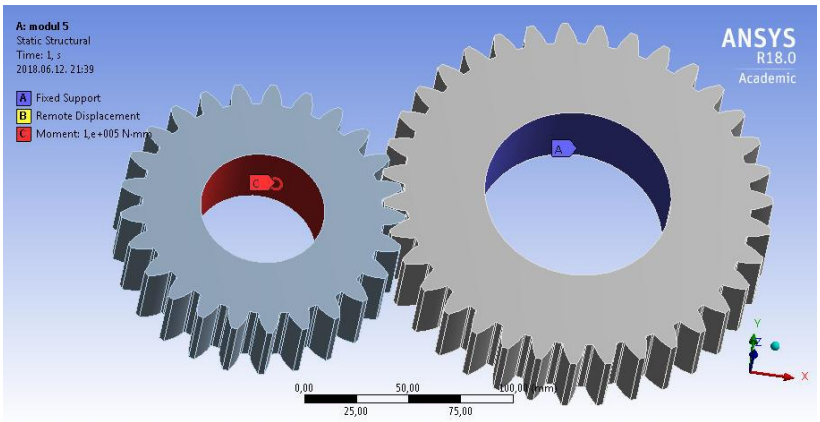

Figure 5. Setting the loads and boundary conditions
Obr. 5. Nastavenia zaťaženia a okrajových podmienok

Five degrees of freedom of the driving spur gear were fixed GONZALES 2015,2017, LITVIN]. Only the rotational movement around the rotational shaft was allowed. In case of the driven cog wheel fixed support was applied (Figure 5).

NORMAL STRESS ANALYSIS IN THE CONTACT ZONE

Figure 6 shows normal tension dispersions – on the driving and driven gears contact tooth surfaces – which are the effect of the load of 100 Nm torque.

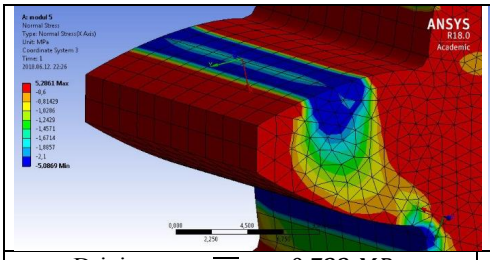	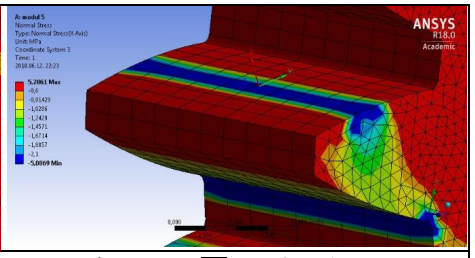
Driving gear, $\overline{\sigma_n} = -0{,}723\ MPa$	Driven gear, $\overline{\sigma_n} = -0{,}441\ MPa$
Module 5 mm	
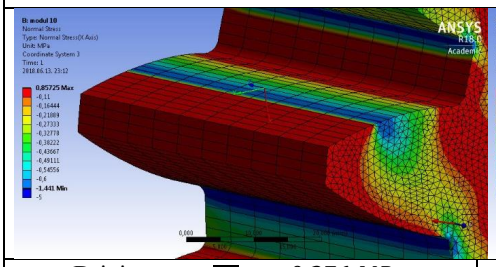	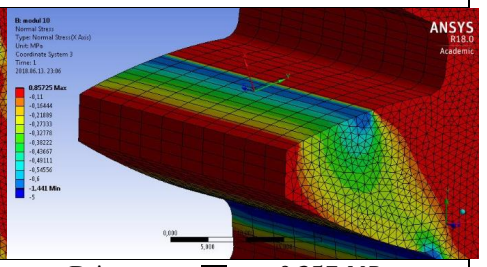
Driving gear, $\overline{\sigma_n} = -0{,}276\ MPa$	Driven gear, $\overline{\sigma_n} = -0{,}257\ MPa$
Module 10 mm	
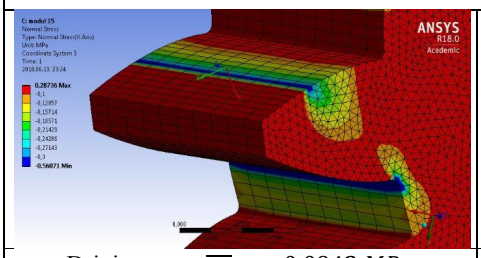	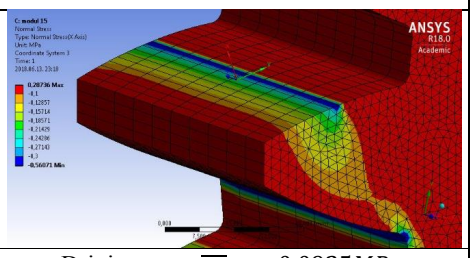
Driving gear, $\overline{\sigma_n} = -0{,}0942\ MPa$	Driving gear, $\overline{\sigma_n} = -0{,}0925 MPa$
Module 15 mm	
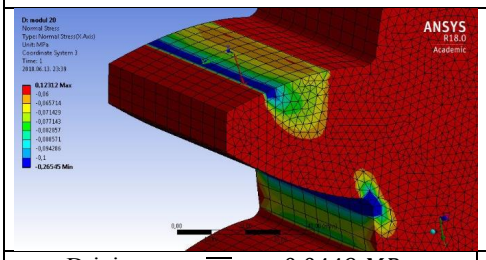	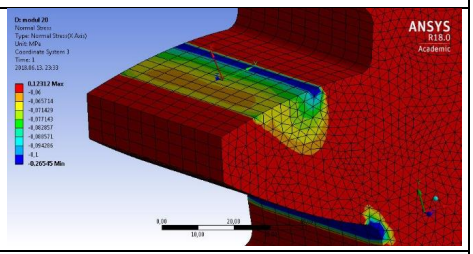
Driving gear, $\overline{\sigma_n} = -0{,}0449\ MPa$	Driving gear, $\overline{\sigma_n} = -0{,}0456\ MPa$
Module 20 mm	

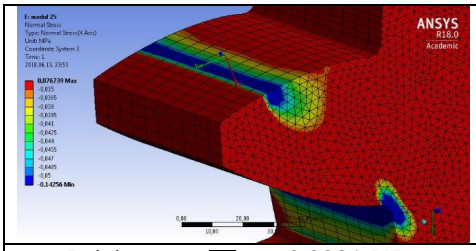

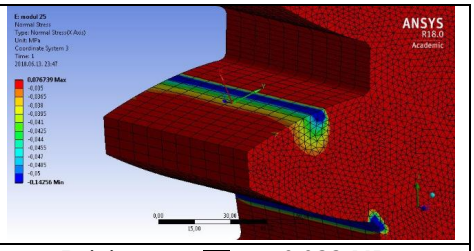

Driving gear, $\overline{\sigma_n} = -0{,}0221\ MPa$	Driving gear, $\overline{\sigma_n} = -0{,}023\ MPa$
Module 25 mm	

Figure 6. Normal stress results on the contact surfaces
Obr. 6. Normálové napätie na kontaktných plochách

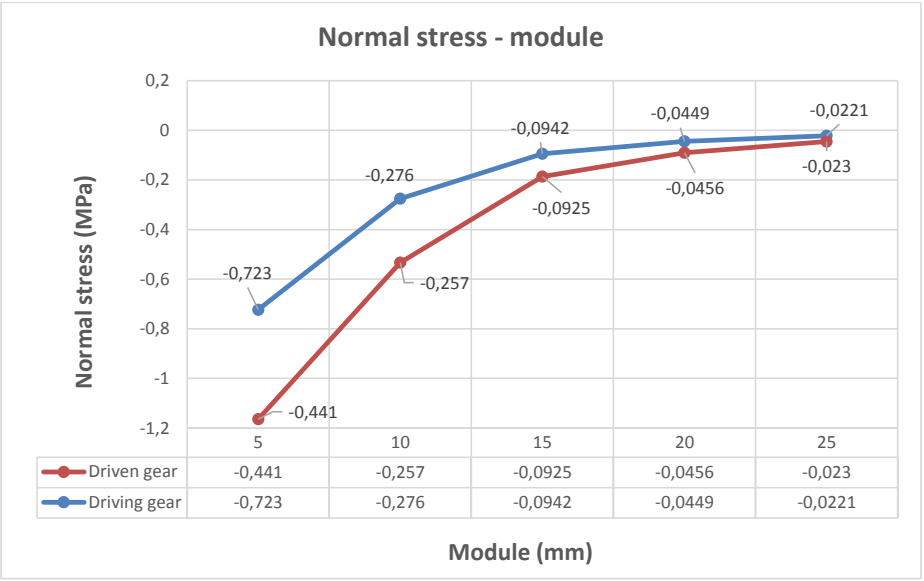

Figure 7. The normal stress results in the function of the module
Obr. 7. Normálové napätie vo funkcii modulu

Based on Figure 6 and 7 it can be stated that on the tooth surfaces of the driving and driven spur gears in the contact zone, perpendicular to the tooth surface, the values of the normal tension decrease in absolute value as a function of enhancing the value of the module.

NORMAL ELASTIC STRAIN ANALYSIS IN THE CONTACT ZONE

Figure 8 shows normal elastic strain dispersions – on the driving and driven gears contact tooth surfaces – which are the effect of the load of 100 Nm torque.

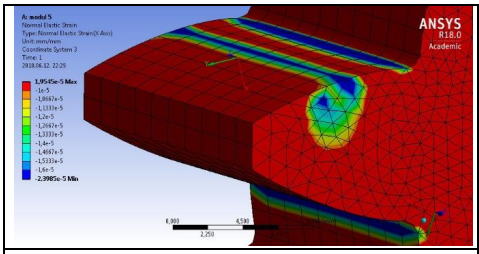	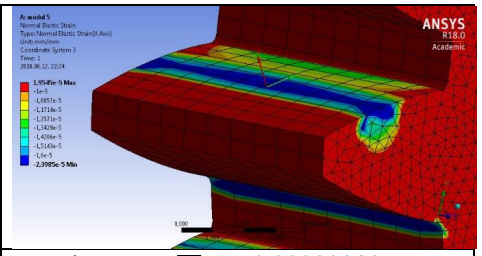
Driving gear, $\overline{\varepsilon_n} = -0{,}00000715\ mm$	Driven gear, $\overline{\varepsilon_n} = -0{,}00000923\ mm$
Module 5 mm	
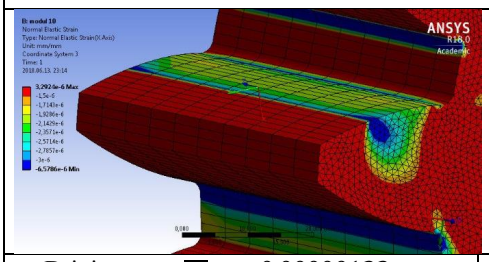	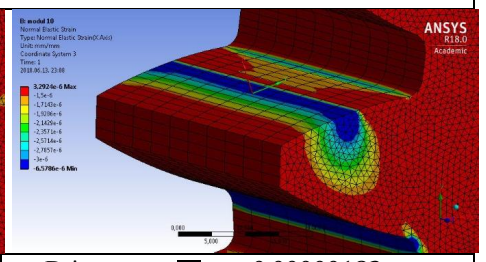
Driving gear, $\overline{\varepsilon_n} = -0{,}00000133\ mm$	Driven gear, $\overline{\varepsilon_n} = -0{,}00000182\ mm$
Module 10 mm	
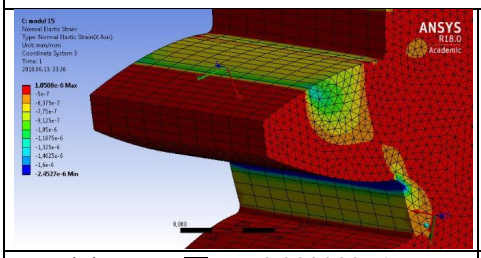	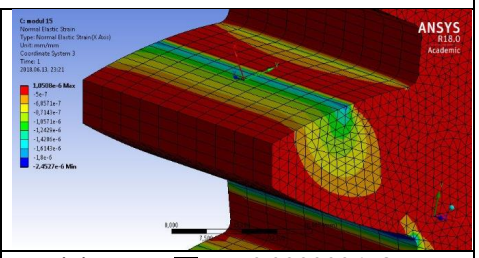
Driving gear, $\overline{\varepsilon_n} = -0{,}00000046\ mm$	Driving gear, $\overline{\varepsilon_n} = -0{,}000000672\ mm$
Module 15 mm	
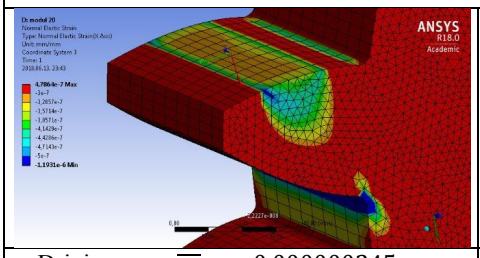	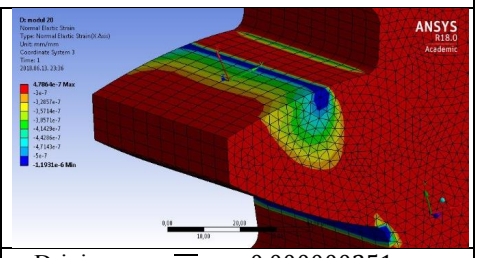
Driving gear, $\overline{\varepsilon_n} = -0{,}000000245\ mm$	Driving gear, $\overline{\varepsilon_n} = -0{,}000000251\ mm$
Module 20 mm	

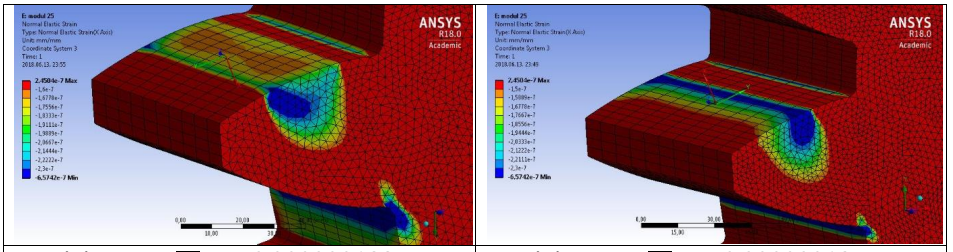

Driving gear, $\overline{\varepsilon_n} = -0{,}000000122\ mm$	Driving gear, $\overline{\varepsilon_n} = -0{,}000000134\ mm$
Module 25 mm	

Figure 8. Normal elastic strain results on the contact surfaces
Obr. 8. Normálová elastická deformácia na kontaktných plochách

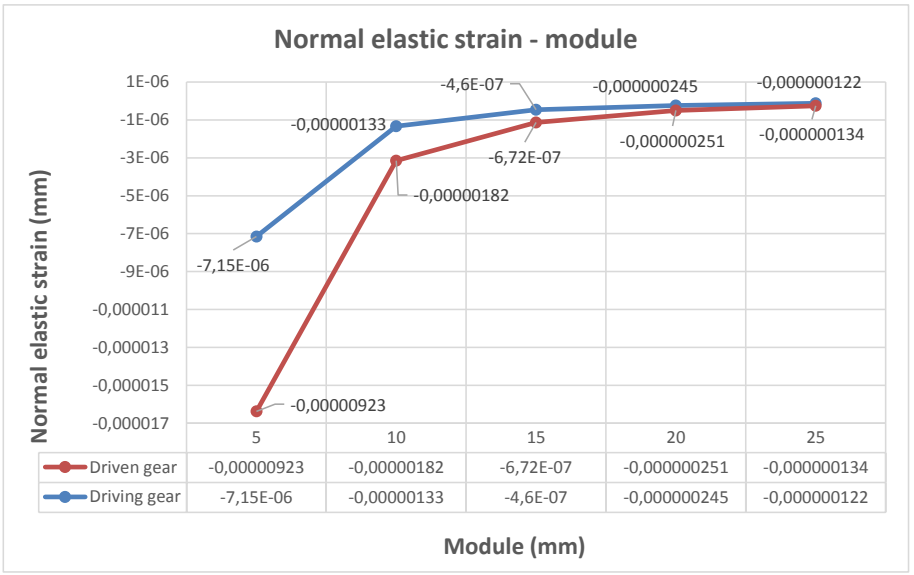

Figure 9. The normal elastic strain results in the function of the module
Obr. 9. Normálová elastická deformácia vo funkcii modulu

Based on Figure 8 and 9 it can be stated that on the tooth surfaces of the driving and driven spur gears in the contact zone, perpendicular to the tooth surface, the values of the normal elastic strain decrease in absolute value as a function of enhancing the value of the module.

NORMAL DEFORMATION ANALYSIS IN THE CONTACT ZONE

Figure 10 shows normal deformation dispersions – on the driving and driven gears contact tooth surfaces – which are the effect of the load of 100 Nm torque.

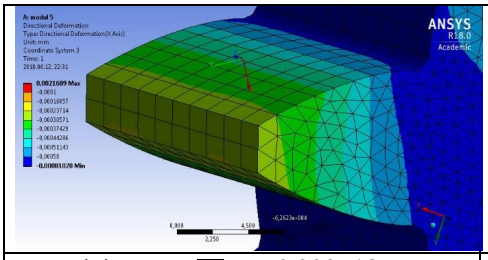	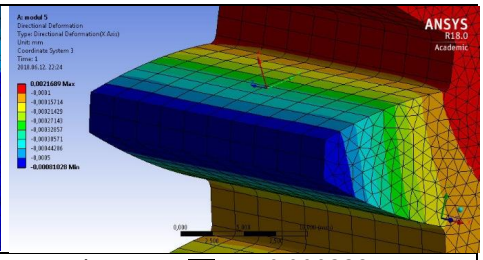
Driving gear, $\overline{u_x} = -0{,}000412\ mm$	Driven gear, $\overline{u_x} = -0{,}000339\ mm$
Module 5 mm	
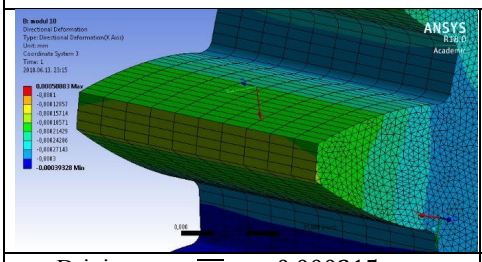	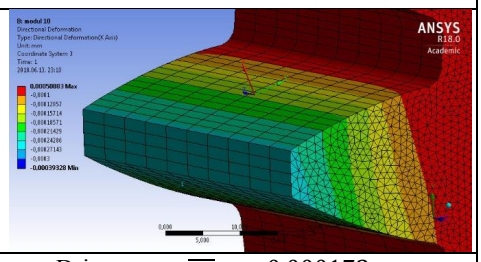
Driving gear, $\overline{u_x} = -0{,}000215\ mm$	Driven gear, $\overline{u_x} = -0{,}000173\ mm$
Module 10 mm	
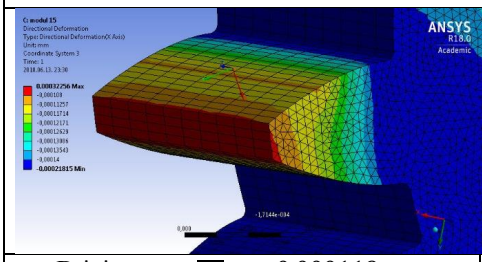	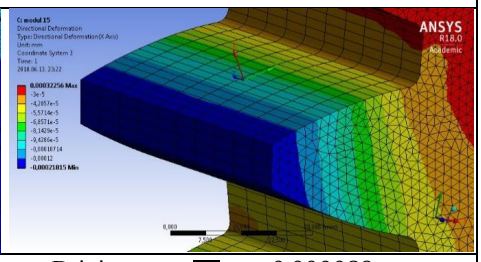
Driving gear, $\overline{u_x} = -0{,}000119\ mm$	Driving gear, $\overline{u_x} = -0{,}000089\ mm$
Module 15 mm	
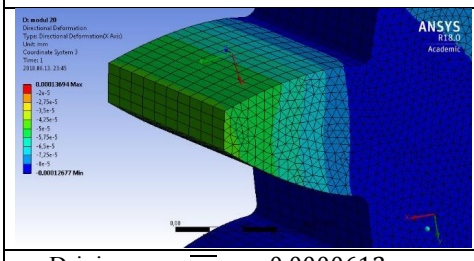	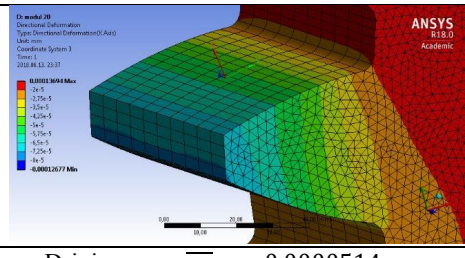
Driving gear, $\overline{u_x} = -0{,}0000612\ mm$	Driving gear, $\overline{u_x} = -0{,}0000514\ mm$
Module 20 mm	

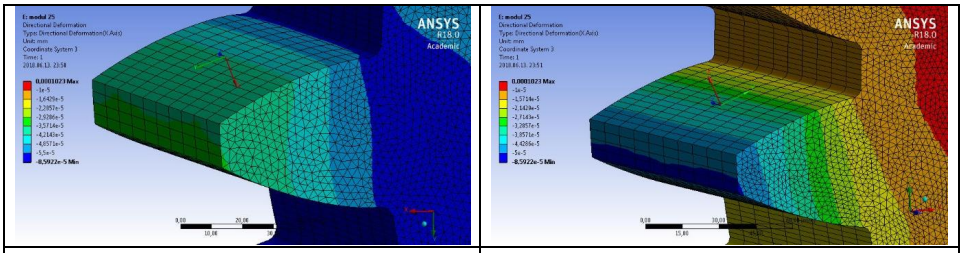

Driving gear, $\overline{u_x} = -0{,}0000428\ mm$	Driving gear, $\overline{u_x} = -0{,}0000348\ mm$
Module 25 mm	

Figure 10. Normal deformation results on the contact surfaces
Obr. 10. Normálová deformácia na kontaktných plochách

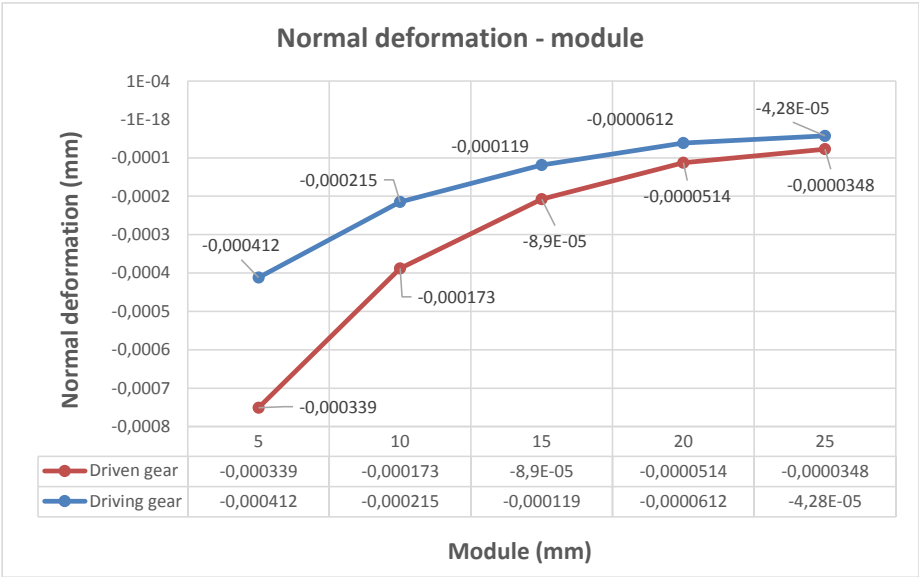

Figure 11. The normal elastic strain results in the function of the module
Obr. 11. Normálová elastická deformácia vo funkcii modulu

Based on Figure 10 and 11 it can be stated that on the tooth surfaces of the driving and driven spur gears in the contact zone, perpendicular to the tooth surface, the values of the normal deformation decrease in absolute value as a function of enhancing the value of the module.

CONCLUSION

Spur gear drives having normal straight is widely used in the machine construction. In this case the tooth connection is on the rolling circle that is why the gears are produced with addendum modification. The objective of the addendum modification is to reach better connection and load conditions on the teeth.

The geometry of this gears were examined. A computer aided program was developed for designing of such gears. Using of this program many gear parameters could be modified that is why special gear CAD models could be created. Based on this CAD models TCA analysis could be done to analyse the gear connection between the teeth.

Five gears were designed in the function of the module. TCA analysis was done to determine the normal stress, normal elastic strain and normal deformation in the function of the module changing. Based on the results the diagrams were prepared to see the changings.

ACKNOWLEDGEMENT

This research was supported by the **János Bolyai Research Scholarship of the Hungarian Academy of Sciences.**

The work/publication is partly supported by the **EFOP-3.6.1-16-2016-00022** project. The project is co-financed by the European Union and the European Social Fund.

REFERENCES

BODZÁS, S., 2017. Computer aided designing and modelling of x-zero gear drive, International Review of Applied Sciences and Engineering, Volume 8, Number 1, Akadémiai Kiadó, pp. 93-97, ISSN 2062-0810, DOI 10.1556/1848.2017.8.1.13

BODZÁS, S.: Computer aided designing and modelling of spur gear pairs having normal and modified straight teeth, International Review of Applied Sciences and Engineering (during publication)

DUDÁS, I., 2011. Gépgyártástechnológia III., A. Megmunkáló eljárások és szerszámaik, B. Fogazott alkatrészek gyártása és szerszámaik, Műszaki Kiadó, Budapest

ERNEY GY., 1983. Fogaskerekek, Műszaki Könyvkiadó, Budapest, p. 460.

GONZALES PEREZ, I., FUENTES, A., 2017. Implementation of a finite element model for stress analysis of gear drives based on multi-point constraints, Mechanism and Machine Theory, Elsevier, pp. 35-47.

GONZALES PEREZ, I., RODA-CASANOVA, V., FUENTES, A., 2015. Modified geometry of spur gear drives for compensation of shaft deflections, Meccanica, DOI 10.1007/s11012-015-0129-9, pp. 1855-1867

LITVIN, F. L., FUENTES, A., 2004. Gear Geometry and Applied Theory, Cambridge University Press, 2004., ISBN 978 0 521 81517 8

TERPLÁN Z., 1975. Gépelemek IV., Kézirat, Tankönyvkiadó, Budapest, 1975., p. 220.

PÁCZELT, I., SZABÓ, T., BAKSA, A. A végeselem módszer alapjai, Miskolci Egyetem, p. 243.

EFFECT OF ELECTROSTATICDISCHARGES ON THE OIL DEGRADATION

VPLYV ELEKTROSTATICKÝCH VÝBOJOV NA DEGRADÁCIU OLEJOV

Michal Holúbek[1], Josef Pošta[1], Martin Pexa[1], Peter Kuchar[2], Michaela Slezáková[1]

[1]Department for Quality and Dependability of Machines, Faculty of Engineering, Czech University of Life Sciences. Kamýcka 129, 16500, Prague 6 – Suchdol, Czech Republic, holubekm@tf.czu.cz
[2]Department of Transport and Handling, Faculty of Engineering, Slovak University of Agriculture in Nitra, Tr. A. Hlinku 2, 949 76, Nitra, Slovakia, xkuchar@is.uniag.sk

ABSTRACT: The purity of lubricants is essential for the flawless condition and reliability of the fluid systems and is also reflected in the economical aspect of operation. Submitted paper is focused on the degradation processes of oils caused by electrostatic discharges, which may arise especially in the elements of hydraulic systems (for example filters) or another parts of machines. When the oil flows through the filter element, the filter layers and the oil are charged electro-statically and electrostatic discharge may occur. The purpose of this fundamental experiment was to verify the hypothesis that electric discharges lead to forming of oxidants (soft pollutants) in the oil. This potentially changes the lubricating ability of the oil and degradation process. To prove the theory, a model created from a car battery ignition was designed to emit electric discharges into four different oil samples. Consequently, a viscosity was measured and analysis of particle pollution were performed to see how was the oil effected. Based on the results, it is clear that the electric discharges have a negative impact on the lubricants properties and proceeding changes of particle amounts in oil are showed.

Key words: lubrication, oil degradation, viscosity, particles, oxidants

ABSTRAKT: Čistota mazív je nevyhnutným predpokladom pre bezchybný stav a spoľahlivosť tekutinových mechanizmov a odráža sa aj v ekonomickom aspekte prevádzky. Predkladaný článok sa zameriava na degradačné procesy olejov spôsobené elektrostatickými výbojmi, ktoré môžu vzniknúť najmä v prvkoch hydraulických systémov (napríklad filtroch) alebo iných častiach strojov. Keď olej prúdi filtračným systémom, vrstvy filtra a olej sa elektrostaticky nabíjajú a môže dôjsť k elektrostatickému iskreniu do oleja. Účelom základného experimentu bolo overiť hypotézu, že elektrické výboje vedú k tvorbe oxidantov (mäkkých znečisťujúcich látok) v oleji. To potenciálne mení mazaciu schopnosť oleja a jeho proces degradácie. Na potvrdenie alebo vyvrátenie teórie bol navrhnutý model s použitím zapaľovania z osobného automobilu a bol vytvorený tak, aby vybíjal elektrické iskry do štyroch rôznych vzoriek oleja. Kvôli overeniu zmien v olejoch sa následne vykonávalo meranie viskozity a analýza znečistenia časticami. Na základe výsledkov je zrejmé, že elektrické výboje majú negatívny vplyv na vlastnosti mazív a sú viditeľné postupujúce zmeny typu a množstva častíc v olejoch.

Kľúčové slová: mazanie, degradácia oleja, viskozita, častice, oxidanty

INTRODUCTION

Electrostatic charge generation occurs in fluid systems as a result of friction between the fluid and system components. Almost all machines are made of metal and their moving parts are lubricated with some lubricants and certain surfaces come in contact with each other. Consequently, the triboelectric effect (or static electricity) appears. Charge generation occurs in liquid systems on the molecular level at the interface of any two unlike materials, so a static charge will be generated in any moving fluid, with positive or negative charges moving from the fluid onto the bounding surface. The magnitude of charge depends on many interrelated factors, including the environment. Although tribology is the science of lubrication, friction and wear, very little has been discussed about the electricity due to friction. [7, 8, 10]

Charges can occur during filtration of hydraulic and lubricating fluids as well as in diesel and gasoline fuels. This effect manifests itself in several ways, the most obvious being an audible noise (clicking sound) as discharge of electrostatic charge accumulation causes sparking internally within the system. Less apparent effects involve migration of the electrical charge downstream of the filter when the charge dissipates by discharging itself to a grounded surface. If the component walls are conductive, then a charge will be induced on the walls, which are of opposite polarity to the fluid. If the exterior surface is grounded, the net charge will be zero. If not, the charge will accumulate to eventually discharge. This will generate an electrostatic discharge where the charge discharges to a surface at lower voltage. In doing so, it can generate a high-energy spark. If the discharge occurs in air, the results can be both spectacular and potentially harmful. [1, 3]

The aim of the experiment was to create a model for testing oil under the influence of electrical discharges and to verify the hypothesis that electrical discharges in hydraulic fluids result in the formation of oxidation products and degradation of oil properties. If there was dependence between electric discharge and oil oxidation, describe the process of degradation changes and interpret the results obtained. For the purpose of demonstrating the effect of electrical discharges on the properties of the oil, a viscosity measuring and particle analysis were performed.

MATERIAL AND METHODS

Four types of oil were selected for the experiment and each of them had a sample of 200 ml of oil. The reason was to compare the effect of electric sparking on the degradation of oils with different chemical composition and properties. After the last analysis of the samples, approximately 120 ml of oil remained in the containers. The results can therefore be influenced by the fact that sparks were each time transmitted to a smaller volume of oil, unlike real hydraulic systems. In this case oils were relatively motionless, except for mixing times and they did not run through the filtration system.

Sample no.1

Sunflower oil – basic edible oil, used in food and cosmetics. Unlike other oils used, sunflower oil does not contain any additives which should prevent degradation of this oil as it is not normally used in machinery. Determined dynamic oil viscosity of the pure oil: $\eta = 29$ mPa·s.

Sample no.2

Plantosyn 3268 ECO is a bio-degradable, ester-based hydraulic oil. It is intended for use in agricultural, forestry and construction machinery. It is not soluble in water, and the leakage or loss of oil is largely captured and maintained by the top layer of soil where it is biodegraded. It is an environmentally friendly alternative to petroleum-based hydraulic oils. The viscosity grade belongs to SAE 5W-20 engine oils. [6] Determined dynamic viscosity of the pure oil: $\eta = 42$ mPa·s.

Sample no.3

Renolin VG 68 is hydraulic mineral oil made from solvent-based raffinate that is highly resistant to oxidation and aging. It can be classified as refined oil with improved corrosion and oxidation protection and wear-reducing additives. [9] Determined dynamic viscosity of the pure oil: $\eta = 61$ mPa·s.

Sample no.4

Titan Ganymet Ultra is a zinc-free synthetic engine oil for stationary gas engines. It is characterized by a high level of protection against corrosion and wear, a very good ability to neutralize acid fumes and oxidative stability. The viscosity class is classified in the SAE 40 class. Determined dynamic viscosity of the pure oil: $\eta = 85$ mPa·s.

Model design solution

The proposed model was designed to simulate electric discharges in hydraulic oil. The model was built from the battery ignition of a Škoda Octavia, with certain voltage of sparks (1-4kV). Each of the four spark plugs was immersed in the container with oil. The basic components in the ignition were: electric coil, distributor and spark plugs. The distributor drive (shaft rotation) was solved by connecting to the lathe spindle. The experiment was best performed at 90 rpm when the sparks were visible. The battery was initially used as a power source, but due to the inability of the battery to maintain a stable voltage (too much resistance in oil), the battery was replaced by a solid source during the experiment. The coil switch and cooling fan were also added to the circuit to prevent overheating of the coil. For the fastening spark plugs, a sheet metal frame was made. The experiment did not take place in a sterile environment and samples were not sealed.

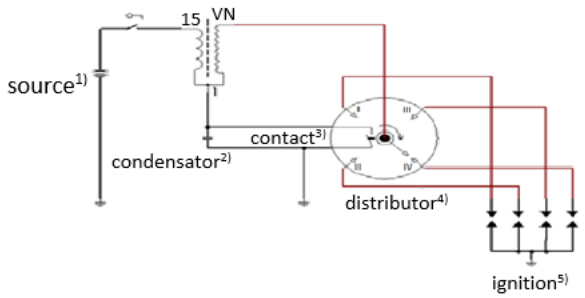

Fig. 1. Basic scheme of ignition
Obr. 1. Základná schéma zapaľovania
[1)]Zdroj napätia, [2)]Kondenzátor, [3)]Kontakt, [4)]Rozdeľovač, [5)]Sviečky zapaľovania

In the Fig. 1. is shown a basic set-up scheme of ignition from combustion engine which was used during the experiment and in the next Fig. 2. is shown practical solution where are samples together with the ignition.

Fig. 2. Demonstration of measuring model
Obr. 2. Ukážka experimentálnej zostavy

Particle analyzer

For the oil analysis was used device called LaserNet Fines (LNF). It is an optical device for automatic detection and identification of faults or incipient failure in mechanical systems due to excess mechanical wear, and for detecting contamination in hydraulic and fuel systems, and identifying underlying causes of that contamination. This analytical tool combines the oil analysis techniques of particle size analysis and particle counting. LNF determines size distributions of wear particles in lubricating systems and classifies the particles according to the mechanical process responsible for their presence. LNF utilizes a pulsed laser diode to form images of debris particles in a flowing fluid system and computer image analysis and classification algorithms to determine the size and concentration of particles and identification of the mechanical wear processes associated with the particles from their shape characteristics. The operator is presented with an assessment of particles found in the fluid sample and a history of previous results for the same equipment.

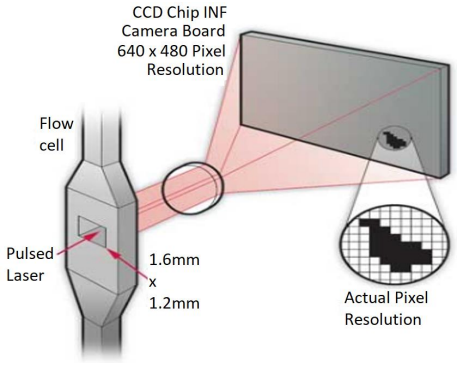

Fig. 3. Basic operation of LaserNet Fines [2]
Obr. 3. Princíp analýzy na prístroji LaserNet Fines [2]

LNF provides shape recognition of all particles greater than 20 µm by using a neural network. An algorithm sorts particles into the following categories: abrasive, adhesive, fatigue, non-metallic and unidentified fibres. The shape recognition software also does a test for circularity so that bubbles and droplets greater than 20 µm are eliminated from the particle counting results. Particles are sized directly and results can be displayed by ISO 4406 Code, or several military codes. While monitoring the electric discharges in oil is not relevant following abrasive, adhesive and fatigue particles because they have metallic origin. We focused only on non-metallic and unidentified particles. [2, 5]

SVM 3000 Stabinger Viscometer

This device measures the dynamic viscosity and density of oils and fuels according to ASTM D7042. From this result, the viscometer automatically calculates the kinematic viscosity and delivers measurement results which are equivalent to ISO 3104 or ASTM D445. The Stabinger measuring principle with Peltier thermostat enables an incomparably wide viscosity and temperature range with a single system. The thermostat works with high-precision stability of 0.005 °C. SVM 3000 is quick, compact and energy-saving, versatile in use, with only small amounts of sample and solvents required. It can measure up to 30 samples per hour. From 2.5 millilitres sample volume (from 1 milliliter without density measurement). This device uses an unique measuring principle. The measuring cell contains a tube filled with sample which rotates at a constant speed. In this tube floats a measuring rotor. This rotational viscometer completely eliminates the influence of bearing friction. [4]

RESULTS

Samples were visually checked before and after the experiment. The difference was clearly visible, even though it is only a subjective appreciation. For all samples, clean oil was clear at first, with no visible contamination. After the experiment, the oil was turbid on all samples, the samples contained particles and sludge and a slight change in oil colour was observed, especially in samples 1 and 2.

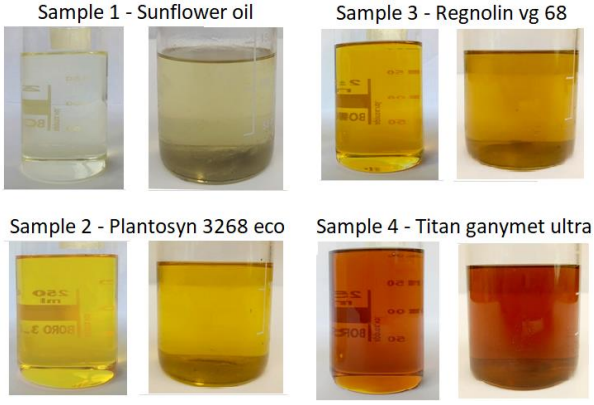

Fig. 4. Visual control of samples before and after experiment
Obr. 4. Vizuálna kontrola vzoriek pred a po experimente

A total of 6 measurements were made by the viscometer, the first measurement being carried out on pure oil and the remaining 5 measurements during the experiment. Measurements were performed after 120, 480, 840, 1200 and 1560 minutes of working time.

The first viscosity results were measured after 120 minutes (16200 revolutions) at a lathe speed of 90 rpm. Results for both dynamic and kinematic viscosity are expressed in the Tab 1.

Table 1. Trend in dynamic and kinematic viscosity during the experiment
Tabuľka 1. Priebeh dynamickej a kinematickej viskozity počas experimentu

		Working time[3] [min.]						
Sample[1]	**Value[2]**	**0 (start)**	**120**	**480**	**840**	**1200**	**1560**	**total change[6] [%]**
1.	**η[4]** *[mPa·s]*	29.247	29.628	30.121	30.823	30.861	31.143	6.48
	ν[5] *[mm².s⁻¹]*	32.185	32.617	33.149	33.893	33.950	34.232	6.36
2.	**η** *[mPa·s]*	42.033	42.173	42.458	42.409	42.357	42.615	1.39
	ν *[mm².s⁻¹]*	46.434	46.594	46.927	46.845	46.756	47.066	1.36
3.	**η** *[mPa·s]*	61.877	61.371	62.186	62.211	61.970	62.298	0.68
	ν *[mm².s⁻¹]*	71.105	70.488	71.462	71.483	71.190	71.564	0.65
4.	**η** *[mPa·s]*	85.178	84.210	85.417	85.339	85.259	85.819	0.75
	ν *[mm².s⁻¹]*	100.03	98.874	100.32	100.210	100.120	100.656	0.63

[1]vzorka, [2]veličina, [3]pracovný čas, [4]dynamická viskozita, [5]kinematická viskozita, [6]celková percentuálna zmena viskozity medzi prvým a posledným meraním

Table 1 shows the total percent change in viscosity. The viscosity significantly changed in sample no.1 by more than 6%, and the change in viscosity in sample no.2 (1.39% and 1.36%) is worth mentioning with a small difference remarked. For samples 3 and 4, a viscosity change of less than 1% was found, and so we can state that oils with additives which are modified to load conditions or potentially electrical discharges were not affected.

The measurement results were also evaluated from a ***statistical point of view*** (determination coefficient, correlation). According to the results of viscosity measurements, for samples 1 and 2, the linear regression model is considered to be prominently significant. Direct correlation of spark viscosity can be described by a linear function and we can apply regression estimates to the base set. According to these results it is possible to predict the behaviour of these oils and we know that the viscosity changes were caused by sparks. For samples 3 and 4, the model did not show statistically significant and it cannot be shown that the change in viscosity was largely due to sparking.

Measurement with LNF-C – particle pollution analysis

First of all, amount and percentage distribution of particles of different size was evaluated as stated in Table 2, and after that particles were evaluated by its type in Table 3.

Table 2. Amount and percentage distribution of particles by its size in 100ml of liquid
Tabuľka 2. Množstvo a podiel častíc podľa ich veľkosti na 100ml tekutiny

Particle SIZE[1)]	Sample no. 1[2)]				Sample no. 2			
	Amount of particles – before[3)] experiment	Ratio of particles before[4)] [%]	Amount of particles – after[5)] experiment	Ratio of particles after[6)] [%]	Amount of particles – before experiment	Ratio of particles before [%]	Amount of particles – after experiment	Ratio of particles after [%]
5-15 µm	56 550	83	2 635 261	90	538 719	99	2 794 113	91
15-25 µm	8 214	12	214 976	7	5 354	1	201 052	7
25-50 µm	2 360	3	72 021	2	787	0	61 028	2
50-100 µm	1 322	2	7 916	1	157	0	3 717	< 1
> 100 µm	0	0	310	< 1	0	0	155	< 1
	Sample no. 3				**Sample no. 4**			
5-15 µm	238 894	98	1 427 908	92	257 307	96	3 134 201	95
15-25 µm	4 728	2	88 694	6	9 172	3	134 927	4
25-50 µm	1 261	1	29 153	2	1 399	1	28 007	1
50-100 µm	0	0	1 234	< 1	0	0	1 547	< 1
> 100 µm	0	0	0	0	0	0	0	0

[1)]Veľkosť častíc, [2)]Vzorka č.1, [3]Počet častíc pred experimentom, [4)]Percentuálne rozdelenie častíc pred experimentom, [5)]Počet častíc po experimente, [6)]Percentuálne rozdelenie častíc po experimente

Generally, all four samples have an evident amount and percentage increase in the particle size in the range of 5-50µm, which could occur in oils due to electric sparks, but also surrounding environments (for example, particles in the range of 5-15µm are commonly found in the air or other pollutants). When we talk about particles in the range of 50-100µm, the increase was less significant, but still obvious and attributed to the impact of the electric discharge to oxidation in oils. For samples 1 and 2, particles of size >100µm appeared as a result of the presence of non-metallic fibrous structures, the formation of oxidation products and the sludge that could have occurred during heat treatment of oils by sparking. These values confirm the lower oxidation stability of samples 1 and 2. For samples 3 and 4, particles of size >100µm were not found what shows their resistance to oxidation and chemical stability.

Next, in terms of particle evaluation according to their type, LNF device can evaluate abrasive, adhesive and fatigue particles as well as non-metallic and unspecified (unknown) particles. For the purpose of evaluating the effect of electric sparks in oil, it is not worthwhile

to consider the presence of metallic particles since there is no logical chance that metallic types of particles in the oil will be generated by electric sparking and thermal degradation. For the experimental purposes, we only mention the content and percentage representation of non-metallic and unspecified (unknown) particles before and after the experiment.

Table 3. Amount and percentage distribution of particles by its type in 1ml of liquid
Tabuľka 3. Množstvo a percentuálne zastúpenie častíc podľa typu v 1ml tekutiny

Particle TYPE[1)]	Sample no. 1[2)]				Sample no. 2			
	Amount of particles – before[3)] experiment	Ratio of particles before[4)] [%]	Amount of particles – after[5)] experiment	Ratio of particles after[6)] [%]	Amount of particles – before experiment	Ratio of particles before [%]	Amount of particles – after experiment	Ratio of particles after [%]
Non-metallic[10)]	232.50	90.08	3 560.00	91.82	69.30	29.51	1 002.80	36.44
Unknown[11)]	0.00	0.00	75.70	1.82	32.70	13.93	87.20	3.17
	Sample no. 3				**Sample no. 4**			
Non-metallic	57.70	24.58	915.00	54.59	171.20	24.58	1 156.80	51.77
Unknown	34.60	14.74	55.90	3.34	52.90	14.74	74.80	1.56

[1)]Typ častíc, [2)]Vzorka č.1, [3]Počet častíc pred experimentom, [4)]Percentuálne rozdelenie častíc pred experimentom, [5)]Počet častíc po experimente, [6)]Percentuálne rozdelenie častíc po experimente, [7)] Abrazívne častice, [8)]Adhezívne častice, [9)]*Únavové častice,* [10)]Nekovové častice, [11)]Neidentifikovateľné častice

From the presented results, it can be stated that all four samples showed a percentage increase of non-metallic particles and also increase of undefined particles. The growth of these particles is attributed to electric discharge and the formation of oxidation products in oils. The results of metal particles are not demonstrated because we do not think it relevant to this experiment, as has been already mentioned above.

Non-metallic particles are partially transparent and indicate the presence of oxidation products. In addition, samples showed the presence of unknown particles where the analyzer could not assess their origin. Obviously, the largest ratio out of all has shown non-metallic particles as was expected before the experiment. These results support our theory about the influence of electric sparking.

CONCLUSION

Based on the percentage increase in particle by its size, the samples 1 and 2 are less resistant to degradation than the samples 3 and 4. The same result can be obtained by comparing the amount of particles according to their type. Oils 3 and 4 showed similar characteristic and results. Higher resistance and stability may in particular be related to the chemical composition of additives. According to results, there is no confirmation of the hypothesis for the significant effect of electrostatic discharges in case of using the oil determined for the certain conditions.

Nevertheless, the electric discharge has a negative effect to the oil properties. The process of degradation is particularly proved by results of the viscosity analysis of all samples, which have increased. Most notably, changes in viscosity for edible sunflower oil and biodegradable oil were noticed. Samples number 3 and 4 has shown good-class stability in viscosity testing as well. The purpose of this fundamental experiment was to verify the hypothesis that electric discharges lead to forming of oxidants (soft pollutants) in the oil. The experiment particularly confirmed expectations in certain conditions, but it should be repeated to a greater number of samples to further development of results.

The results of this paper can be used in practical application as a proof, that engine oils with certain properties should be resistant to impact of electrostatic discharges, however, testing is necessary. Especially for hydraulic and other oils used under the high pressure or high flow rates. There was recorded increasing trend of particle pollution for all four samples and after longer operating time, samples number 3 and 4 could potentially degrade their qualities, as well. Engine oils are tested by manufacturers in many different stress tests, but testing for resistance to electric discharges is not common. Presented paper might be used by oil producers as inspiration for further testing of oils. The system, which we used was simple and effective and it is applicable in different variants (voltage, number of discharges, etc.). With some minor improvements, this idea represents an easy and interesting way, how to get new and useful information about oil properties.

REFERENCES

[1] DAY, M., BENSCH, L., 2015. Electrostatic charge generation – in hydraulic and lubrication systems. In: *Practicing Oil Analysis*. Noria: USA, roč. 11. ISSN 1536-3937.

[2] FILICKY, D., SEBOK, T., MATLE, L., ANDERSON, D., 2002. Laser Net Fines – A New Tool for the Oil Analysis is Toolbox. In: *Practicing Oil Analysis*, Noria: USA, roč. 9. ISSN 1536-3937.

[3] Filtration without any static charging of the system [online]. 2015. RT – Filtertechnik: Germany [cit. 2018-04-21]. Dostupné z: <http://www.rt-filter.de/en/kompetenz/medientechnologie /sfree.html>.

[4] FITCH, B., 2013. Anatomy of a Viscometer. In: *Practicing Oil Analysis*. Noria: USA, roč. 8. ISSN 1536-3937.

[5] KUČERA, M., ALEŠ, Z., PEXA, M., 2016. Detection and characterization of wear particles of universal tractor oil using a particles size analyser. In: *Agronomy Research*. Estonian University of Life Sciences: Estonia, roč. 14, č. 4, s. 1351 – 1360. ISSN 1406-894X.

[6] Plantosyn 3268 eco [online]. Hazmioil: ***Tábor*** [cit. 2018-04-13]. Dostupné z: <http://www.hazmioil.cz/PI/plantosyn.3268.eco.pdf>.

[7] SASAKI, A., KAWAI, S., HONDA, T. and IWAI, Y., 2002. Measurement of the potential of static electricity generated by the friction of oil lubricated metal on metal. In: *Tribology Transactions*. Roč. 45, č. 1, s. 55-60. ISSN 0569-8197.

[8] ŠÍMA, M., 2008**.** ESD – ElectroStatic Discharge [online]. Portál ZČU: Plzeň [cit. 2018-04-10]. Dostupné z: <https://portal.zcu.cz/CoursewarePortlets2/DownloadDokumentu ?id=69855>.

[9] Technické informace – RENOLIN VG – Řada 32,46,68,100 [online]. Hazmioil: ***Tábor*** [cit. 2018-04-13]. Dostupné z: <http://www.hazmioil.cz/PI/PI-P-X04.pdf>.

[10] VAN RENSSELAR, J., 2012. Static discharge. In: *Tribology and Lubrication Technology*. Roč. 68, č.9, s. 46-53. ISSN 1545-858X.

Contribution has been prepared within the solving of scientific grant project CULS IGA 2017: 31190/1312/3119 – "Analysis of the impact of biofuels on the pressure profile in the combustion chamber of turbocharged diesel engine"

Corresponding author:
Michal Holúbek, +421 902611630, holubekm@tf.czu.cz